EARTHQUAKE PROTECTION OF MEDIUM-RISE REINFORCED CONCRETE BUILDINGS BY BASE ISOLATION

A THESIS

submitted in fulfilment of the
requirements for the award of the degree
of
DOCTOR OF PHILOSOPHY
in
EARTHQUAKE ENGINEERING

By

SAJAL KANTI DEB

DEPARTMENT OF EARTHQUAKE ENGINEERING
UNIVERSITY OF ROORKEE
ROORKEE - 247 667 (INDIA)

SEPTEMBER, 1993

Gratis

Dedicated To My Parents

CANDIDATE'S DECLARATION

I hereby certify that the work which is being presented in the thesis entitled **"Earthquake Protection of Medium Rise Reinforced Concrete Buildings by Base Isolation"** in fulfilment of the requirement for the award of the Degree of *Doctor of Philosophy* and submitted in the Department of Earthquake Engineering of the University is an authentic record of my own work carried out during a period from 31.7.1989 to 10.9.93 under the supervision of **Dr. S.K. Thakkar** and **Dr. D.K. Paul** .

The matter presented in this thesis has not been submitted by me for the award of any other degree of this or any other University.
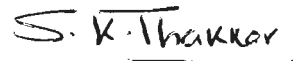
Sajal Kanti Deb

This is to certify that the above statement made by the candidate is correct to the best of our knowledge.
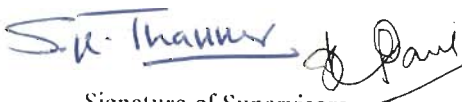
Dr. D.K. Paul
Professor
Deptt. of Earthquake Engineering
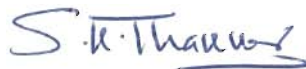University of Roorkee

Dr. S.K. Thakkar
Professor
Deptt. of Earthquake Engineering
University of Roorkee
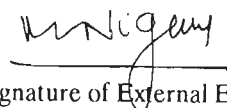
Date: 10-09-93

The Ph.D Viva-Voce examination of Sajal Kanti Deb, Research Scholar, has been held on

Signature of Supervisors   Signature of H.O.D.   Signature of External Examiner

ACKNOWLEDGEMENT

ABSTRACT

Earthquake protection by base isolation of buildings has attracted considerable attention in recent years. The main concept here is to isolate the structures from ground instead of the conventional techniques of strengthening the structural members. This new design methodology appears to have considerable potential in preventing damages to the structures and non-structural elements. Loose contents in the building are also protected.

In the present study, earthquake protection of medium rise reinforced concrete framed building by base isolation has been studied - both analytically and experimentally. Model laminated rubber bearing (LRB) has been designed for seismic isolation of a three storeyed r.c. framed building during Shake Table test. Analytical studies are carried out to asses the suitability of pure friction isolator (P-F), lead rubber bearing (LLRB), sliding-elastomer bearing (EDF) for seismic isolation of medium rise r.c. framed buildings.

Stability theories of LRB, proposed by different investigators, have been studied in connection with design of model LRB. Static testing of model bearing has been carried out to determine bearing parameters. Compressive test has been carried out to determine the vertical stiffness of the model bearing, which should have a very large value to avoid rocking and other unwanted modes of vibration. Shear test of model bearing under reversible lateral load shows that shear force-displacement relationship is non-linear in nature.

Shake Table Tests of the three storeyed base isolated 1/6th scale model has been carried out to assess the effectiveness of the base isolation in controlling the response of the superstructure. Additional loads are attached to each floor level for gravity load simulation. Simulated earthquake motions generated from a time scaled average spectra for alluvial soil, have been used as the input table acceleration histories. The model did not suffered any damage, even when it was subjected to high peak table acceleration of the order of 0.55g. Higher modes contribution in the seismic response of isolated structure are effectively filtered out by model bearing.

Relative performances of P-F bearing, LRB, LLRB and EDF bearing in controlling the response of a three storeyed r.c. structure, subjected to unidirectional earthquake motion is studied. Geometry and post yielding stiffness of all LRB based isolation system are kept same, while coefficient of friction in P-F and EDF isolators are considered to be 0.1. The bilinear hysteretic behaviour of LRB and lead rubber bearing are represented by equivalent linear stiffness and damping factor. Frictional force developed at the sliding interface is modelled by rigid plastic model. Superstructure is idealized as a rigid body and flexible model to understand the effects of flexibility of superstructure on overall response of base isolated buildings. Koyna (Long., 1967) and El-Centro (N-S, 1940) accelerogram is used as input excitations to understand the behaviour of base isolated building subjected to earthquakes with different characteristics. A unified solution algorithm has been developed for analysis of base isolated building supported over selected isolation systems, based on Newmark's method in predictor-corrector form.

Effects of superstructure flexibility on the base displacement for LRB, LLRB and EDF isolation systems are not significant, although acceleration response increases slightly, when the flexibility of superstructure has been taken into account. But, both base displacement and acceleration response for P-F bearing are largely influenced by flexibility of the superstructure. It is observed that base isolation technique is more effective in controlling the response of the structure for earthquake excitation with most of its energy contents in high frequency range. Fourier decomposition of roof acceleration for both excitations show that LRB acts as low pass filter and higher modes contribution is lowest for this system as compared to LLRB and EDF bearing. P-F is not able to filter out high frequency contribution in the response.

When isolated structure experiences multidirectional motion due to asymmetry in the structure and/or due to multidirectional excitation, it becomes very difficult to compute the response of the base isolated structure by modelling the hysteretic behaviour of LRB based isolation systems by bilinear model and that of sliding systems by rigid plastic model. In the present study, hysteretic non-linear model developed by Wen and modified visco-plastic model developed by Constantinou et al.

have been considered for modelling different types of isolation system under both unidirectional and bidirectional motions. Close form solution of stiff differential equation of hysteretic model for forces mobilized in non-linear elements of different isolation systems are obtained. Experimental shear force-displacement relationship obtained from uniaxial test of present study and that obtained by other investigator from both uniaxial and biaxial tests, have been simulated. Simulated hysteresis loops of different isolation system under both uniaxial and biaxial motion are found to be in good agreement with experimentally obtained hysteresis loops.

A unified solution algorithm has been developed for computation of response of medium-rise base isolated structures, considering non-linear behaviour of isolation systems, subjected to general plane motion. This solution algorithm is based on Newmark's method in predictor-corrector form. The centre of mass of all the floors and the base are assumed to be on the same vertical axis.

The response of a three storeyed r.c. framed building supported over either - P-F bearing, LRB, LLRB or EDF system, subjected to bidirectional motion of Koyna earthquake (1967), has been studied. Comparison of response of isolated structure in a particular direction for unidirectional and bidirectional excitations reflects the effects of biaxial interaction between orthogonal components of restoring force of isolation bearings. Response of solution algorithm and the computer programs developed in this study are in good agreement with that obtained from the more complex numerical studies reported in the literature.

Slender shape of model LRB used for isolation of the test structure during Shake Table test, induced rocking mode of vibration in the overall response of the isolated structure. When, an additional rocking degree of freedom is incorporated only at the rigid base of the superstructure, computed response obtained from flexible model is found to be in close agreement with the experimental response of the model. Thus, response of the base isolated medium-rise framed buildings can be predicted reliably by solution algorithm and computer programs developed in the present study.

CONTENTS

LIST OF FIGURES

LIST OF PHOTOGRAPHS

LIST OF TABLES

NOTATIONS

A = Dimensionless constant

A_b = Area of the bearing

a = Width of LRB

a' = Constant to care of variation of bearing pressure at sliding interface

α = Ratio of post yielding stiffness to pre yielding stiffness

α_1 = Mass ratio

b = Length of LRB

β = Newmark's constant

β' = Dimensionless constant

C = Superstructure damping matrix

C_b = Damping matrix of viscous isolation elements

C_{eq} = Equivalent Damping of LRB/LLRB

d_{max} = Maximum displacement in the bearing

d_{min} = Minimum displacement in the bearing

d_o^+ = Positive displacement in hysteresis loop for zero shear force

d_o^- = Negative displacement in hysteresis loop for zero shear force

d_r = Ratio of u_{bmax} and u_{by}

$\Delta\mu$ = Difference between μ_{max} and sliding friction value at very low velocity

Δt = Time interval for direct integration

E = Young's modulus of elastomer

E_c = Compression modulus of the bearing

ε_u = Euclidean norm

F_{max} = Maximum shear force in the bearing

F_{min} = Minimum shear force in the bearing

F_o^+ = Positive shear force in hysteresis loop for zero displacement

F_o^- = Negative shear force in hysteresis loop for zero displacement

F_y = Yield force in lead core

f = Vector of hysteretic part of restoring force in the isolation bearing

f_o = Natural frequency of SDOF base isolated model

ϕ_s = Vector of residual force in superstructure

ϕ_b = Vector of residual force in base of isolated structure

ϕ = Residual force in rigid body

G = Shear modulus of elastomer

g = acceleration due to gravity

g' = Dimensionless constant

γ = Newmark's constant

γ' = dimensionless constant

h = Thickness of one elastomer layer

h_t = h + thickness of one steel shim

I = Moment of Inertia of LRB

i = Iteration number counter

K = Superstructure stiffness matrix

K_b = Stiffness matrix of non-hysteretic part of isolation elements

K_e = Pre yielding stiffness matrix of the bearing

K^* = Effective stiffness matrix of superstructure

K_b^* = Effective stiffness matrix of isolation system

K^* = Effective stiffness matrix of isolation system (1 dof)

K_e = Pre yielding stiffness of the bearing

K_p = Post yielding stiffness of the bearing

K_{eq} = Equivalent stiffness of LRB/LLRB

k = material modifying factor

K_h = Total horizontal stiffness of the isolation bearings

K_t = Tangent stiffness at zero displacement

$(K_h)_{eff}$ = Effective stiffness of the LRB

k_h = Horizontal stiffness of individual bearing

k_l = Effective length factor of LRB

k_v = Vertical stiffness of individual bearing

l = Combined height of elastomer layers and steel shims

l_r = Total height of elastomer/rubber in LRB

M = Diagonal mass matrix of the superstructure

M_b = Diagonal mass matrix for base motion

m_t = Total mass of isolated structure

μ = Static coefficient of friction

μ_s = Sliding coefficient of friction

μ_{max} = Maximum sliding coefficient of friction at large velocity of sliding

N = Number of degrees of freedom

n	=	Time step counter
n_f	=	Number of floors
n_r	=	Number of elastomer layers
ν	=	Poisson's ratio of elastomer
P_c	=	Buckling load of the bearing
R	=	Matrix of earthquake influence factor
r	=	Vector of earthquake influence factor
r	=	Radius of gyration
S	=	Shape factor
s	=	Scale factor
$Sign(\dot{u}_s)$	=	Sign of sliding velocity
σ_{cr}	=	Buckling stress
θ_b	=	Instantaneous direction of bearing displacement
U_b	=	Instantaneous resultant bearing velocity
u	=	superstructure displacement vector w.r.to base
$\dot{u}$	=	superstructure velocity vector w.r.to base
$\ddot{u}$	=	superstructure acceleration vector w.r.to base
u_b	=	Bearing displacement vector w.r.to ground
$\dot{u}_b$	=	Bearing velocity vector w.r.to ground
$\ddot{u}_b$	=	Bearing acceleration vector w.r.to ground
$\ddot{u}_{bt}$	=	Absolute base acceleration vector
$\ddot{u}_s$	=	Sliding acceleration vector at the frictional interface
$\dot{u}_s$	=	Sliding velocity vector at the frictional interface
u_s	=	Sliding displacement vector at the frictional interface
u_b	=	Bearing displacement w.r.to ground
$\dot{u}_b$	=	Bearing velocity w.r.to ground
$\ddot{u}_b$	=	Bearing acceleration w.r.to ground
u_{by}	=	Yield displacement of the bearing
u_{bmax}	=	Maximum displacement of the bearing
$\ddot{u}_g$	=	Ground acceleration
u_m	=	maximum displacement
u_s	=	Sliding displacement at the frictional interface
$\dot{u}_s$	=	Sliding velocity at the frictional interface
$\ddot{u}_s$	=	Sliding acceleration at the frictional interface
u_t	=	Total displacement of the rigid body
W	=	Total load at the frictional interface
W_d	=	Dissipated energy (hysteresis loop)
W_s	=	Stored energy
ω	=	Angular frequency

ω_{eq} = Equivalent natural circular frequency

Y = Yield Displacement

ζ_b = Damping ratio of model LRB

ζ_{eq} = Equivalent damping ratio of the bearing

z = Vector of dimensionless hysteretic constant

z = Dimensionless hysteretic constant

CHAPTER 1

INTRODUCTION

1.1 General

In conventional medium-rise buildings, the fundamental frequency of vibration is in the range of frequencies where earthquake energy is maximum. This means that the building acts as an amplifier of the ground vibrations and the accelerations experienced at each floor level increase to the top. This also causes additional stresses in the frame and more interstorey drifts which may cause damage to the columns between floors. The amplified accelerations at each floor act on the contents and occupants of the floor. It can cause severe damage to these contents and non-structural elements even when no damage occurs to the structure itself. Earthquake resistant design of structure can be broadly classified into two categories (i) Conventional Earthquake Resistant Design (ii) Non-conventional Earthquake Resistant Design. These are briefly discussed here.

1.1.1 Conventional Earthquake Resistant Design:

Conventional design of practice for seismic safety of structure permits mobilization of inelastic action in its suitable components, which will provide that structure with significant energy dissipation potential to enable it to withstand a severe earthquake without collapse. This inelastic action is typically intended to occur in especially detailed critical regions of the structure, usually in the beams, adjacent to the beam-column joints. Inelastic behaviour in these regions, while able to dissipate substantial energy, also results in often significant damage to the structural member and although the regions may be well detailed, their hysteretic behaviour will degrade with repeated inelastic cycling. The interstorey drifts required to achieve significant hysteretic energy dissipation in critical regions are large and would usually result in substantial damage to non-structural elements such as infill walls,

partitions, doorways, and ceilings.

1.1.2 Non-conventional Earthquake Resistant Design: To overcome the shortcomings inherent in the philosophy of conventional earthquake resistant design a number of innovative approaches have been developed. An overview of non-conventional systems for earthquake resistant design is presented in Fig.1.1. In passive control, the behaviour of the structure depends on characteristics of the input motion. Earthquake protection of structures by passive control can be divided into two classes - (a) Base Isolation Techniques and (b) Energy Absorbing Devices. In base isolation technique the superstructure is decoupled from foundation by means of seismic isolation system, which reduces the transmission of damaging earthquake motion to the building. Energy absorbing devices control seismic response of the building by dissipating earthquake energy transmitted to the building. These devices are placed in suitable position in different floor levels of the building.

Active control is other form of non-conventional earthquake resistant design in which earthquake input and response motion are measured by sensors and response of the building are controlled by adding a force using external energy supply or changing the dynamic stiffness and damping characteristics of the structure.

In this study, earthquake protection of medium-rise r.c. framed buildings using base isolation technique is studied.

1.2 Base Isolation

A recent break through in earthquake engineering called "Base Isolation" is likely to revolutionize the way buildings are engineered in earthquake-prone areas. Buildings are mounted on rubber-steel-combination pads or on other isolators that during an earthquake, prevent most of the damaging horizontal component of the ground vibration from being transmitted to the buildings. Contrary to conventional design, loose contents of the buildings and non-structural components are also protected, therefore, buildings can be expected to remain functional even after an earthquake.

Base isolation is based on a new principle: rather than tying a building firmly to its foundation, the two are decoupled, which permits the building to float on top of isolation systems during earthquakes. Figure 1.1 shows three of the existing base isolated buildings constructed in New Zealand, Japan, U.S.A. respectively and Table 1.1 gives a directory of base isolated structures constructed in different parts of the world. This new principle opens the door to further research and improvements in our search for better seismic safety.

1.2.1 Basic Elements of Base Isolation System

It is helpful when reviewing current world wide development in seismic isolation to first identify the basic elements of a practical base isolation system. These are - (a) Flexible mounting (b) Energy absorbing device and (c) Rigidity for low lateral load.

■ **Flexible Mounting:** The elastomeric bearings are made of many alternate elastomer layers and reinforcing steel plates and their performance as bridge bearings are well proved because these bearings can accommodate thermal expansion and creep movement of bridges. It is possible to support buildings on elastomeric bearings and in excess of 150 examples exist in Europe and Australia, where buildings have been successfully mounted on these pads. To date laminated rubber bearing made from elastomer or natural rubber has been used not only for seismic protection but also for vertical vibration isolation due to traffic and other disturbances. By increasing the thickness of the elastomer layer in the bearing, desired lateral flexibility and period shift can be attained for achieving safety against earthquakes.

A laminated rubber bearing is not only a means of introducing flexibility into a structure, but it certainly appears to be most practical and the one with widest range of application to date. Other possible devices include rollers, sliding bearing, sleeved piles, rocking foundations, air cushions and coil springs.

The reduction in lateral force with increasing period (flexibility) is shown schematically in the acceleration response spectra of Fig.1.1(a). Substantial reductions in base shear are possible as the

period of vibration is lengthened but the degree of reduction depends on the initial fixed base period and the shape of response spectra curve.

However, the additional flexibility needed to lengthen the period will also give rise to large relative displacements across the flexible mount. Fig.1.1(b) shows an idealized displacement response curve from which displacements are seen to increase with increasing period (flexibility). These displacements can be reduced if additional damping is introduced at the level of the isolators (Fig.1.1(b)).

■ Energy Absorbing Device: One of the most effective means of providing a substantial level of additional damping is through hysteretic energy dissipation. The term hysteretic refers to the offset in the loading and unloading curves under cyclic loading. The work done during loading is not completely recovered during unloading and difference is lost (dissipated) as heat. Fig.1.1(c) shows an idealized force-displacement loop where the enclosed area is a measure of the energy dissipated during one cycle of motion.

Elastomers or natural rubber exhibit this property to some extent. By the addition of special purpose fillers to these materials, it is possible to increase their material hysteresis without unduly affecting their mechanical properties. Such a technique gives a useful source of damping but so far, it has not been possible to achieve the same level of energy dissipation as it is possible with the plastic deformation of a metal or utilizing frictional energy dissipation. Mechanical devices which use the plastic deformation of metals or frictional couple to achieve supplemental damping have been developed. Hydraulic damping has been used successfully in many special purpose structures. Potentially high damping forces are possible from viscous fluid flow, but maintenance requirements and high initial cost have restricted the use of this particular device.

■ Rigidity for Low Lateral Loads: While lateral flexibility is required to isolate against seismic loads, it is clearly undesirable to have a structural system which will vibrate perceptively under frequently occurring loads such as minor earthquakes or wind loads.

Specially formulated elastomers or natural rubber take advantage of

4

the dependence of shear modulus on strain amplitude to provide initial resistance to wind. At low strains, these elastomers and natural rubber exhibit high moduli than their moduli at high strains. Softening occurs with increasing strain and the desired isolation is then achieved. This behaviour is evident from the Fig.1.1(c). In pure friction isolation system this can be achieved by selecting coefficient of friction appropriately.

1.3 Identification of the Problem

Medium-rise multistoreyed building is chosen for base isolation for earthquake protection, since shorter buildings could easily be made strong enough to resist the fixed base inertia forces, while taller ones would not benefit because they would already have periods comparable to the two seconds typical of present day isolated structures.

In conventional seismic design of a fixed base structure the designer accepts a priori that the ground motion will impart to the structure a certain amount of energy. This energy must be dissipated if it is not to cause high floor accelerations or strong drifts, and it is generally achieved through inelastic deformation of the structural framing members as discussed earlier. This leads to the paradoxical conclusion that the integrity of the structure is assured only by deliberately inflicting damage on it. However, seismic isolation makes use of the idea of prevention rather than cure. The energy is largely prevented from entering the structure by decoupling the latter from the ground motion, thereby reducing both the ductility demand and the floor accelerations. Design for this double benefit is not possible in fixed base structures.

The perfect isolators would completely separate the structure from the ground by mounting it on a medium with no shear resistance, such as invicid fluid or perfect roller bearings. The ground movement then could not influence the movement of the structure at all. Practical versions of such devices have not yet been developed and probably never will be, however substantial but imperfect separation can be achieved by flexible mounting.

5

In the present study, the performance of four isolation system have been studied for seismic isolation of medium-rise multistoreyed framed reinforced concrete building. These bearings are (1) Laminated rubber bearing (2) Lead rubber bearing (3) Pure sliding bearing and (4) Sliding-elastomer bearing. These four isolation systems are chosen, because they are relatively simple in construction and cost effective, and these would be suitable for technologically developing countries. The dynamic response of the isolated system must be predictable for seismic isolation to be successful. Keeping this in view, simple yet accurate mathematical models have been investigated for modelling the structure and in particular the isolators. A 1/6th scale three storeyed base isolated reinforced concrete model was tested on the computerized shake table facilities of University of Roorkee. Measured responses are compared with the computed response for validation of analytical models.

1.4 Objectives

The work has been undertaken for earthquake protection of medium-rise multi storeyed r.c. framed building by base isolation, with following objectives:

(i) to review the literature, covering various base isolation systems developed and behaviour of base isolated buildings.

(ii) to develop seismic isolation systems suitable for medium-rise buildings.

(iii) to perform earthquake simulator tests of a model base isolated r.c. frame building.

(iv) to investigate analytical methods suitable for simulation of behaviour of buildings isolated by different base isolation systems.

(v) to develop the necessary computer programs for analysis of response of base isolated building.

(vi) to validate the analytical model by comparing the computed response with the experimental response.

1.5 Scope of the Study

To develop efficient and cost effective isolation system and to understand the behaviour of base isolated building following tasks were

6

undertaken:

1.5.1 Experimental study

(i) Investigation of available stability theories for LRB, design of the LRB model for seismic isolation of the test model and its testing to determine isolator parameters which influence the behaviour of base isolated system.

(ii) Free vibration testing of the base isolated test model to determine dynamic characteristics of the isolated system.

(iii) Earthquake simulator testing of the base isolated test model on a computerized shake table for observation of its dynamic behaviour.

1.5.2 Analytical study

(i) Mathematical idealization of the building-isolator system for prediction of its dynamic behaviour. The isolated building is idealized as (i) rigid body model, (ii) lumped mass model, (iii) 3-D model (3 dof per floor). Non-linear behaviour of isolators is modelled in light of experimental observations.

(ii) Development of computational algorithm for analysis of dynamic responses of the building isolated by various isolation systems for both unidirectional and general plane motion.

(iii) Development of simplified equivalent linear method of analysis for practical design purpose.

(iv) Comparative study of behaviour of the LRB isolation system with that of the other isolation systems.

   Validation of analytical models investigated in this study, by correlating the analytical results with experimental results and results of other investigators.

1.6 Outline of the Thesis

A review of earlier investigations on different types of base isolation systems developed in different parts of world, analytical and experimental behaviour of the base isolators and base isolated building as a whole under dynamic loading condition are presented in Chapter 2.

7

Chapter 3 describes the design and testing of the selected isolators for the base isolated test structure for determination of important parameters.

Chapter 4 presents free vibration test and earthquake simulator test of the base isolated test model. Base isolated test structure supported on selected isolation system are subjected to a artificially generated earthquake input motion. Measured responses of the test structure are presented in this chapter.

Chapter 5 presents the analysis of base isolated building under uniaxial excitation. In this chapter the building is idealized as rigid body model and lumped mass model. Force-displacement characteristics of isolation systems are idealized by conventional hysteretic models. Computed responses of base isolated test model is compared with measured responses of earthquake simulator tests.

Chapter 6 presents the analysis of base isolated building for general plane base motion. For modelling bidirectional motion of non-linear isolation elements, the coupled differential equation have been used. Medium-rise multistorey shear building is idealized as simplified 3-D model in the analysis. The response obtained from the solution algorithm developed in the present study are compared with that reported in the literature.

The conclusions of the present work and suggestion for future studies are included in Chapter 7.

Table 1.1 (a) Directory of Worldwide Base-Isolation Activity (1)
by Buckle and Mayes(1990)

Country	Constructed Facilities	Activity Organizations
BELGIUM		D'Appolonia
CANADA	1 coal shiploader, Prince Rupert B.C.	Univ. British Columbia,Vancouver Pall Dynamics, Montreal Swan Wooster Engg., Vancouver Khanna Consultants Intl.
CHILE	1 ore shiploader, Guacolda	University of Chile
CHINA	2 houses (1975), 1 weigh station (1980), 1 4-story dormitory, Beijing (1981)	Central Research Inst. of Building and Construction, Beijing
ENGLAND	1 nuclear fuel reprocessing plant	Malaysian Rubber Producers Research Association Rubber Consultants, Ltd. Imperial College of Science and Technology, London University of Southhampton
FINLAND		Imatran Voima Company
FRANCE	4 houses (1977-1982) 1 3-story school, Lambesc (1978) 1 nuclear waste storage facility (1982) 2 nuclear power plants Cruas and Le Pellirin	Centre National de la Recherche Scientifique, Marseille Centre d'Etudes Nucleaires de Saclay Electricite de France Spie Batignolies
GERMANY		GERB-Gesellschaft fur Isolierunge; Berlin; Kraftwerke Union; Engineering Decision Analysis; Polensky and Zolher, Frankfurt Jupp Grote
GREECE	2 office buildings, Athens	University of Patras
HUNGARY		Technical University of Budapest
ICELAND	5 bridges	Iceland Highway Dept.
INDIA		University of Roorkee Bhabha Atomic Research Center
IRAN/IRAQ	1 nuclear power plant, Kanun River (1978) 1 12-story building.Teheran (1968)	
Israel		Israel Institute of Technology Haifa

9

Table 1.1 (b) Directory of Worldwide Base-isolation Activity
by Buckle and Mayes(1990)

Country	Constructed Facilities	Activity Organizations
ITALY*	3 viaducts	Autostrade, Roma TESIT, Milano Polytechnic of Milan
JAPAN*	4 houses/apartments 7 research laboratories 2 museums 5 office buildings	Taisei Corp., Tokyo Kenchiku. Okumura Corp., Ohbayashi-gumi, Ltd., Oiles Industry, Sumitomo Construction, Takenaka Komuten Co., Kajima Corp., Shimizu Construction Co., Ministry of Construction, Univ. of Tokyo., Tohoku Univ., CRIEPI/Federation of Electric Power Companies
MEXICO	1 4-story school, Mexico City (1974)	Gonzales Flores, Cons. Engr.
MIDDLE EAST	storage tanks for liquid propane and butane**	
NEWZEALAND	2 office buildings Auckland and Wellington(1982 and 1983) 37 bridges 2 industrial structures (chimney and boiler)	Physics and Engg. Lab., DSIR University of Auckland Ministry of Works and Devp. Beca,Carter, Hollings & Ferner Holmes, Wood, Poole & Johnstone
RUMANIA		Polytechnic Institute of Jassy
U.S.S.R.	1 7-story building, Sevastopol	
SOUTH AFRICA	1 nuclear power plant, Koeberg	
SWITZERLAND		Swiss Federal Inst. of Tech. Zurich Seisma A.G.
U.S.A.	6 bridges 3 buildings 3 industrial structures	Dynamic Isolation Systems Univ. of California, Berkeley Reid and Tarics/Base Isolation Consultants Forell/Elsesser, Reaveley Engineers, California and Illinois Departments of Transportation
YUGOSLAVIA	1 3-story school (1969), Skopje	Univ. of "Kiril and Metodij"

* Both Italy and Japan also have a large number of partially
isolated bridges which are not included in above tabel.

** These five tanks are only partially isolated for seismic loads and
have therefore not been counted in above table
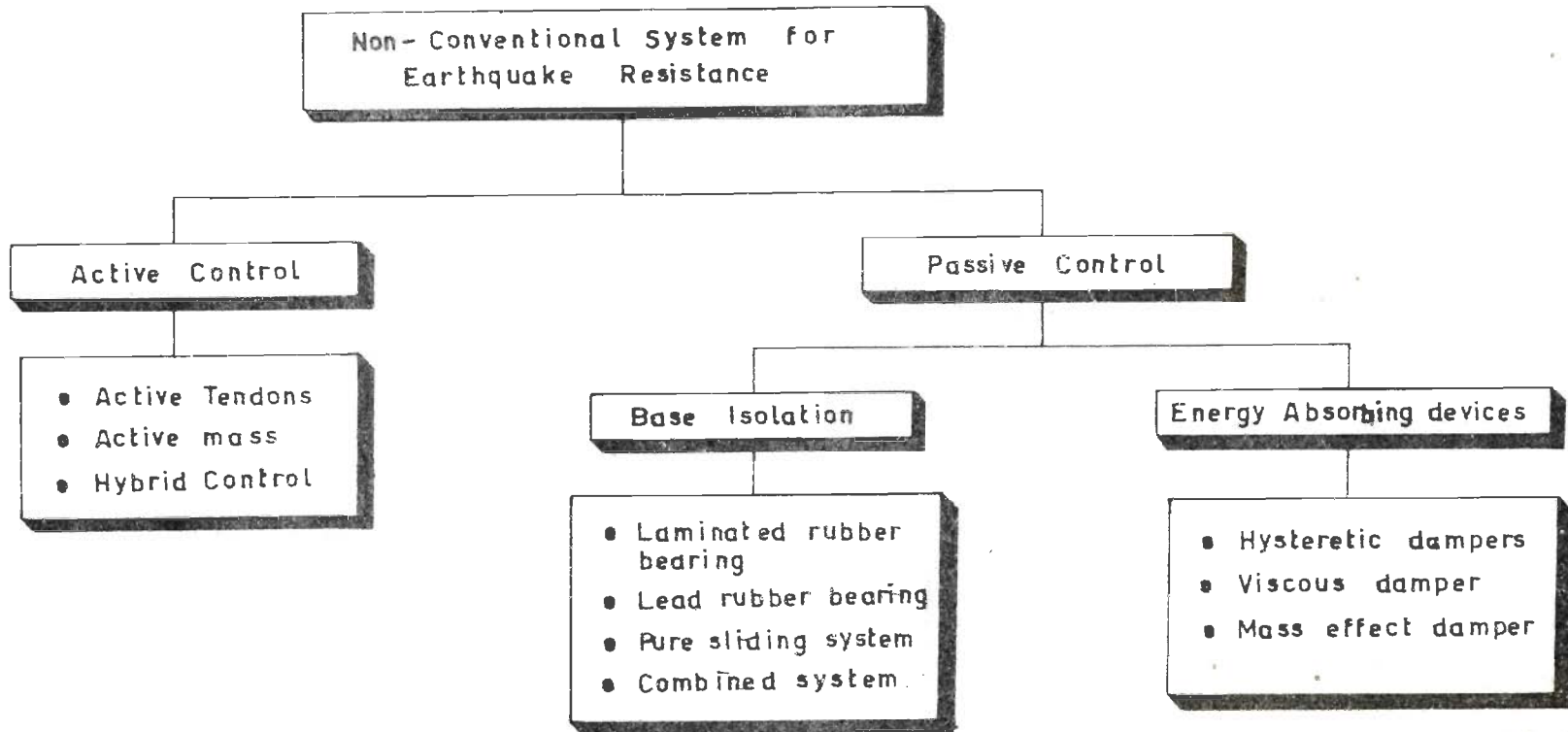
Fig.1.1 Non-conventional Systems for Earthquake Resistant Design
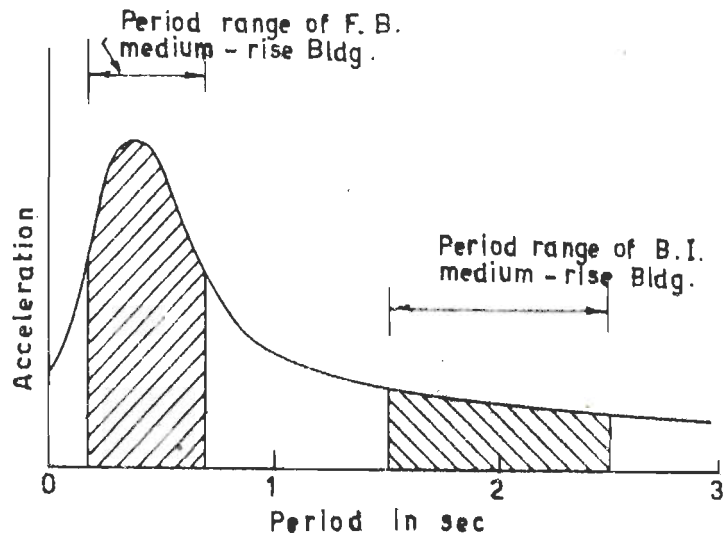
(a) Idealized Acceleration Spectrum
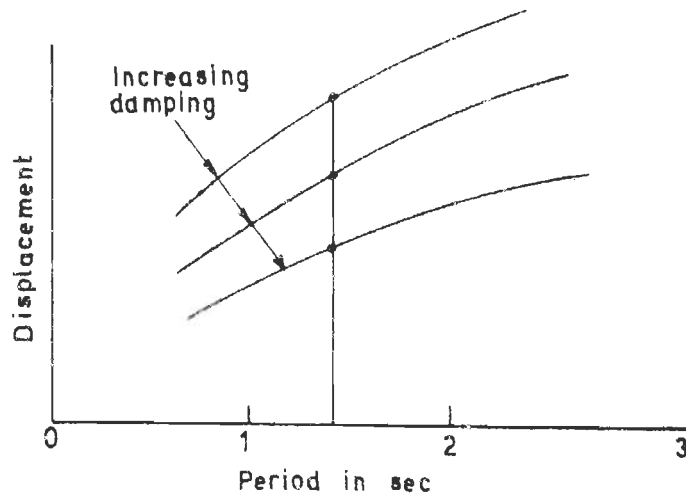
(b) Idealized Displacement Spectrum
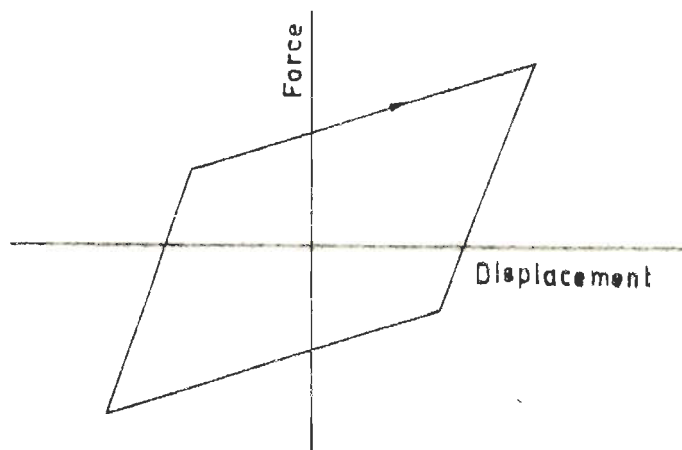
(c) Bilinear Force-Displacement Response
of Isolation System

Fig.1.2 Idealized Response Spectra for Base Isolated
Structure and Isolator Behaviour

12
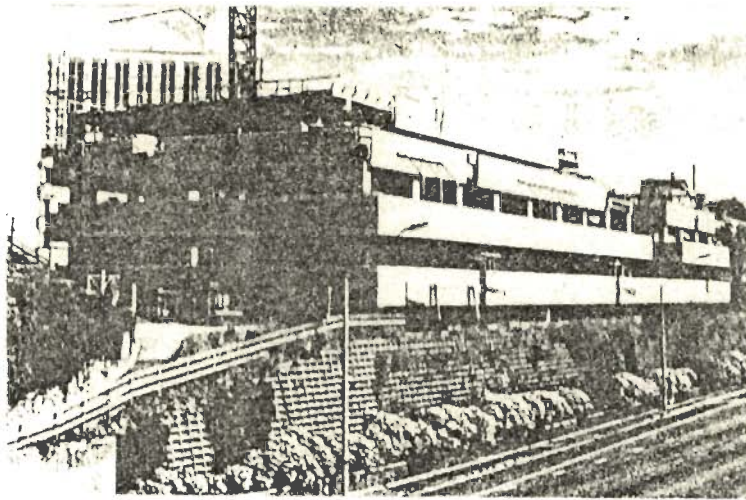
(a) William Clayton Building (1982), NZ
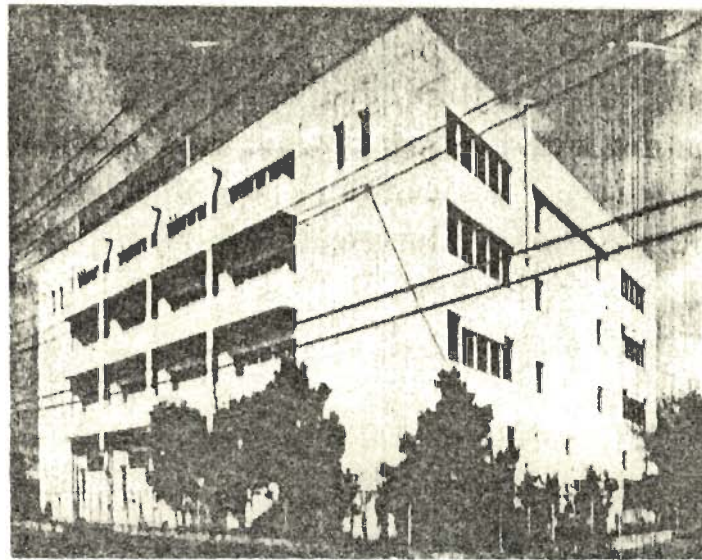
(b) Technical Center Building (1987), Japan
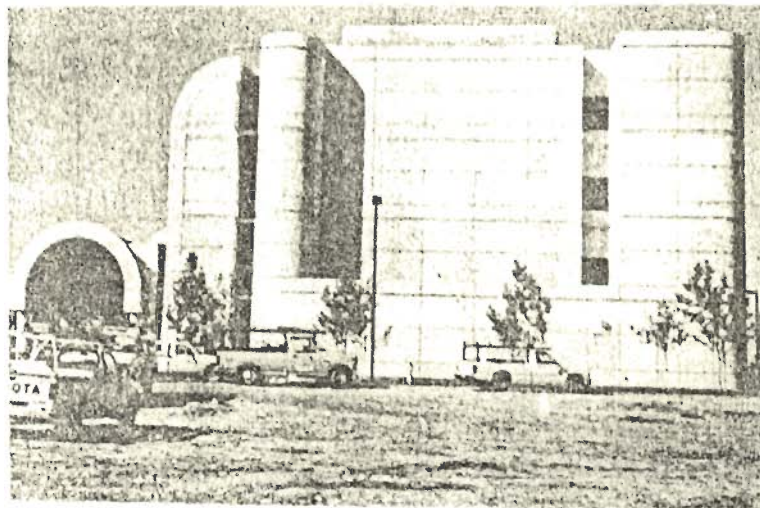
(c) Law and Justice Center (1986), U.S.A.

Fig.1.3 Photographs of Base Isolated Buildings

CHAPTER 2

REVIEW OF LITERATURE

2.1 Introduction

The idea of protecting buildings by base isolation is so appealing that inventors have found it irresistible and number of ways to do this have been patented or proposed. The goal of all isolation system developed so far is to reduce the accelerations in the buildings below the ground accelerations. In low or medium-rise buildings this is achieved by incorporating flexibility at the foundation level by the use of base isolation. Recent developments in rubber technology have made the idea of base isolation a practical reality. In this Chapter a brief review of seismic base isolation and its applications to buildings are presented.

2.2 Early Development on Isolation System

Frank Lloyd Wright designed the Imperial Hotel in Tokyo in 1921 and possibly this was the first building constructed using seismic isolation concept. Under the site was an 8 ft layer of fairly good soil and below that a layer of soft mud. This layer appeared to Wright as a good cushion to relieve the terrible shocks. The building performed extremely well in the devastating 1923 Tokyo earthquake.

Fintel and Khan(1969) developed a new approach of earthquake resistant design, called the soft first storey method, in which the first storey column is allowed to yield during an earthquake, producing an energy absorbing action and controlling displacements. However in this approach, large sideways in the first storey level could produce severe damage, causing collapse of the building a distinct possibility.

In the process of search for better isolation system many types of roller bearing system have been proposed, and several have been patented

14

and tested [Capse(1984)]. Since the ground movement can be in any direction, it is necessary to use spherical bearings or two crossed layers of rollers. The rollers and the spherical bearings are very low in damping and have no inherent resistance to wind so some other mechanism that provide wind restraint and energy absorbing capacity is needed. Since a roller isolation system could sit unattended, unmaintained for several decades in the basement of building, it is likely that its performance when called on could be disastrous. When steel presses against steel for a long period, there is a possibility of cold welding which could cause the system to become rigid after a time.

A three storeyed concrete building was constructed in Skopje, Yugoslavia in 1969 for a elementary school. This building rests on large blocks of natural rubber for earthquake protection. In contrast with more recent rubber bearings, these blocks are completely unreinforced so that the weight of the building causes them to bulge sideways. The vertical stiffness of the system is about the same as the horizontal so that the building will bounce and will rock backwards and forwards. It is unlikely that this approach will be used again.

2.3 Recent Isolation Systems and Their Behaviour

2.3.1 Laminated Rubber Bearing:

Many isolation system have been proposed since the turn of the century to achieve the seismic isolation of structures, but so far only a very limited number have actually been implemented. Among the isolation systems that have gained acceptance, the most common is the laminated rubber bearing system (Fig. 2.1). The bearings are made by vulcanization bonding of rubber/elastomer sheets to thin steel reinforcing plates. The steel reinforcement increases the compressive stiffness of the unit while maintaining the desired low horizontal stiffness. Their action under seismic loading is to isolate the building from the horizontal components of the earthquake ground motion, while the vertical components are transmitted to the structure relatively unchanged. Vertical accelerations are not normally a problem for most buildings. Laminated rubber bearings (LRBs) are suitable for medium-rise reinforced concrete buildings. For buildings up to seven storeys wind load will not be important and also uplift on the bearings will not occur. The LRBs are similar to bridge bearings and experience with these gives confidence in their longevity, reliability, and

resistance to various environmental degradations.

When a combined system of building supported over LRB is modelled as a linear viscously damped system, very simple solution will result. If the fixed base fundamental frequency of the building is much higher than that of the isolated, say 3 Hz as compared with 0.5 Hz for the isolated case, the first mode of the isolated building is mainly a rigid body mode with all deformation in the rubber. The second mode has a frequency about 50 % to 100 % above the first fixed base frequency [Kelly (1986)]. The seismic input to the structure can be treated as an equivalent lateral load which is proportional to the rigid body mode. Since it is a characteristic of a linear vibrating system that all modes are mutually orthogonal, this means that all modes higher than the first will be orthogonal to the input motion, so that if there are high energies in the earthquake ground movement at the frequencies of these higher modes, this energy can not be transmitted into the building. Thus, the isolation system works not by absorption of these energies but by deflecting them.

ISOMETRIC VIEW

PLAN VIEW   SECTION VIEW
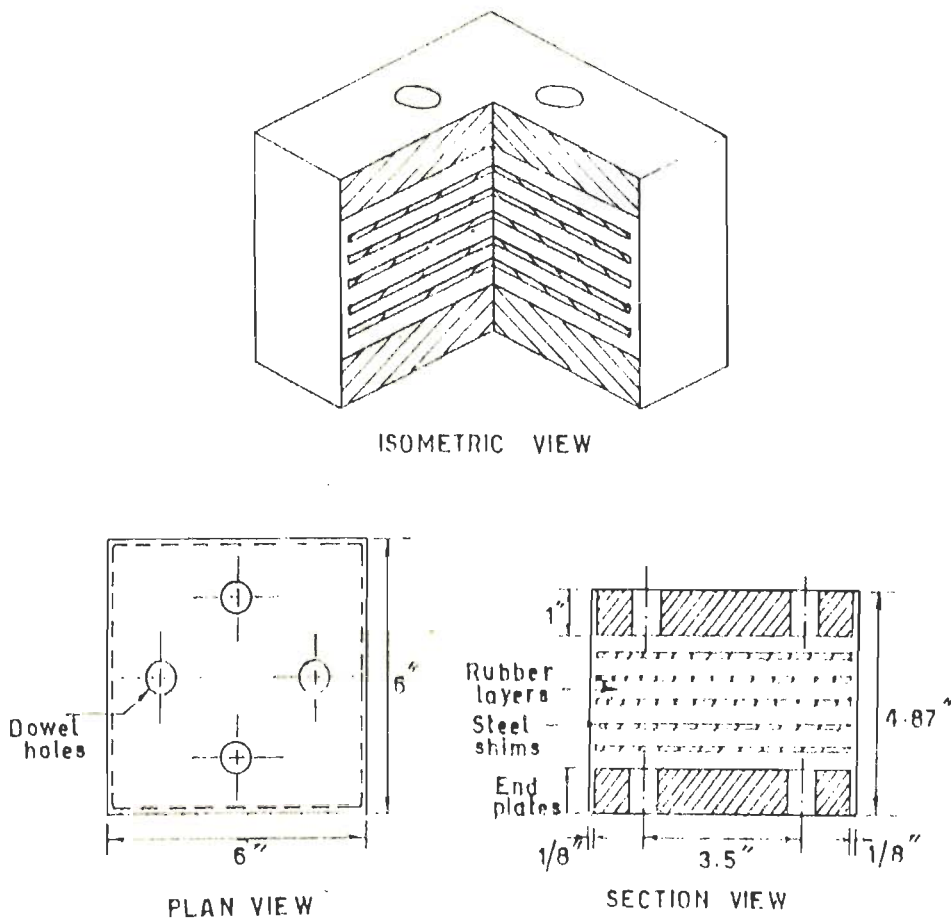
Fig.2.1 Laminated Rubber Bearing [Aiken et al.(1989)]

A simple form of rubber bearing isolation system was used for a three storey school in the small town of Lambese near Marseilles in France [Delfosse(1977, 1980)]. In this building there are no wind restraints or additional elements to enhance damping and the period of the isolated building is around 1.70 sec. Since this school has been completed, the designer of the isolation system, Giles Delfosse, has built three houses in the neighbouring community of Saint-Martin de Castillon. Delfosse has also designed an isolation system (GAPEC) of this kind for a three storey building for the storage of radioactive waste [Delfosse and Delfosse(1984)]. If it were not isolated, the period of the structure would be 0.30 sec and the peak acceleration would have been 0.61g. With isolators the period becomes 0.73 sec and acceleration is reduced to 0.33g. In recent years there has been a considerable amount of research into improving rubber compounds used in the bearing [Derham(1982)].

Base isolated building have coincident periods in both lateral directions and in torsion. They can also have coincident periods in pure vertical mode and rocking mode. Analytical study of torsional and lateral modes coupling [Pan and Kelly (1983)] and vertical and rocking modes coupling [Pan and Kelly (1984)] shows that with the degree of damping that is possible in rubber/elastomer bearings the influence of such coupling is unlikely to be of importance. The use of base isolation for unsymmetrical buildings would be very beneficial in that the bearings could be located to balance the centre of mass and the centre of resistance, it would thus cancel the negative structural effects of the configuration [Nakamura et al.(1988)].

Skinner et al.(1992) have studied analytically the effects of the degree of isolation on the modal profiles and periods, and on the seismic motions and loads, of a linearly isolated system and the effects of isolator nonlinearity in the seismic response calculation. They observed that, by the time isolation factor 'I' (the ratio between the flexibility of the isolator and the flexibility of the structure) has been increased to 2.0, the mode shapes are already close to their completely isolated (I = α) profiles. To study the effects of non-linearity, isolator has been modelled as bilinear hysteretic and a isolator non-linearity factor was defined. It has been established that non-linearity factor, if not suppressed by high elastic phase isolation factor, can

17

give rise to substantial higher mode contribution to seismic loads and to large increases in floor acceleration spectra at shorter periods.

Mizukoshi et al.(1992) carried out experimental studies in order to find the effect of geometric shapes on shear failure limit characteristics. The geometric shape of laminated rubber bearing with circular section is determined by two shape factors - primary and secondary shape factors. The tests were conducted to grasp the effect of the primary and secondary shape factors of the rubber bearings on the failure limit characteristics. The test results have shown that the influence of the geometric shapes were significant on shear deformation capacity of rubber bearings under high axial pressure.

2.3.2 Lead Rubber Bearing: Pioneering works on base isolation was carried out in New Zealand since early 1970's [Skinner et al.(1975, 1976), Skinner(1984)]. Damping that is inherent in usual rubber compounds as well as neoprene is rather low at that time, for use in aseismic design. Research in New Zealand resulted in the development of several energy absorbing devices that could enhance damping in rubber bearing. Of these the laminated rubber bearing with lead core (LLRB) as shown in Fig.2.2 is one of the most highly developed in the late 1970's [Robinson and Tucker(1977)]. The lead plug produces a substantial increase in damping from approximately 10 % of critical damping in the available rubber to about 20 % and also increases the resistance to wind loading. The building in which these isolators are used is in Wellington which is in a region of high seismicity. The building is four stories high and has a reinforced concrete frame [Meggett(1984)].

Analytical studies of the response of buildings supported over LLRB isolation system has been carried out [Lee and Medland(1978)]. Earthquake simulator tests of a model building on LLRB have been carried out by Kelly and Hodder(1982). The theoretical studies and the experimental results show that the lead plugs generally reduce the base displacement but increases the response contribution of higher modes. There have been problems with the lead working into the rubber and problems with the lead plug fracturing thereby reducing its effectiveness. Extensive studies were carried out by Robinson(1982) to understand the behaviour of this system and improve its performance.
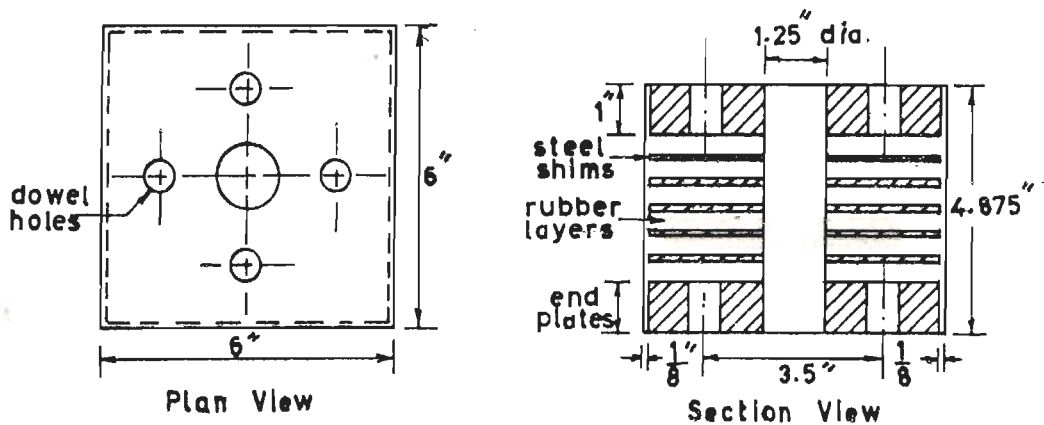
Fig.2.2 Lead Rubber Bearing [Aiken et al.(1989)]

A comprehensive series of tests on such bearings were carried out in New Zealand [Built(1982)]. The test series revealed a problem of substantial reduction in energy dissipation with reductions in load carried by the bearing. The tests also showed a deterioration of damping properties with the number of cycles caused by fracture of lead plug. Mitigation of these problems was achieved by confining the lead plug by coils or steel washers [Tyler and Robinson(1985)] and by reducing the thickness of individual rubber layers.

LLRB isolation system got wide acceptance in Japan and about ten numbers of base isolated buildings were constructed in Japan in mid 1980's. Extensive testing of this isolation was carried out [Shimoda et al.(1988), Hirasawa et al.(1988)]. These studies show that the equivalent damping ratio and equivalent stiffness are function of the strain level and the vertical load. These also indicate that the equivalent damping ratios are more affected by the vertical load than the strain level, while the equivalent stiffness are more affected by the strain level than the magnitude of the vertical load. Detailed analytical work of base isolated building supported over LLRB was carried out by Miyazaki et al.(1988). It indicates that the maximum acceleration and displacement response are almost the same, these neither depend on floor levels nor on the input waves. The maximum acceleration and displacement response depend on intensity level of earthquake input. This isolation system shows the better performance when subjected to severe excitation.

2.3.3 High Damping Laminated Rubber Bearing: High damping LRBs was used for the first time for seismic isolation of Foothill Communities Law and Justice Centre, in San Bernardino County, California [Derham et al.(1985)]. This happened to be the first base isolated building in the United States. The site of the building is 20 km from the San Andreas fault. The isolators are made from highly filled natural rubber which has mechanical properties that make it ideal for base isolation system with high damping property. Its shear stiffness is high for small strains but decreases by a factor of about four or five as the strain increases, reaching a minimum value at a shear strain of 50 %. For strains greater than 100 % the stiffness begins to increase again. Thus for small loading caused by wind or low intensity seismic loading the system has high stiffness and as load intensity increases the stiffness drops. For very high load, say above the maximum credible earthquake, the stiffness increases again providing fail-safe action. The damping follows the same pattern but less dramatically, decreasing from an initial value of 20 % to a minimum of 10 % and then increasing again. In the design of the system the minimum values of stiffness and damping are assumed and the response is taken to be linear. The high initial stiffness is invoked only for wind load design and the large strain response only for fail-safe action. These characteristics of the bearings make the structure distinctly different from other base isolated buildings.

In Japan, experimental work on base isolation by laminated high damping rubber was carried out [Takeda et al.(1988)]. In this study, several tests were performed on the base isolated building with laminated high damping rubber, which was developed aiming at isolating both of micro vibration and earthquake. As for micro vibration it is important to consider vertical vibration as well as horizontal vibration which is dominant in earthquake. Therefore, the high damping rubber is designed aiming at isolating vibration in vertical direction also. The forced vibration tests were carried out in wide frequency range from 4 Hz upto 400 Hz and earthquake observation were also made at this building. This study showed that during an earthquake, this base isolation system isolates the building proper from the earthquake, while during normal times it effectively isolates the building from traffic vibrations and machinery and equipment vibrations. Therefore, its use in buildings close to railway tracks and buildings and terminals above

20

subways, is considered promising.

Aiken et al.(1989) carried out experimental and analytical studies of low shape factor (LSF) elastomeric seismic isolation bearings. These bearings were designed for a seismic isolation application to provide horizontal and vertical isolation. This dual requirement led to a bearing design with a shape factor smaller than usual for a bearings designed to provide horizontal isolation only. Bearings were manufactured from both filled, high damping and natural rubber compound. An extensive series of test was under taken in the test set-up shown in Fig. 2.3(a) to investigate the performance characteristics of bearings with dowelled and bolted end connections. On the basis of the test results a number of comparisons were made of different bearings. The influence of axial load and shear strain on bearing characteristics of shear stiffness, vertical stiffness, and damping behaviour were investigated, with particular emphasis on evaluating the consequences of a low shape factor. Fig. 2.3(b) and 2.3(c) show two force-displacement hysteresis loops of a high damping LRB for two different shear strain levels and vertical loads. The shear tests demonstrated that the LSF bearings posses stable stiffness and damping properties. The bearings also showed a general reduction of stiffness with increasing axial load.

Suzuki et al.(1992) developed a high damping seismic isolation system using ferrite mixed high damping laminated natural rubber, which is temperature independent viscous in nature. They also developed 'equivelent linear method' for practical design of isolation system, the accuracy of which is verified by shake table testing. A damping factor of the order of 10 % was provided by high damping ferrite rubber isolator.

An extensive series of tests were carried out by Aiken et al. (1992) to identify the mechanical characteristics of two types of high damping isolation bearings and one type of LLRB. Cyclic horizontal displacement tests, varying the test parameters of shear displacement amplitude, axial load and loading frequency were performed on all of the bearings. Fundamental bearing stiffness and damping characteristics were studied in terms of shear strain, axial load, and rate of loading. In general, it was found that variations in axial load and rate of loading did not significantly affect bearing stiffness and damping properties

horizontal
actuator

force
transducer

vertical
actuator 1

vertical actuator 2

(a) Test Set-up

Vertical load = 31·46 kips
Strain = 100 %

(b) Shear Force - Displacement Loop _ I

Vertical load = 62.96 kips
Strain = 159.2 %

(c) Shear Force - Displacement Loop - II
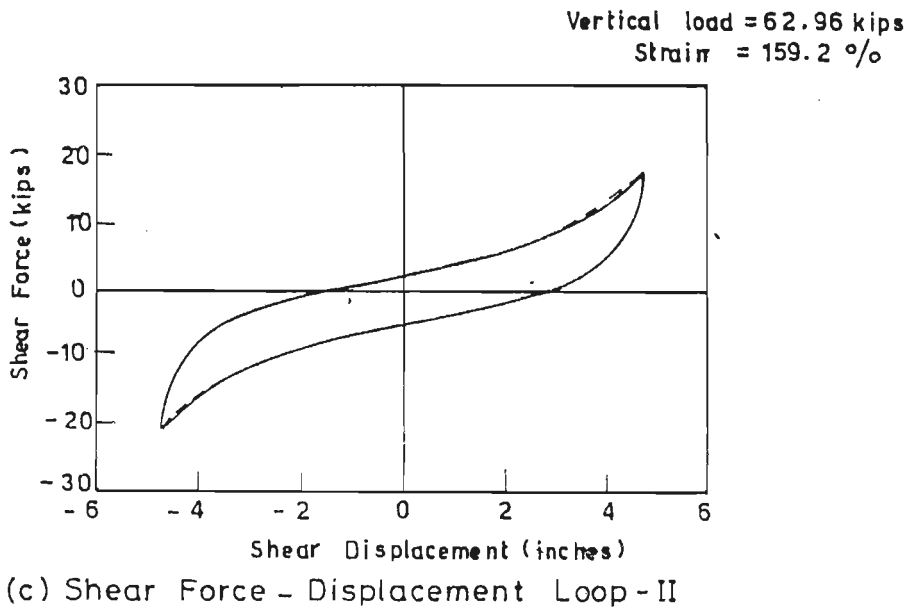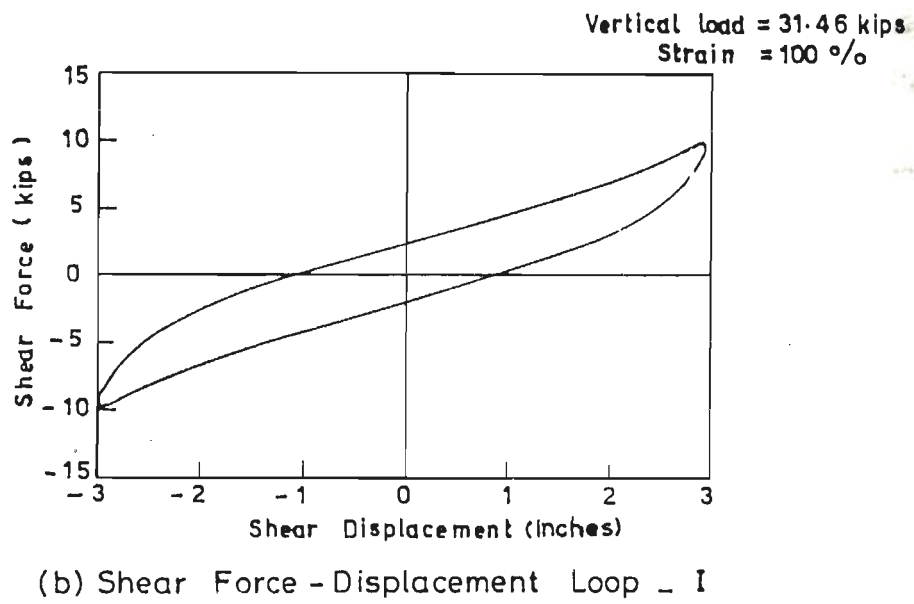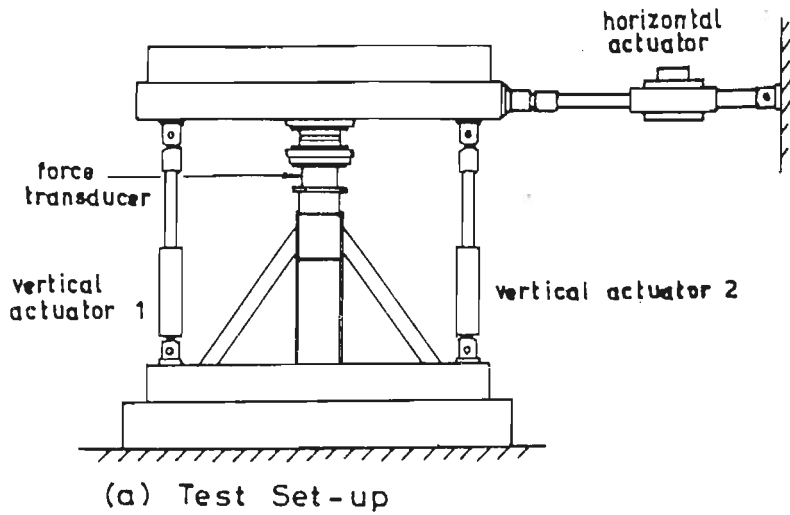
Fig. 2.3_ Test Set-up and Results of Shear Test of
LRB [Aiken et.al.(1989)]

for moderate shear strain levels. The ultimate-level shear tests achieved bearing shear strain in excess of 500 percent before failure occurred. The tension failure tests revealed the very large tension capacity of bolted high-damping bearings.

Serino *et al.*(1992) carried out shake table testing of a 394 kN isolated mock-up for studying performance of high damping steel-laminated rubber bearings under seismic inputs, alongwith development of non-linear model of isolation system. Significant reductions of the peak acceleration (upto 90 %) have been observed during the seismic tests, which have also demonstrated the small influence of the bi- and tri-axial interaction effects in the isolation bearings.

2.3.4 LRB with Additional Energy Absorbing Device: Extensive studies were carried out [Skinner *et al.*(1975)] in New Zealand on hysteretic dampers. These dampers used in parallel with isolation systems acts as energy absorbers which limit the quasi-resonant build-up of structural deformations and forces. These dampers utilize solid steel beams to deform plastically in various combination of torsional, flexural and shear deformations. The design schemes for use of rubber bearings in parallel with hysteretic dampers for effective earthquake protection of buildings and other types of structures were suggested [Skinner *et al.*(1975)]. Experimental works on use of bars and curve plates of hot rolled mild steel as energy absorbing device for controlling displacement was carried out [Stiemer and Zhou(1984)]. The proposed devices were used in parallel with isolation systems in buildings or other structures. They were designed to deform elastically under minor loads such as wind load and deform plastically when subjected to major earthquake loadings to provide necessary damping for controlling displacement.

Yasaka *et al.*(1988a) carried out experimental studies to develop LRB and steel rod damper for isolating a acoustic/ environmental vibration laboratory building from ground borne micro tremors, earthquake motion and vibration induced by strong winds. Vertical spring of rubber bearing was to be determined so as to have a natural frequency of 5 Hz to cut off ground borne micro-tremor by more than 20 dB. The post yield spring of the system correspond to a natural frequency of 0.5 Hz. The steel rod damper was made from mild steel with yield stress 2.87

23

tf/cm^2. Reinforced concrete deformation restrainer was used to protect the steel rod from local damage at the fixed end. Measurement of micro tremor, earthquake and wind observations have established its satisfactory performance. The steel rod damper alongwith its restoring force characteristics is shown in Fig. 2.4.
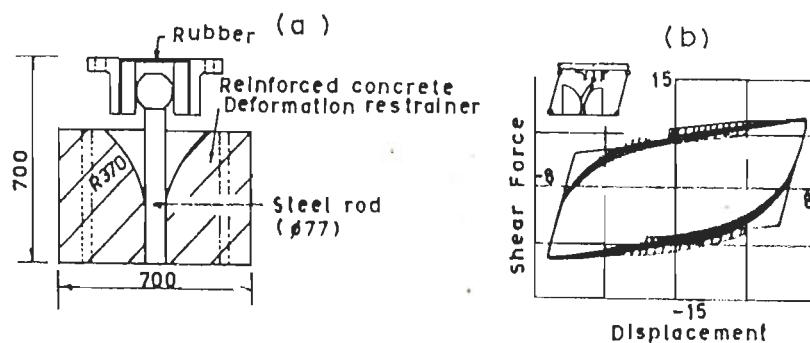
Fig.2.4 Hysteretic Behaviour of Steel Rod Damper [Yusaka et al.(1988)]
(a) Steel Rod Damper and (b) Force-Displacement Loop

Teramura et al.(1988) developed natural rubber bearing and special steel bar damper fitted with spherical bearings. They used this system for construction of 5 storeyed High Tech R&D centre building. Their analytical studies showed that the building would behave satisfactorily in severe earthquakes, particularly against high frequency earthquakes.

Aoyagi et al.(1988) carried out experimental and analytical studies on seismic isolation of a four-storey reinforced concrete building. The seismic isolation device consists of LRB and elasto-plastic steel dampers. The elastoplastic dampers consists of four spiral steel bars which allow to provide almost same functional characteristics for every direction. Based on vibration test, earthquake response observation and numerical analysis of the base isolated building they concluded that in the large deformation region of isolation devices, the natural period becomes longer considerably and large damping as designed and acceleration response during earthquake differs accordingly to the frequency characteristics of the ground motion.

Higashino et al.(1988) designed LRB and viscous dampers for seismic isolation of building and analyzed their performance against actual earthquake. Viscous dampers developed employs the shear deformation of viscous fluid. The viscous fluid used is called SA-P. The fluid is

mainly composed of poly-butene and its viscousity is very high. The ozone proof, water proof, acid proof and bacteria proof characteristics of viscous fluid was found to be good according to the accelerated aging test. Effectiveness of this isolation system was confirmed by the earthquake observation tests. Suzuki et al.(1992) developed a simple viscous damper, which is shown in Fig. 2.5 alongwith its restoring force displacement characteristics.
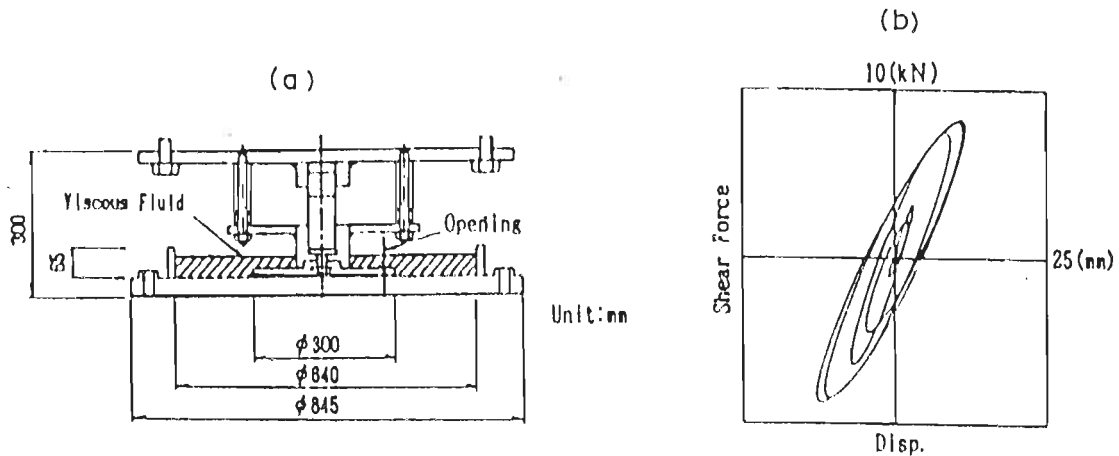
Fig.2.5 Hysteretic Behaviour of Viscous Damper [Suzuki et al.(1992)]
(a) Viscous Damper and (b) Force-Displacement Loop

Izumi *et al.*(1988) studied the effectiveness of LRB and oil damper for seismic isolation of two buildings both experimentally and analytically. They observed that the oil damper provides certain advantages since it has a reliable damping effect for not only large amplitude of motion but also small amplitude of motion.

Shimosaka *et al.*(1988) developed a new isolator consisting of LRB and ball screw type dampers with magnetic damping device. They claim that using magnetic damper the relative base displacement may be attenuated by 20 or 30 % compared with the case of other conventional hysteretic dampers. They studied the seismic responses of a seven storeyed building isolated by employing laminated rubbers with oil damper and laminated rubbers with magnetic dampers and also the seismic response of non-isolated one. Results show that the displacement response spectra from both isolated cases have narrower band peaks than the non-isolated one, while the acceleration response spectra belonging to both isolated cases have wider band characteristics as compared with

that of the non-isolated one.

Nakamura et al.(1992) developed a 'Soft-Landing Mechanism' in a effort to develop a base isolation system designed to reduce the seismic forces acting on nuclear fuel facilities and to secure the safety of such facilities even in case of excessively strong ground motion. The soft-landing base (Fig. 2.6) has a sliding surface on which the superstructure is set to land softly by using the subsidence of rubber bearing accompanying lateral deformation in an earthquake. Soft-landing functions without applying large acceleration to the superstructure and reduces the deformation of the rubber bearings. Soft-landing load supporting function prevents buckling caused by the deformation of the rubber bearing.
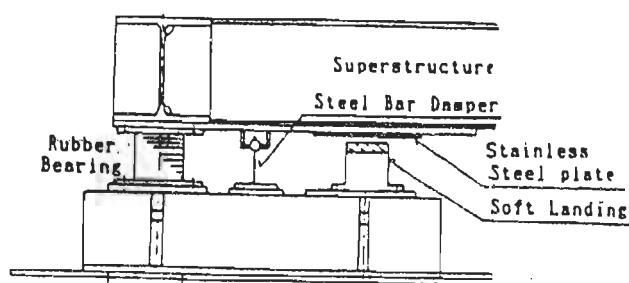
Fig.2.6 Base Isolation System with Soft-landing Mechanism
[Nakamura et al.(1992)]

2.3.5 Pure Friction System: Pure friction (P-F) isolation system are the simplest of all seismic isolation system developed so far. The isolation mechanism in this system is purely sliding friction. There has been a large amount of theoretical studies of pure friction isolation system. Mostaghel and Tanbakuchi(1983), Kelly and Beucke(1983), Younis and Tadj-bakhsh(1984) studied the behaviour of pure friction base isolation system under unidirectional horizontal sinusoidal and earthquake excitations. These studies established the effectiveness of pure sliding isolation system in controlling the level of acceleration and displacement response. For low coefficient of friction, the

acceleration does not vary with the frequency content of the ground motion. This implies that this system can be effectively used for all kind of sites. Lin and Tadjbakhsh(1986) studied the effect of vertical acceleration on the horizontal response of isolation system. They concluded that the force of friction and horizontal displacement response are significantly affected by the vertical ground motion and later on this study was extended by Liauw et al.(1988) to incorporate the effect of soil flexibility.

Arya et al.(1978), Arya(1984) carried out tests, where the performance of half-size single storey brick buildings were subjected to shock loading on a railway wagon impact facility. Several types of model buildings were tested, including both isolated and non-isolated, and it was concluded that the buildings with a sliding isolation system performed better than a conventional building.

In China, this system was incorporated for construction of four numbers of earthquake resistant masonry buildings. The approach adopted there is providing a separation layer under the floor beams above a wall foundation [Li(1984)]. A thin layer of specially screened sand is laid on the sliding surface and the building constructed on this. Since low-rise concrete block or masonry buildings are very stiff and heavy structures, they are very susceptible to earthquake damage, but the presence of the sliding layer allows a degree of flexibility which reduces the seismic risk.

Tyler(1977) carried out tests on PTFE (Poly Tetra Flouro Ethelene) /stainless steel sliding bearing under earthquake conditions. Representative normal loads were applied together with a sliding action, giving a maximum acceleration of 0.2g and a maximum velocity of 36 cm per sec, i.e. motions equivalent to a moderate to severe earthquake. At 0^0C friction was found to have maximum coefficient which fell from 17 to 13% as the normal pressure was increased from 15 to 25 MN/mm^2. At 20^0C corresponding values were reduced from 15 to 10 %. Maximum friction generally occured in the first cycle of loading after which values fell. After two 5 cycles the range of coefficient friction was typically from 9 to 5 %. Tests on the lubricated PTFE layers showed coefficient of friction less than 2 % under the above test conditions. The maintenance of this low value, over the years, would depend on the effective

retention of the grease.

Mokha *et al.*(1990) carried out extensive testing to model the frictional properties of sheet type Teflon-steel interfaces in relation to their application in sliding bearings for base isolated building and bridge structures. A series of laboratory experiments in the test set-up shown in Fig. 2.7(a) has been conducted on Teflon-steel interfaces to determine the effect of sliding velocity, sliding acceleration, bearing pressure, type of Teflon, and surface finish on frictional characteristics of sliding bearings. It was found that sliding acceleration has insignificant effects on the recorded values of frictional force. However, sliding velocity and bearing pressure have important effects as shown in Fig. 2.7(b). Further, the breakway friction coefficient (before initiation of sliding)decreases with increasing bearing pressure [Fig. 2.7(c)]. At the initiation of sliding, the ratio of breakway to sliding values of friction was 1.5 to 4.5.

Constantinou *et al.*(1990) developed a mathematical model of frictional behaviour of Teflon sliding bearings for conditions of interest in base isolation. The calibration of the model is based on extensive experimental data that were presented by Mokha *et al.*(1990). This model is capable of accounting for: (1) unidirectional and multidirectional motion at the teflon steel interfaces; (2) velocity and pressure dependence of coefficient of sliding friction and (3) breakway (or static) friction effects.

2.3.6 Combined Systems: Sliding-elastomer base isolation system [Gueraud *et al.* (1985)] developed under auspices of Electricite De France (EDF). This system is standardized for nuclear power plants in regions of high seismicity and is constructed by the French company Framatome. Typically the power plant is built over a huge monolithic concrete raft that covers several thousands of square metres. This base raft is supported by hundreds of isolators that are in turn supported by a foundation raft built directly on the ground. The main component of EDF (Fig. 2.8) system consists of a laminated neoprene pad topped by a lead bronze plate which is in frictional contact with stainless steel plate ($\mu = 0.2$) anchored to the structure. The EDF base isolator, which essentially uses an elastomeric bearing and friction plate in series. At lower level of ground excitation, lateral flexibility of the neoprene
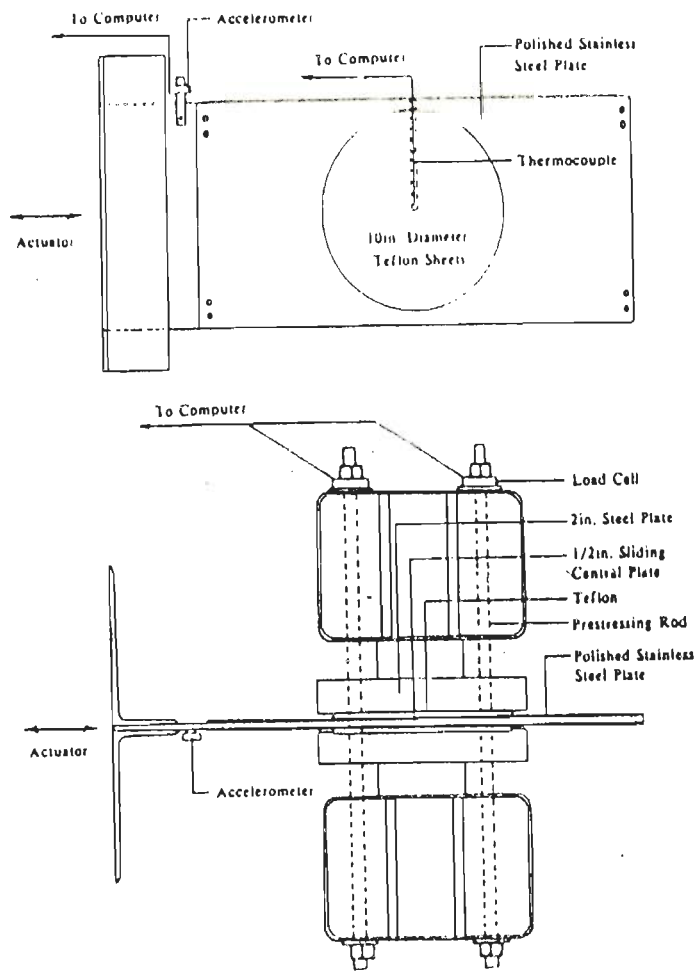
(a) Test Set-up
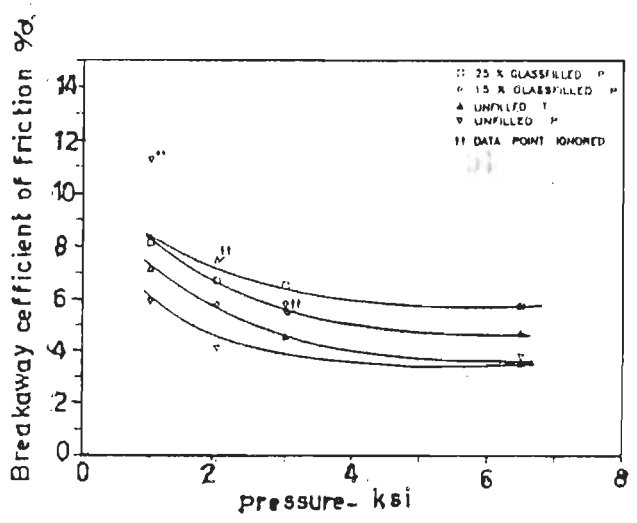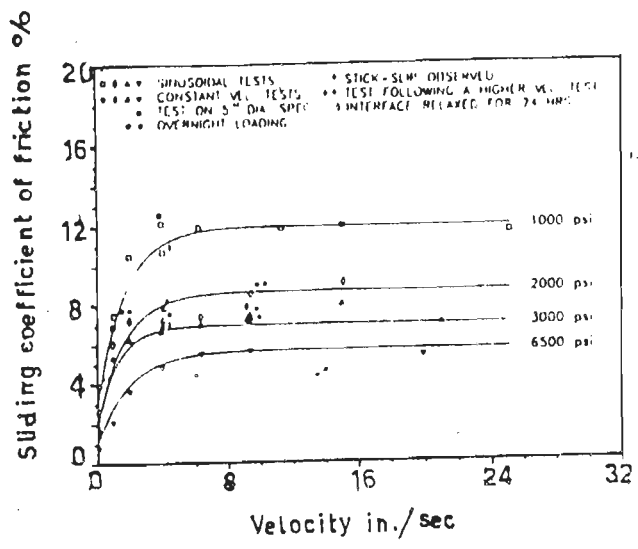
(b) Variation of Sliding coefficient of friction with Velocity and pressure

(c) Effect of bearing pressure on Breakaway coefficient of friction

Fig.2.7 Test Set-up and Results of Shear Test of Teflon/Stainless Steel Frictional Interface [Constantinou et al.(1990)]

pad lengthen the period of the structure above to achieve seismic isolation. However, slip in frictional interface provides additional safety at high level of excitations.
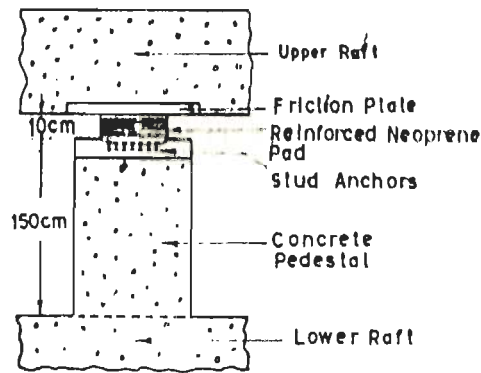
Fig.2.8 EDF Isolation System
[Gueraud et al.(1985)]
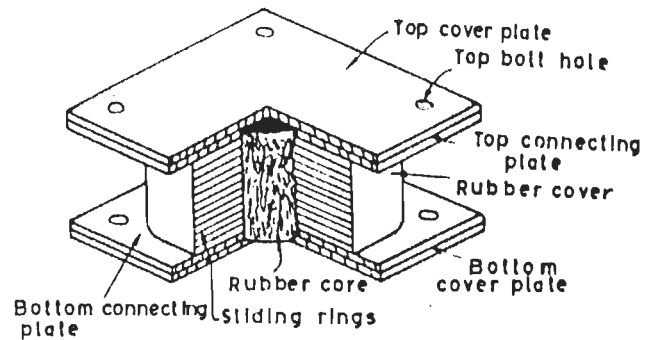
Fig.2.9 R-FBI Isolation System [Mostaghel
and Khodaverdian (1987)]

Mostaghel and Khodaverdian(1987) developed the resilient-friction base isolator (R-FBI). This base isolator consists of concentric layers of Teflon coated plates that are in frictional contact with each other with a central rubber core is fitted but not bonded to the sliding plates (Fig. 2.9). The rubber core distributes the lateral displacement across the height of the isolator and carries no gravity loads. The interfacial friction force acts both as the structural fuse and as energy absorber. This system combines the beneficial effects of friction damping with that of the resiliency of rubber to filter out the high energy carrying frequencies of the ground motions, thus providing isolation over a wide frequency range.

Su et al.(1989) proposed a new isolation system named as Sliding Resilient-Friction (SR-F) base isolator combining the desirable features of the EDF base isolator and R-FBI system. It was suggested to replace the elastomeric bearings of EDF base isolation system by the R-FBI units. That is, the upper surface of the R-FBI system in the modified design is replaced by a friction plate. As a result, the structure can slide on its foundation in a manner similar to that of EDF base isolati-

on system in the event of severe ground excitation and thus provides additional safety. Analytical study confirms that the SR-F isolator performs remarkably well under a variety of severe loading conditions.

Kawamura *et al.*(1988) developed a sliding type base isolation system to reduce horizontal seismic acceleration, which was named TASS system (TAISEI SHAKE SUPPRESSION SYSTEM). TASS system is (Fig. 2.10) generally composed of sliding bearing, bearing plates and horizontal springs. Sliding bearings are placed on bearing plates and support the weight of the super structure. Horizontal springs are fixed between the superstructure and foundation, connecting both parts. Slip occurs between sliding bearings and bearing plates and Coulomb damping is generated to absorb seismic energy. Horizontal springs are used to reduce seismic displacement response.
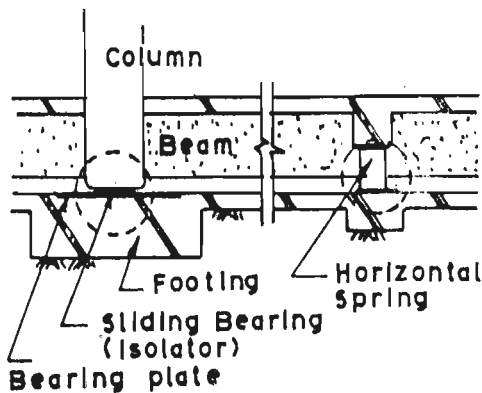
Fig.2.10 TASS Isolation System
[Kawamura et al.(1988)]
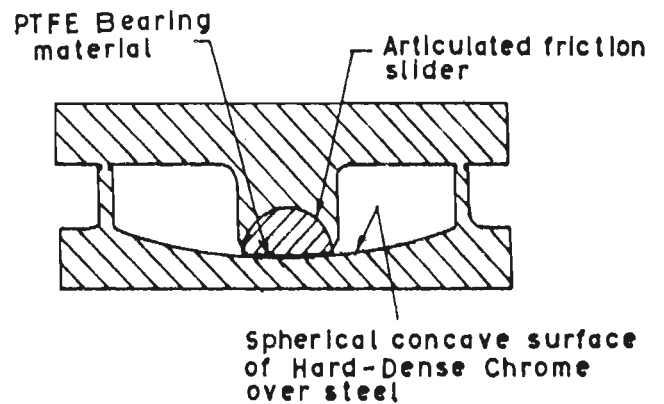
Fig.2.11 FPS Isolation System
[Zayas (1989)]

Zayas *et al.*(1989) developed Friction Pendulum System (FPS) using principle of simple pendulum for achieving seismic isolation is shown in Fig. 2.11. The FPS uses geometry and gravity to achieve the desired seismic isolation results. It is constructed of materials with demonstrated longevity and resistance to environmental deterioration. Mokha *et al.*(1991) carried out shake table study of the FPS installed in a six storey, quarter scale, 52 Kip model structure. The isolated structure is found to be capable of withstanding strong earthquake forces of different frequency content. The system is shown to have

quantifiable properties. Analytical techniques have been presented which provide accurate prediction of response.

GERB [Huffmann(1985)], a company specializing in vibration isolation has developed a new system for the three dimensional earthquake protection of whole structures, based on helical springs with definite linear flexibility of similar order in all three dimensions and velocity proportional visco-dampers, also highly effective in all degrees of freedom. A five storey steel frame building supported over GERB isolation system have been tested on shake table of Earthquake Research Institute at Skopje and the test results have shown the effectiveness of this system in minimizing structural response.

Caspe and Reinhorn(1986) developed an isolation system known as Earthquake Barrier System, which uses woven Teflon-steel inter-faces under very high pressure (about 8,000 psi) in an attempt to reduce friction to very low levels. Restoring force and energy absorption capacity are provided by a combination of high friction interfaces and steel beams designed to yield in bending.

2.4 Optimum Isolation Damping

Optimum viscous isolation damping in isolation mechanism for minimum acceleration response of base-isolated structures subjected to stationary random excitation was investigated by Inaudi and Kelly(1992). In this study optimum damping has been obtained based on minimum peak acceleration response to Gaussian excitation. The minimization of acceleration variances renders very similar values for the optimum damping values and this is because of the fact that the peak factor is not sensitive to changes in the isolation damping. The results obtained in this study show that the optimum isolation damping decreases with an increase in the number of degrees of freedom. An increase in the damping of the superstructure produces an increase in the optimum damping value while an increase in the flexibility of the superstructure tends to decrease the optimum damping and amplify the peak floor accelerations. The low-pass filter characteristics of a base-isolated structure are deteriorated by a heavily damped isolation system. Special care should be taken in defining the isolation damping when designing an isolated structure for sensitive equipment protection.

Shustov(1992) observed that the damping force is an active driving force, although it is mostly conceived as a force of inelastic resistance during an earthquake type of excitation. The negative pushing effect in damping mechanism is immediate, where as its positive dissipating effect needs more time to fully develop. It was concluded that the low damping base isolation would perform better than high damping system because there will be greater frequency separation in the former.

2.5 Base Isolation on Soft Soil

Although, the concept of base isolation is gaining widespread acceptance in different parts of the world, a question is being raised over the performance of base isolated building located at soft soil sites as to the effect of a low-site natural frequency on isolated structures. To address these concerns, Kelly(1991) carried out an experimental study on shake table at the Earthquake Simulator Laboratory of Earthquake Engineering Research Center of the University of California at Berkeley. Two different isolation systems were used in the shake table tests. One isolation system was designed to provide the model with a natural period that corresponds to the period of a proposed nuclear facility. The second system made use of a newly developed high damping rubber with a low shear modulus which provides a frequency about twenty five percent lower than that given by the first system. This allowed the assessment of (i) the benefits of lengthening the period of isolation system where the site is particularly soft and (ii) the practicality of long-period isolation systems based on elastomeric components. The test series has shown that the base isolation systems can be used at soft-soil sites under circumstances where the isolator loads and, consequently, the isolator sizes are sufficiently large to accommodate the resulting large displacement.

2.6 Comparative Study

Fan et al.(1990) carried an extensive comparative study for evaluating performances of various isolation systems. This study reveals that the acceleration time histories of a structure with Pure Friction system and the R-FBI/SR-F isolators show many sharp peaks. These sharp peaks are generated by the slip-stick and reversal transitions for which the discontinuous changes of friction force exert shock loadings on the base

33

of the structures. The continuous but non-linear transitions of the Pure Friction and the R-FBI/SR-F system generate high frequency components in the absolute acceleration time histories. While, acceleration responses with the LRB system, show relatively smooth time variations. It was also observed that the acceleration response provided by the EDF system is smoother in comparison to those of the Pure friction and the R-FBI/SR-F systems.

2.7 Concluding Remarks

Base isolation systems reviewed in the previous sections can be broadly classified as (i) laminated rubber bearings (LRB) (ii) lead rubber bearings (LLRB) (iii) high damping LRBs (iv) LRBs with additional energy absorbing devices (v) Pure sliding systems (P-F)(vi) Combined systems. Fig.11 shows broad classification of different types of recent seismic isolation systems and energy absorbing devices.

In mid seventies LRBs were used in France for seismic isolation of buildings although inherent damping available in elastomer is low. In New Zealand and Japan, additional energy absorbing devices were developed, which act in parallel with LRBs for supplemental damping for restricting base displacement within acceptable limit. Most of the energy absorbing devices utilize plastic deformation of metals, although other forms of energy absorbing devices like oil dampers, viscous dampers, friction dampers have also been developed. Presence of energy absorbing device makes the connection details at the base of the isolated building more complicated and some of the energy absorbing devices have to be replaced after experiencing an earthquake.

LLRB and high damping LRB combines the function of isolator and energy absorbing device in one unit and therefore, connection details at the basement are relatively simple. Experiments carried out on LLRB revealed that a deteriorations of damping properties with the number of cycles caused by fracture of lead plug. Higher mode responses increase in both LLRB and high damping LRB. It was also observed that the low damping base isolation would perform better than high damping system because there will be greater frequency separation in the former.

Pure sliding systems are very simple in construction but sharp peaks are seen in the response of isolated structure because of stick-

slip behaviour of this system and this phenomenon imparts shock type of loading in the isolated structure. EDF combines LRB and P-F bearing in series and thereby posses advantages of both LRB and P-F bearing.

Combined systems which includes isolators like R-FBI, TASS and FPS systems are highly sophisticated systems and implementation of this category of isolation system for seismic isolation of structures in developing countries like ours is not practical considering cost effectiveness at present.

Based on the above study, LRB with moderate damping (around 10 to 15%) is found to be suitable for seismic isolation of medium-rise framed buildings. Experimental and analytical studies are carried out to evaluate the behaviour of medium-rise r.c framed building isolated by LRB. Analytical studies are also carried out to assess the suitability of LLRB, P-F bearing, EDF bearing for seismic isolation of medium-rise r.c. framed building.

Seismic Isolation System

- **Laminated Rubber Bearing (LRB)**
  - **Simple LRB**
    - Natural Rubber
    - Neoprene
  - **Lead Rubber Bearing**
    - Simple lead core
    - Confined core
  - **High Damping LRB**
    - Carbon filler
    - Ferrite filler
    - Others
  - **LRB + Energy Absorbing Device**
    - Steel bar damper
    - Viscous damper
    - Oil damper
    - Spring damper
    - Friction damper
    - Magnetic damper
- **Pure Sliding System**
  - Sand layers
  - Carbon layers
  - Teflon/stainless steel interface
  - Others
- **Combined System**
  - EDF
  - R-FBI
  - TASS
  - SR-F
  - FPS
  - GERB
  - Others

Fig.2.12 Broad Classification of Base Isolation System

CHAPTER - 3

DESIGN AND TESTING OF SEISMIC ISOLATION BEARING

3.1 Introduction

Properly designed isolators in a base isolated structure provide necessary flexibility and energy dissipation capacity to safe guard the building against the damaging horizontal components of earthquake motion. The laminated rubber bearing used for seismic isolation of structures are development of elastomeric bridge bearings and their process of manufacturing are similar. The difference between these two types of bearings are in proportions of rubber and steel and in maximum lateral deformation capacity for which they are designed. In this chapter design and testing of laminated rubber bearing for the r.c. framed test structure (as described in the Chapter 4) are presented.

3.2 Essentials of a Seismic Isolation System

Design principle of seismic isolation bearings are similar to that of the mountings of buildings for isolation from ground borne road and rail vibration. However, there are number of uncertainties that are related with seismic events and consequently there are number of specific requirements which must be met by a practical base isolation system. These are listed below:

1. The base isolators must support the vertical load of the structure with a large safety factor.

2. The isolators must be stiff enough vertically to prevent significant amplification of any vertical component in the earthquake.

3. The shear stiffness of the isolators must be low enough to filter out the majority of the frequency components in an earthquake at a site.

4. During an earthquake the building will move sideways on the isolators. At the extremes of these movements the bearings must

continue to support the vertical load of the structure.

5. The damping in the isolators must be sufficient to prevent a build-up of amplitude in the structure during an earthquake.

6. Motion of the base isolated structure during strong winds should not be sufficient to disturb the occupants.

7. The isolation should not cause excitation of higher modes in the structure or contents.

8. The isolators should be, if possible, be intrinsically fire resistant.

9. The isolators should have a lifetime at least equal to that of the structure.

3.3 Design of Laminated Rubber Bearing

The design of laminated rubber bearing for seismic isolation must ensure following three parameters:

(i) the horizontal stiffness of the bearings, so that the specified horizontal natural frequency can be achieved.

(ii) the vertical stiffness of the bearings, so that no undesirable vertical or rocking mode will occur.

(iii) the stability of the bearings under combined vertical load and lateral displacement. This combined loading condition must be checked to ensure that a reasonable factor of safety exists against instability caused by extreme loading.

In the design of laminated rubber bearing, a number of trials are necessary to find out an optimum size of elastomer layers, steel shims and the bearing as a whole, which will satisfy the above three requirements. Model LRB has been moulded by vulcanizing elastomer layers with powdered carbon fillers and m.s. plates. Carbon fillers are added to increase the damping provided by the bearing.

Base isolated buildings are generally designed for a natural frequency of 0.5 Hz for deflecting energy associated with higher modes of vibration, while keeping the base displacement within the acceptable limit. For 0.5 Hz prototype frequency corresponding model (1/6th scaled) frequency = $\sqrt{\text{Scale factor}}$ x 0.5 = 1.225 Hz

Assumed elastomer properties are:

Hardness IRHD = 50

Shear modulus G = 600 kN/m^2

Elongation at break > 400 %

Plan dimension of the bearing = 90 mm x 90 mm

Numbers of bearings supporting test model = 6

3.3.1 Horizontal Stiffness: The simple single degree-of-freedom natural frequency (f_o) of the base isolated model structure is given by

$$f_o = \frac{1}{2\pi} \sqrt{\frac{K_h}{m_t}} \qquad \dots (3.1)$$

where, m_t is the total mass of the model structure and K_h is the total horizontal stiffness of the bearings. Substituting the values of f_o and M in the Eqn.(3.1), gives $K_h = 302.53$ kN/m.

Therefore, horizontal stiffness of single bearing k_h

$$k_h = \frac{K_h}{no.\ of\ bearings} = 65.422\ kN/m$$

Again, the horizontal stiffness k_h is given by simple shear formula

$$k_h = \frac{G\ A_b}{l_r} \qquad \dots (3.2)$$

where, l_r is height of rubber in the bearing and A_b is area of the bearing. The equation assumes that lateral deformation of the bearings is due to shear. Substituting the values of k_h, G and A_b in (3.2), gives $l_r = 74$ mm.

3.3.2 Vertical Stiffness: To achieve high vertical stiffness of the bearings, 19 layers of elastomer, each of 4 mm thick, is selected. The elastomer layers are separated by 2 mm thick mild steel shims. The compression stiffness can be calculated from the relation

$$k_v = \frac{E_c A_b}{l_r} \qquad \dots (3.3)$$

where, E_c = bearing compression modulus. The commonly used equation for the compression stiffness of rubber [Gent and Lindlay(1959)] is

39

$$E_c = E (1 + 2 k S^2) \qquad \qquad \dots (3.4)$$

where, E = Young's modulus = 2.3 MPa for IRHD 50

     k = material modifying factor = 0.75 for IRHD 50

     S = shape factor, which is the ratio of one loaded area of

         a single rubber layer to its unloaded faces

      = 5.625

From (3.3) compressive stiffness k_v = 12043.42 kN/m is obtained. Therefore, ratio of the compressive stiffness to shear stiffness is equal to 184. This ratio is of importance in the design of bearings as the vertical stiffness has to be many times greater than the horizontal stiffness to minimize the rocking and other unwanted modes of vibration. Corresponding ratio of the vertical and horizontal frequencies of the base isolated building will be 13.56. Photo 3.1 shows model laminated rubber bearing designed for seismic isolation for the test model. Details of the model laminated rubber bearing alongwith its attachments for connection are shown in Fig.3.1.

3.3.3 Stability-Buckling Load:

For estimation of buckling load of multilayer elastomeric bearing, number of theories were proposed by different investigators. Some of these theories are briefly discussed in connection with the calculation of buckling load of the model elastomeric isolation bearing for test structure.

Haringx(1948-49) developed a stability theory for steel helical springs and subsequently applied to the rubbers by Gent(1964). Taking into account the shear and flexural stiffness, the buckling load of the bearing is expressed as:

$$P_c = \frac{P_s}{2} \left[\left(1 + 4 \frac{P_e}{P_s} \right)^{1/2} - 1 \right] \qquad \qquad \dots (3.5)$$

where, $P_s = GA_b$, $P_e = \dfrac{\pi^2 (EI)_{eff}}{l^2}$ and $(EI)_{eff} = \dfrac{1}{3} E_c I$

    l = combined height of the elastomer layers and the steel shims

Isolation bearings are generally quite squat, with height of the bearings comparable to its lateral dimension. This leads to a reasonable

approximation for P_c given by

$$P_c = \sqrt{P_s P_e} \qquad \qquad \dots\dots(3.6)$$

In Haringx theory as extended by Gent for application to laminated elastomeric bearing restraint provided by the steel shims against lateral expansion of elastomer layer was not taken into account. Koh and Kelly (1989) defined effective shear and flexural rigidity as:

$$(GA_b)_{eff} = GA_b \frac{l}{l_r} \qquad \qquad \dots\dots(3.7)$$

where, l_r = the total thickness of all elastomer layers.

The scaling factor l/l_r is to account for the presence of the steel plates, which are assumed to be rigid as compared to the elastomer and

$$(EI)_{eff} = EI \; g'(S^2, \nu) \frac{l}{l_r} \qquad \qquad \dots\dots(3.8)$$

where, $g'(S^2, \nu)$ is a dimensionless function, ν is Poisson's ratio.

For incompressible rubber ($\nu = 0.5$)

$$g'(S^2, \nu) = 96 \; S^2 \sum_{n_r=1}^{\infty} \frac{1}{n_r^4 \, \pi^4} \left[1 - \frac{\tanh n_r \pi}{n_r \pi} \right] = 0.7425 \; S^2 \quad \dots\dots(3.9)$$

For a square shaped bearing, thus,

$$(EI)_{eff} = 2.23 \; S^2 \; r^2 (GA_b)_{eff} \qquad \qquad \dots\dots(3.10)$$

where, r = radius of gyration, n_r = number of layers.

$(GA_b)_{eff}$ and $(EI)_{eff}$ as defined above, can be used for more realistic estimate of buckling load.

Derham and Thomas(1983) proposed the following relation for estimation of buckling load of multilayer elastomeric bearing taking into account the rigidity provided by the steel shims.

$$P_c = \frac{G\, A_b h_t \left(\sqrt{1 + \pi\, a^2 r^2 / l^2} - 1 \right)}{2h} \qquad \ldots\ldots(3.11)$$

where,
$$f = \frac{6\, a^2 q}{\pi^4 h^2} + 1$$

$$q = \sum_{n_r=1}^{n_r} \frac{1}{n_r^4} \frac{a}{n_r^5 \pi b} \tanh(n_r \pi b / a)$$

where, h is the thickness of one rubber layer, h_t = h + thickness of one steel shim, a is the shorter side, b is the longer side, n_r is the numbers of layers and $l = n_r \times h_t$.

Stanton et al.(1989) carried out extensive analytical and experimental studies on the stability of laminated elastomeric bearing. They observed that buckling load of the bearing is strongly influenced by axial deformations in addition to flexural and shear deformations. Existing theories ignore the effect of axial deformation and become very conservative in predicting the buckling load. Based on analytical and experimental studies they proposed the following empirical relation for the estimation of buckling stress.

$$\sigma_{cr} = \frac{G}{\dfrac{1.92\, k_l l_r}{S \sqrt{1 + 2b/a}} - \dfrac{1.33}{S(S+2)(1+b/4a)}} \qquad \ldots\ldots(3.12)$$

where, a and b are the width and length of the bearing, k_l is the effective length factor, l_r is the total rubber thickness and S = shape factor in unloaded condition.

Buckling load of the model LRB estimated from formulae proposed by different investigators are listed in Table 3.1. As the maximum column load is 16 kN, therefore, the elastomeric isolation bearing have a high factor of safety against the buckling and a high safety factor is justified in the light of prevailing uncertainties, namely the difference between the theoretical and measured stiffnesses and difficulties inherent in characterizing the material behaviour. Further, it is also necessary to avoid rocking and vertical modes of vibration of

42

the structure.

Table 3.1 Predicted Buckling Load of Model LRB

Sl. No.	Investigator	Buckling Load (kN)
1	Gent	27.92
2	Koh and Kelly	43.88
3	Derham and Thomas	40.94
4	Stanton et al.	67.11

Thomas(1982) observed that the factor of safety against buckling of LRB is proportional to mass of the structure above, for a particular natural frequency. Therefore, design of LRB with high factor of safety against buckling is very difficult for small loads. Model LRB for seismic isolation of test structure is designed with 19 layers of elastomer to achieve high factor of safety and required frequency of isolated system simultaneously. In this process, shape of the bearing became slender, unlike that of the prototype isolation bearing.

3.4 Testing of Elastomer

3.4.1 Hardness: (as per Indian Standard IS 3400, II)   The international standard hardness test is based on measurement of the indentation of a rigid ball into the rubber specimen under specified conditions. The measured indentation is covered into International Rubber Hardness Degrees (IRHD). The scale being so chosen that zero represents a material having an elastic modulus 0 and 100 represents a material of infinite elastic modulus. A direct reading of hardness in IRHD was thereby recorded as 48 to 50 for elastomer used in the moulding of model bearing.

3.4.2. Tensile Stress-Strain Properties: (as per IS 3400, I)   In this test, test piece of dumb-bell shape has been stretched by a movable grip of tensile testing machine at a constant rate. Readings of the load and elongation were taken during the uninterrupted stretching of the test piece when it breaks. Tensile strength was calculated by dividing the load at break by initial area of cross-section of the test-piece. The elongation at break was calculated by subtracting initial distance

between reference lines on the dumb-bell test piece from the distance between the same lines at break point and expressing the result as percentage of the initial distance. Tensile strength and elongation at break were found to be 18.57 MPa and 425 % respectively.

3.4.3 Compression Set at Constant Strain: (as per IS 3400, X)   A Test piece in the shape of a cylindrical disk has been subjected to a constant strain under compression in compression device for a given time (24 hrs) and it was allowed to recover for a given time. The difference between original thickness and thickness after recovery is expressed as percentage of initially applied compression. Compression set was found to be 19.35 %.

3.4.4 Adhesion of Rubber to Metal: (as per IS 3400, XIV)   The test consists of measuring the force required to cause separation of a rubber part adhering to a metal surface. The angle of separation is 90. Before the load is applied, the rubber was stripped from the metal plate for a distance of approximately 1.5 mm by using a sharp knife. The tab so formed was placed in the grip, which is then moved at the rate of 50 mm/min until separation was complete. The maximum force required to cause separation over the distance of 25 mm was recorded. The adhesion value was expressed in N/mm of width. Adhesion value was found to be 14.91 N/mm.

Test results of elastomer testing are summarized in Table 3.2.

Table 3.2 Properties of Elastomer

Average Hardness (IRHD)	Tensile Strength (MPa)	Elongation at Break (%)	Compression Set (%)	Adhesion Strength (Mpa)
49	18.57	425	19.35	14.91

3.5 Analysis of Shear Force-Displacement Hysteresis Loops

The parameters influencing the performance of laminated rubber bearing are obtained from analysis of shear force-displacement hysteresis loops. Depending on axial load and shear strain level, the bearing stiffness has been found to be highly non-linear in some instances. It has been found that bearing undergoes a substantial change

44

of stiffness from the small strain to large strain portion of hysteresis loop. Two different shear stiffnesses have been defined for laminated rubber bearings by Aiken *et al.*(1989).

The effective (overall) stiffness of the bearing based on the values of peak force and peak displacement is defined as:

$$(K_h)_{eff} = \frac{F_{max} - F_{min}}{d_{max} - d_{min}} \qquad \dots (3.13)$$

where, F_{max}, F_{min}, d_{max}, d_{min} are the maximum and minimum values of shear force and displacement respectively.

A stiffness K_t may be defined as the slope of the tangent to the hysteresis loop at zero displacement, is expressed as:

$$K_t = \frac{F_o^+ - F_o^-}{d_o^+ - d_o^-} \qquad \dots (3.14)$$

where, d_o^+, d_o^- are the positive and negative displacement data on either side of $d = 0$ on the displacement axis and F_o^+, F_o^- are corresponding force values on the hysteresis loop. Figure 3.2 shows the definition of $(K_h)_{eff}$ and K_t.

The hysteresis loop are also analyzed to obtain the equivalent viscous damping ratio of bearings. A hysteresis loop is a plot of force against displacement, and the area contained within such a loop represents the energy dissipated by the bearing. The equivalent damping ratio of the bearings is evaluated from the following relation.

$$\zeta_{eq} = \frac{W_d}{4 \pi W_s} \qquad \dots (3.15)$$

where, W_d = dissipated energy (hysteresis loop)

W_s = Stored (elastic) energy

$$= \frac{1}{2} (K_h)_{eff} d_{max}^2$$

3.6 Static Testing of Model Laminated Rubber Bearing

The aim of the tests carried out was to assess the performance of

designed isolation bearing, which will be used for earthquake simulator testing of the test structure and therefore, tests performed were non-destructive in nature. Further, elastic properties, damping properties and stiffness of the model bearing are estimated in this section.

3.6.1 Test Set-up: The testing of model bearing was carried out in a specially designed test rig, in which it is possible to apply vertical and lateral loads simultaneously to the bearing. For studying the behaviour of the bearing under the lateral load, two bearings have been placed one above the other with a mild steel spacer plate in between them and lateral load was applied to the plate by a reversible hydraulic jack. Vertical and lateral displacements were measured by dial gauges of least count 0.01 mm.

3.6.2 Compressive Load Test: Test set-up for compressive load test is shown in Photo 3.2. Compressive load was applied gradually with an increment of 5 kN and corresponding axial deformation was measured with four dial gauges. Maximum compressive load applied was 50 kN and at this load slight lateral bulging was noticed. Compressive stress-strain behaviour of the isolation bearing subjected to vertical load is shown in Fig.3.3, which shows that compressive stress-strain characteristic of model bearing is nearly linear and therefore, it is expected that buckling load will approach the predicted critical load obtained from formula proposed by Stanton et al.(1989). Compression modulus of bearing was found to be 126 MPa from Fig.3.3.

3.6.3 Shear Test: Shear test of seismic isolation bearing is the most important of all because parameters determined in this test will govern its performance during seismic events. In this test, two bearings have been placed one above the other to facilitate application of varying reversible lateral load under constant vertical load, which simulate structural load on bearing. The test was carried out for two different vertical loads. Maximum shear strain level was restricted to 55 % because this is the predicted maximum bearing strain under earthquake input to be excited during earthquake simulator testing of the test model. Test arrangement of shear test is shown in Photos 3.3 and 3.4.

Figure 3.4 shows shear stress-strain characteristic of the isolation bearing, which is nonlinear in character and the shear modulus G decreases with increasing strain level. The value of G at 25% and 50% strain level are 0.63 MPa and 0.57 MPa respectively. Figure 3.5 shows the horizontal shear force-displacement hysteresis loops under reversible lateral load for a vertical 10 kN and 20 kN vertical loads respectively and in both the cases maximum shear strain is limited to 55%. Shear stiffness of the bearing as revealed by the test hysteresis loops is highly nonlinear. It is clear that the bearing undergoes a substantial change of stiffness from low to high strain levels. The values $(K_h)_{eff}$ and K_t for Test-1 are 93.37 and 89.26 kN/m respectively and that for Test-2 are 88.70 and 82.80 kN/m respectively. Damping ratio obtained for Test-1 and Test-2 are 0.104 and 0.137 respectively. Thus, damping ratio increases with the increase of vertical load. Test results of static testing of laminated rubber bearing are summarized in the Tables 3.3 and 3.4.

Table 3.3 Elastic Properties of the Bearing

Parameter	Maximum Strain Level (%)	Value (MPa)
Compression Modulus E_c	5	126
Shear Modulus G	25	0.63
	50	0.58

Table 3.4 Results of Shear Test

Test No.	Vert. Load (kN)	Max. Shear Strain (%)	F_{max}, F_{min} (kN)	d_{max}, d_{min} (m)	F_o^+, F_o^- (kN)	d_o^+, d_o^- (kN)	$(K_h)_{eff}$ (kN/m)	K_t (kN/m)	ζ_{eq} (%)
1	10	55	3.29 -3.90	0.040 -0.037	0.49 -1.34	0.015 -0.006	93.37	89.26	0.104
2	20	55	3.05 -3.78	0.040 -0.037	0.61 -1.46	0.018 -0.007	88.70	82.80	0.137

3.7. Concluding Remarks

In this Chapter, design procedures of laminated rubber bearing has been discussed in connection with seismic isolation of 1/6th scaled

three storeyed, two bay r.c. framed building. The formulae for estimation of buckling load of the elastomeric bearing proposed by different investigators have been studied. Testing procedure of elastomer and multilayer elastomeric bearing are described and test results are presented.

Buckling load predicted by the Haringx theory as extended by Gent(1964) are highly conservative as this theory do not take restraint provided by the steel shims into consideration. When bearing parameters are modified [Koh and Kelly(1989)] to take into consideration the restraint provided by the steel shims, results predicted by this theory improved noticeably. Formula proposed by Derham and Thomas(1983) estimates critical load nearly equal to that obtained by using modified bearing parameters in Haringx formula. But the buckling load predicted by the formula proposed by Stanton et al.(1989) gives much higher value of buckling load because they have taken the effect of axial deformations in addition to restraint provided by the steel shims.

Shear modulus assumed in the design of elastomeric bearing is very close to that obtained from the test results, but the horizontal stiffness of the bearing calculated from the shear formula differs from that obtained from the test results by nearly 20 %. This is due to the fact that the contribution of side covers to the shear stiffness was not taken into account. Shear modulus and lateral stiffness decreases with increasing strain level and increasing vertical load. Damping provided by the model laminated rubber bearing increases with increasing vertical load.

2nos x 5th x 80sq. SS Plate

6   6

5

8

152   12

4

22

25   5

8th x 90 x 90 LG
MS Plate

18 nos x 2 th x 90 x 90 LG
MS Plate

19 nos x 4 th Internal
elastomer layer

Ø 25 dia x 2 th MS Plate

M 24 Hex screw
x 30 LG

25 th x 120 x 200 LG
MS Plate

102

4 nos Ø 22 dia
Holes for M 20
Bolts

120   60 C/C   102

140 C/C

200
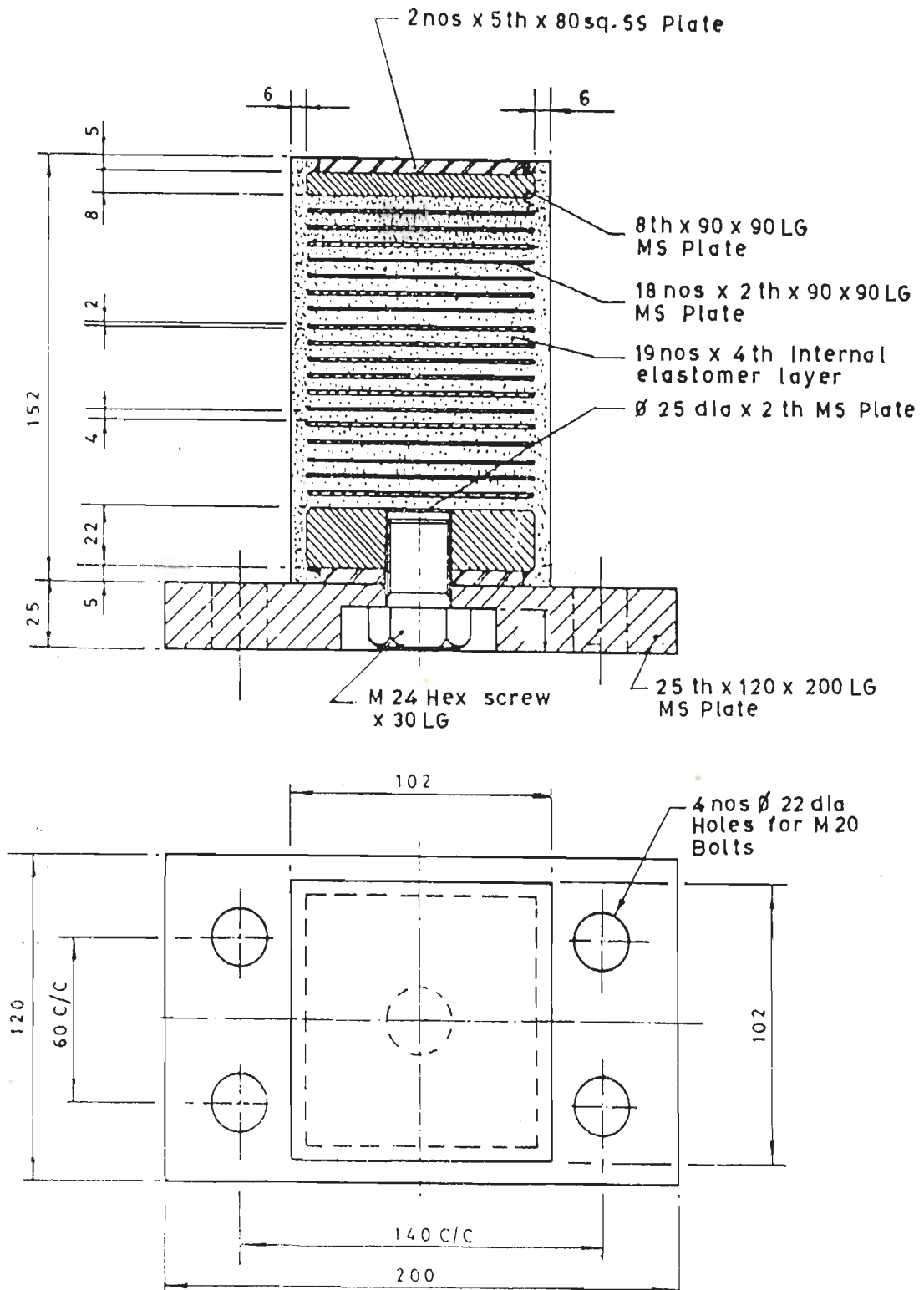
Fig.3.1 Details of Laminated Rubber Bearing Model

49
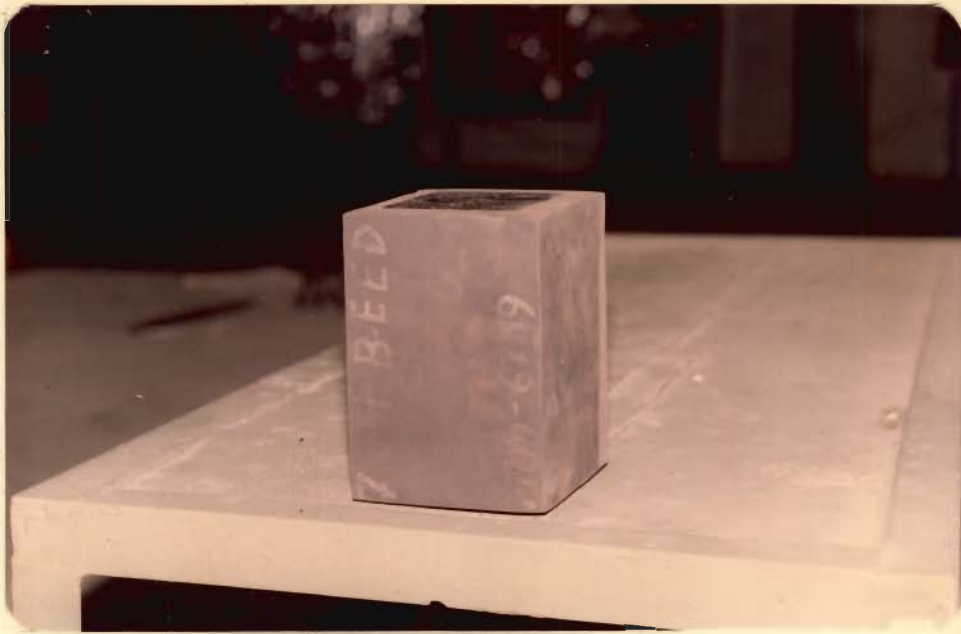
Photo 3.1 : A model of Laminated Rubber Bearing

Photo 3.2 : Test Set-up for Compressive Load Test
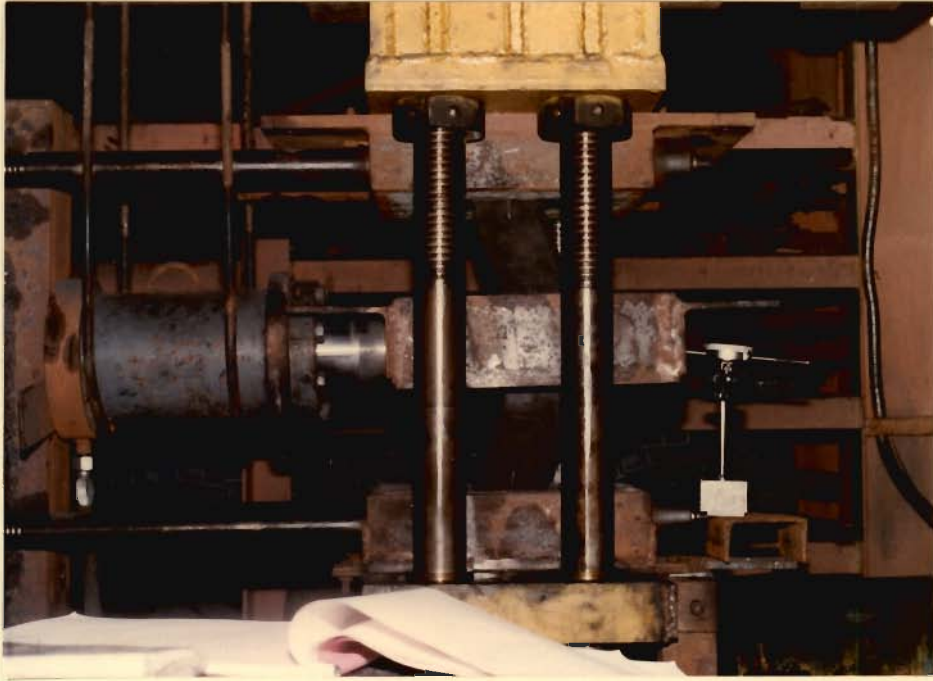
Photo 3.3 : Test Set-up for Shear Test - Front View

Photo 3.4 : Test Set-up for Shear Test - Side View
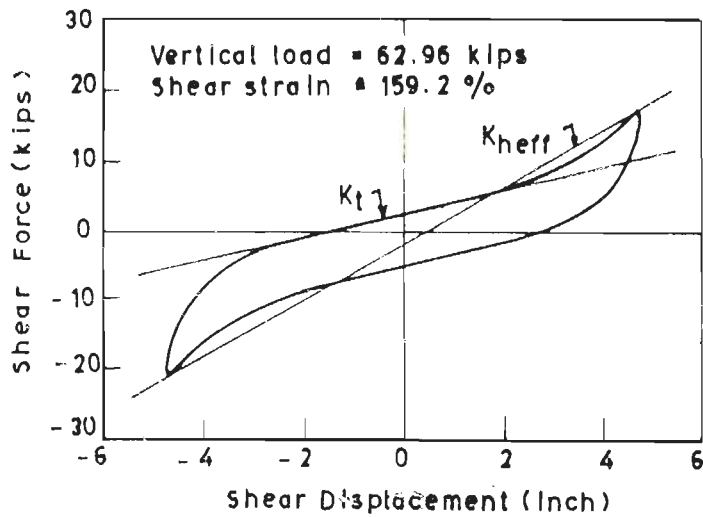
Fig.3.2 Typical Shear Force-Displacement Hysteresis Loops
[Aiken et al.(1989)]
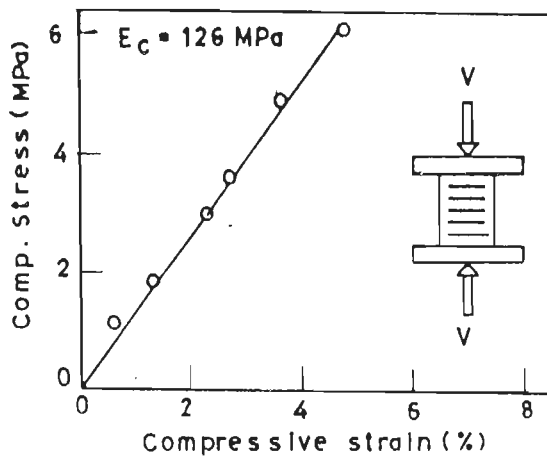
Fig.3.3 Compressive Stress-Strain Characteristic
of LRB Model
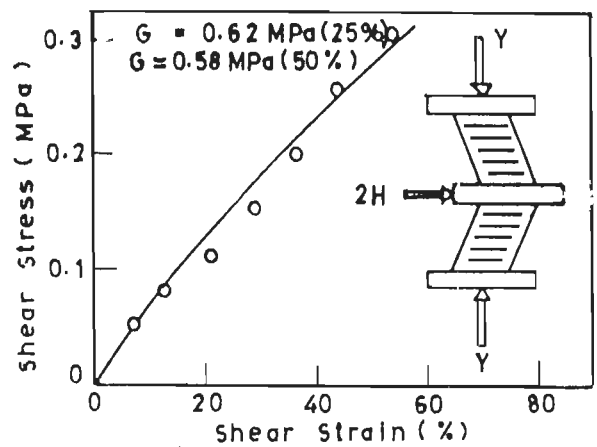
Fig.3.4 Shear Stress-Strain Characteristic
of LRB Model
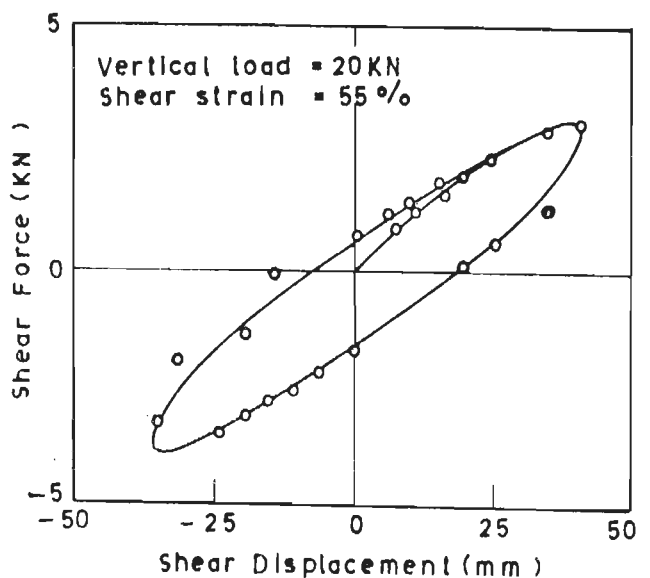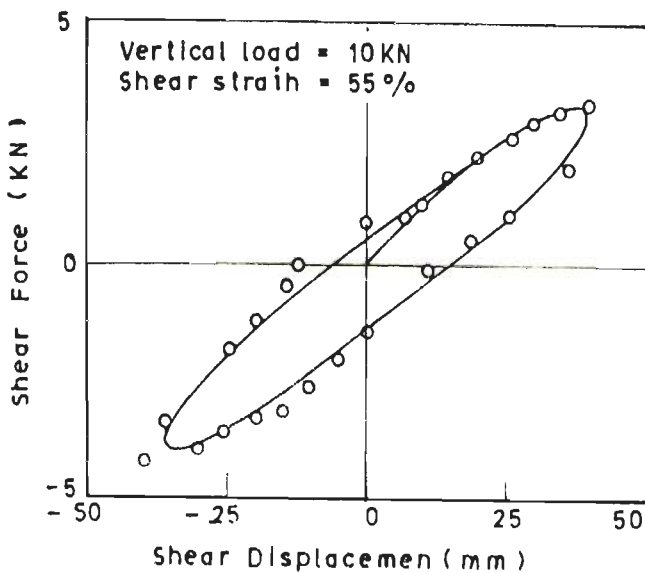
Fig.3.5 Shear Force-Displacement Hysteresis Loop

52

CHAPTER-4

SHAKE TABLE TESTING OF BASE ISOLATED TEST MODEL

4.1 Introduction

This chapter describes the tests performed on 1/6th scaled three storeyed r.c. test model supported over LRB isolation system. The earthquake simulator facilities and control system are described briefly. The instrumentation of the test model is detailed. The simulated earthquake motions and the measured response of the model are presented. This Chapter concludes with analysis and discussion of the experimental results.

4.2 Details of the Test Structure

4.2.1 Similitude and Scaling: A scale factor of 1:6 has been considered for the present experimental investigation considering the size of the available shake table (3.5 m x 3.5 m) and its load carrying capacity. Scaling is performed to satisfy geometrical and gravity load simulation requirements. Additional concrete blocks are placed on the model to simulate the gravity load so as to have almost same stress level in the columns of the model as that of the prototype. The total weight of test model is 11 kN while the additional load provided for gravity load simulation is 52 kN. The scaling relationships for gravity load similitude are presented in the Table-4.1.

4.2.2 Construction and Connection Details: A three storey two bay reinforced concrete framed model is constructed for the experiment. Photos 4.1 and 4.2 show two stages of construction of the test model. Material used for fabrication of test model are M20 grade of concrete and Fe250 steel reinforcement. The dimensions of elements of the test model are obtained by geometrical scaling of the corresponding elements

of the prototype, which are designed for Zone-V as per seismic zoning

Table-4.1 Seismic Scaling Relationships

| Parameter | Scaling | Protype |
		1/6 - scale model
length	s	6
mass	s^2	36
displacement	s	6
acceleration	1	1
stress	1	1
strain	1	1
force	s^2	36
area	s^2	36
time	$\sqrt{s}$	2.45

map of India. The design of the model elements are also checked for the handling stresses due to shifting the test structure from the place of construction to the shake table.

The storey height of the model is 0.67 m. The total height of the test model is 2.38 m. The basement slab has a plan area of 2.30 m x 1.30 m and the other floors and roof have a plan area of 2.07 m x 1.07 m. Figure 4.1 shows the plan and elevation of the model. The basement beam are designed as inverted T-beam to provide necessary bearing area for the isolation bearings. Basement, floor and roof slabs of thickness of 30 mm, beams of size 70 mm x 100 mm and columns of size 70 mm x 70 mm are provided. Details of reinforcements are provided in the Fig.4.2. Hooks of 12 ϕ m.s. bars with appropriate development lengths are provided for lifting of the model.

A steel plate of size 200 mm x 200 mm and 2 mm thick has been attached to the basement slab directly below each column. The model is simply resting over the isolation bearings with only frictional contact between the stainless steel topping of the bearings and steel plates below each of the columns. There is no possibility of slip at the interface in general, because of high coefficient of friction. Development of tension in the isolation bearing is prevented by this arrangement in case of slight uplift of the basement slab from bearings due to the rocking mode of vibration.

A mild steel base plate of size 2.55 m X 1.35 m and 8 mm thick, stiffened by grids of ISMC 100 channels is fabricated for shifting model structure to the Shake Table and to facilitate necessary connections between isolated structure and the Shake Table. During fabrication of base plate necessary restraints are provided to prevent bending of the base plate due to welding works. Photo 4.3 shows the arrangement for shifting of the test structure and placing it on the Shake Table.

Isolation bearings are connected to base plate, which in turn is connected to the shake table firmly by high tension bolts as shown in the Fig.4.3. Connection detail of additional loads for gravity load simulation and slab panels is shown in Fig.4.4.

4.3 Earthquake Simulator Facilities and Control System

A digitally controlled shake table facility capable of reproducing specified real earthquake accelerogram or simulating synthetic accelerogram compatible with a specified design spectra for testing structures is available in the Department of Earthquake Engineering, University of Roorkee. The driving mechanism of the table is of servo-hydraulic type. The size of the table is 3.5 m x 3.5 m. This table can give motion in a plane containing vertical and one horizontal direction. The table is driven by three actuators, two vertical and one horizontal. A square grid pattern of bushes of special alloy steel is provided at 400 mm c/c on the top plate of the shake table platform for mounting model/prototype on the table. This shake table can support a pay load of 200 kN. The zero-period acceleration (ZPA) can be upto 3g depending on payload.

The digital control of table is done by Micro PDP 11/23 computer. It contains 2 digital to analog converters (DAC) and 16 analog to digital converters (ADC) to monitor the motion of the table and the test structure. Photo 4.4 shows the control panel and data acquisition system. The table is controlled by monitoring the desired acceleration in a closed loop system by the computer.

4.4 Free Vibration Test

Free vibration tests of the isolated structure have been carried

out to determine its dynamic characteristics. Free vibration tests have been performed after placing it on the Shake Table. The Shake Table was inactive during free vibration tests, with motion prevented by locking it against the surrounding foundation. Static lateral load was then applied to the structure to the predetermined level. Once the required lateral load was applied, the free vibration in the structure was initiated by suddenly releasing the load. Photo 4.5 shows the arrangement of a free vibration test. This procedure was undertaken with the load applied at first floor level. Practical constraints prevented pulling the model from higher levels, nonetheless, it was hoped that by pulling at this level, free vibration response would be induced in atleast first two modes of the model.

The entire structure was pulled back for a base displacement of 7.5 mm, which corresponds to a shear strain of 10%, approximately, and then released. Absolute roof acceleration of the test structure was recorded by a Force Balance Accelerometer. Using the successive acceleration peaks, a_n and a_{n+1} in the recorded roof acceleration response history damping (ζ_b) available in the isolation system can be estimated from the following formula.

$$\zeta_b = \frac{1}{2\pi} \ln \frac{a_n}{a_{n+1}} \qquad \ldots \ldots (4.1)$$

The fundamental frequency of vibration is obtained from Fourier amplitude spectra of the roof acceleration. The estimation of damping and fundamental frequency from the free vibration record are given Section 4.6.

4.5 Shake Table Test

Shake Table testing of base isolated model subjected to unidirectional simulated earthquake motions has been carried out to study the effectiveness experimentally of the isolation system designed in the present study in controlling the overall response of the isolated structure. In the following sections, details of simulation of earthquake excitations, instrumentation of the test model and filtering of the acquired signals have been presented.

56

4.5.1 Simulated Earthquake Motion: A time scaled average spectra (Fig.4.5) representative of alluvial soil [Moharz(1976)] is selected for synthesizing earthquake motion for Shake Table testing of base isolated model. A spectrum compatible motion simulated on the Shake Table platform by multifrequency waves using random vibration theory [Kimura and Izumi(1989)] as required response spectra (RRS) is broadband. A record of 20.48 sec is generated with a rise and decay time of 2 sec each having 100 samples/sec. The spectrum compatible motion is generated by an iterative procedure using a software. An amplitude modulated random signal with the specified rise and decay time is obtained initially as drive signal. This drive signal is given as the input to the shake table and response of the table is recorded from the accelerometers fixed on the table. These accelerometers are connected with antialiasing filter with a cutoff frequency of 33 Hz. The filtered signal is then are sampled by sample and hold circuit. These sampled data are quantified by the analog to digital converter (ADC) and recorded in the memory of the computer. Thus recorded motion have a bandwidth of 33 Hz. The test response spectra (TRS) is computed from the recorded table motion. TRS is compared with RRS and any deficiencies and excesses in the TRS are removed by suitably adjusting the drive signal from the acquired table motion data. The adjusted drive signal is again used as input to the Shake Table and the entire steps of readjustment of drive signal as described above is performed till a good match between TRS and RRS is obtained. The drive signal thus generated is essentially a voltage waveform which is to be given as input to the servo valve for controlling the flow of servo oil in the pressure side of double acting actuators. Various level of zero period acceleration (ZPA) are obtained by changing gain of the stored voltage waveform generated by the iterative method to produce a spectrum compatible table motion. Thus as the gain increases an almost similar table acceleration history is created except for the possible feedback from the table and model interaction. The gain of voltage waveform in Test runs 1, 2 and 3 are 1.5, 2 and 5 respectively.

Figures 4.6 and 4.7 show the measured table acceleration histories alongwith their respective Fourier amplitude spectra for Test runs - 1 and 2 respectively. The peak table acceleration for Test runs - 1 and 2 are recorded as 0.18g and 0.23g respectively. Frequency components of both the accelerograms are in the same range, between 0 to 16 Hz, as

these are simulated from the same spectra. The table acceleration history of the Test run - 3 is not recorded due to malfunctioning of the particular channel acquiring the response. The peak table acceleration of the Test run - 3 is estimated to be of the order of 0.55g to 0.60g, because the gain of voltage waveform in this test run is 2.5 times higher than that of the Test run - 2 and also the frequency contents of the accelerogram expected to be almost same as that of the Test runs - 1 and 2.

4.5.2 Instrumentation:

The test model has been instrumented with Force Balance Accelerometers (FBAs) to record the response of the structure to all input excitations. A total of 6 channels of data have been acquired to record the model response. One accelerometer was placed at each floor level of three storeyed model and one accelerometer was placed at the basement floor to measure the horizontal acceleration. The calibrations of the accelerometers are performed prior to the testing. The calibration factor used by the data acquisition system through out the test is conservative i.e. the measured acceleration is always on the lower side of the acceleration produced. The setting of antialiasing filters are 50 Hz for free vibration testing and 33 Hz for the earthquake type excitation.

4.5.3 Filtering of Acquired Signal:

All data have been passed through signal conditioners that removed all frequency components of the signals above 33 Hz at the time of data acquisition. Subsequent filtering during data reduction used Butterworth low pass filter of the order - 6 [Lam(1979)] to remove all frequency components above 16 Hz. This cut-off frequency was chosen for the following two reasons - (i) the first three modes of vibration of the test model was contained below 16 Hz, and (ii) Fourier amplitude spectra of test signals were small above 16 Hz.

Photos 4.6 shows the arrangements of shake table testing of the base isolated test model.

4.6 Results and Discussion

In this section, measured response of a isolated three storeyed r.c. framed test model obtained from free vibration test and shake table

tests for three unidirectional simulated earthquake motions are presented. Fourier amplitude spectra of absolute roof acceleration histories of three test runs and amplitude envelops and linear acceleration response spectra of measured table acceleration for Test runs 1 and 2 are also plotted for analysis of the test results.

Figure 4.8(a) shows the absolute roof acceleration history recorded during free vibration test. The ripples around the amplitudes of the record indicate the presence of rocking mode of vibration. The slender shape of the bearing is responsible for this phenomenon. Damping calculated from the logarithmic decrement of acceleration history is found to be 8.50 % of critical damping. This damping value corresponds to very low level of strain and it is expected that damping will increase for high level of strain during Shake Table Tests. Figure 4.8(b) shows the Fourier amplitude plot of roof acceleration. The fundamental frequency and the second mode frequency of the isolated model are found to be 1.75 Hz and 6.3 Hz respectively, have been indicated in this figure.

Figures 4.9 to 4.11 show the absolute acceleration response histories at the each floor levels and base for the three test runs. Figure 4.12 shows the Fourier amplitude spectra of the absolute roof acceleration of the isolated test model. Comparison of Fig.4.6(b) with 4.12(a) and Fig.4.7(b) with 4.12(b) show that the high frequency components of the table acceleration histories of the Test runs -1 and 2 have been filtered out by model LRB and it essentially, behaves as a low pass filter. In the three test runs, the fundamental frequency of the isolated system is found to be same with a value of 1.51 Hz and this value is much lower than that indicated by free vibration test. This may be due to the non-linear behaviour of the LRB model. There was also no damage in the model bearing or superstructure during high level of table acceleration (peak of the order of 0.55g). In the Test run - 3 residual slip of the order of 5 mm has been observed between top plates of the bearings and steel plates provided below each column.

Figures 4.13(a) and (b) show the linear acceleration response spectra calculated from measured table acceleration of the Test run 1 and 2 using 8.5% damping provided by the model bearing. The measured peak roof acceleration is also shown on the spectra with the time

periods of the isolated test structure. It is observed that measured maximum values are underestimated by linear spectra by approximately 15%. The higher experimental values may be attributed to slight uplift of the structure from bearings due to rocking and non-linear behaviour of the isolation system.

Figures 4.14(a) and (b) show the amplification envelops for the Test runs 1 and 2. The amplification envelops are plots of maximum horizontal storey acceleration for each level divided by the maximum horizontal table acceleration versus the storey height. All the peak storey acceleration values used for these plots did not necessarily all occur at the same time. Amplification factor for the Test runs 1 and 2 are found to be 0.52 and 0.54 respectively as shown in Figs. 4.12(a) and (b) and this shows the effectiveness of the model isolation system in controlling the level of response transmitted to the test structure.

4.7 Concluding Remarks

In this chapter, the response of a three storeyed r.c. framed test model isolated by model laminated rubber bearing, recorded during free vibration test and shake table test are analyzed. On the basis of this study following conclusions are drawn:

o   High frequency components of table acceleration are effectively filtered out by model LRB, which behaves as a low pass filter.

o   The behaviour of the model LRB is essentially non-linear in nature with high stiffness at low strain level.

o   Rocking mode contribution is present in the response of the isolated structure, because of slender shape of the model LRB.

o   No damage have been observed in the model bearing or superstructure, although small amount of residual slip has been noticed in the interface between top plates of the bearings and steel plates provided below each column.

o   Model LRB, designed in this study, is found to control the motion transmitted to the test model effectively.

Photo 4.1 : Construction of the Test Structure - Stage I

Photo 4.2 : Construction of the Test Structure - Stage II

Photo 4.3 : Placing of the Test Structure on the
Shake Table
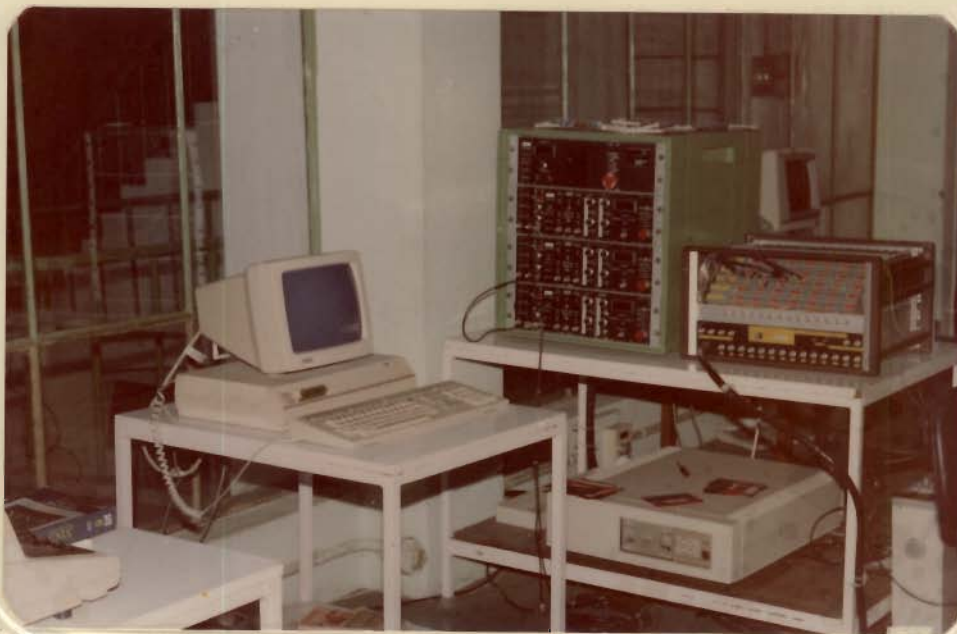
Photo 4.4 : Control Panel and Data Acquisition System
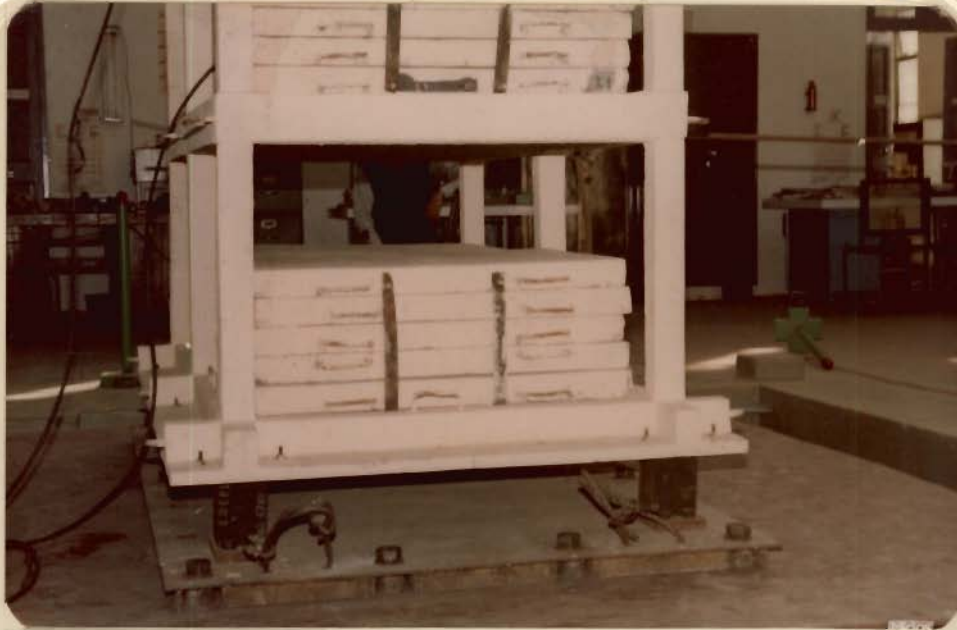
Photo 4.5 : Free Vibration Testing of the Test Structure

Photo 4.6 : Arrangement for Shake Table Test
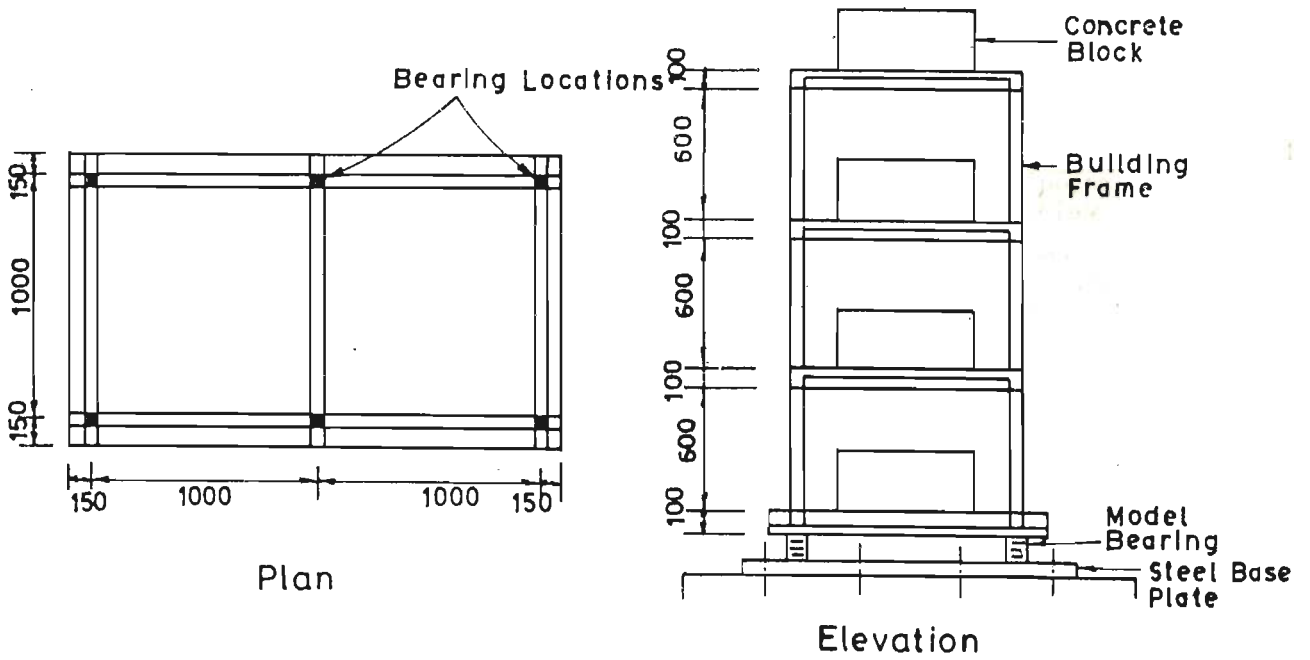
Fig.4.1 Plan and Elevation of Test Model
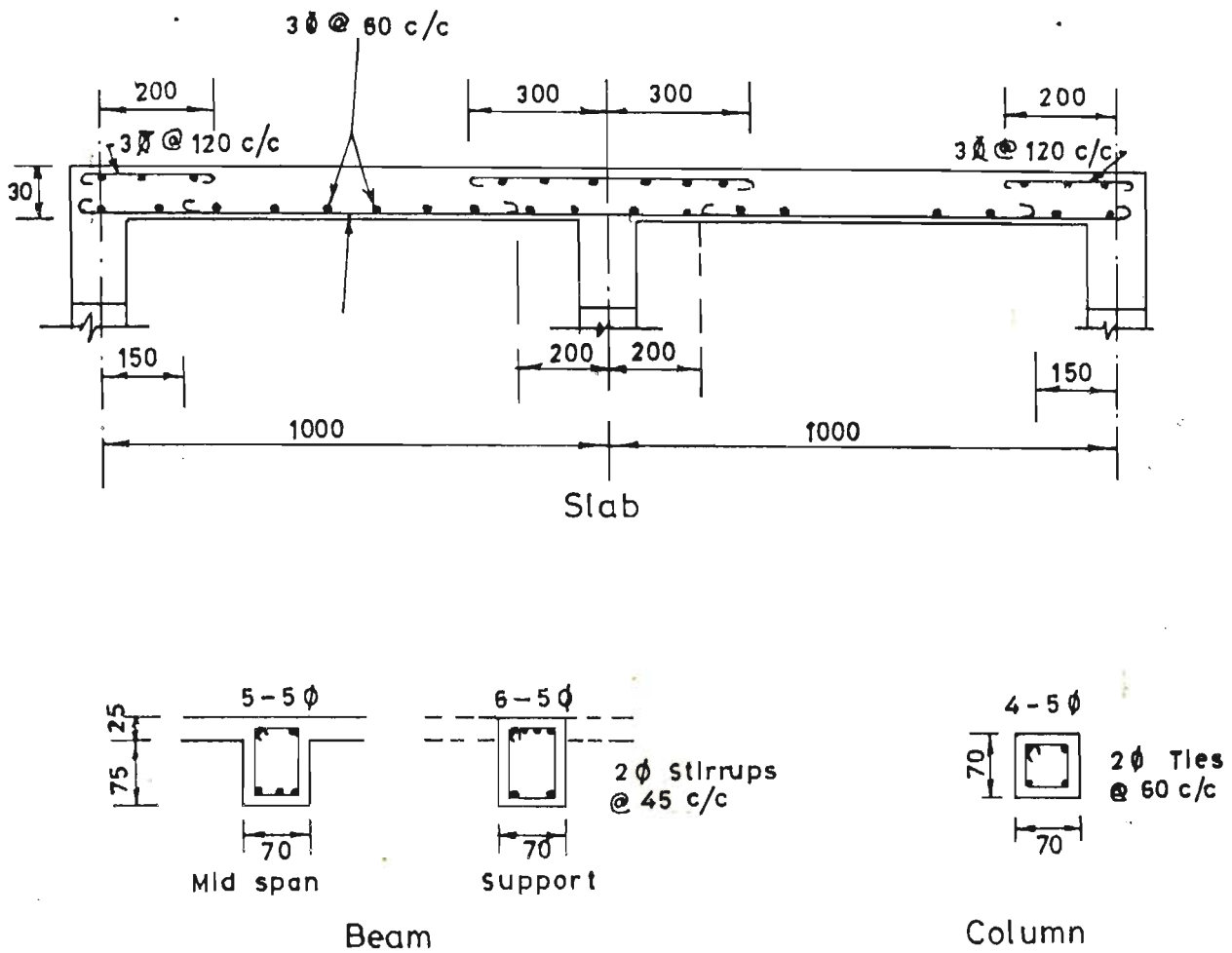
Fig.4.2 Details of Reinforcement
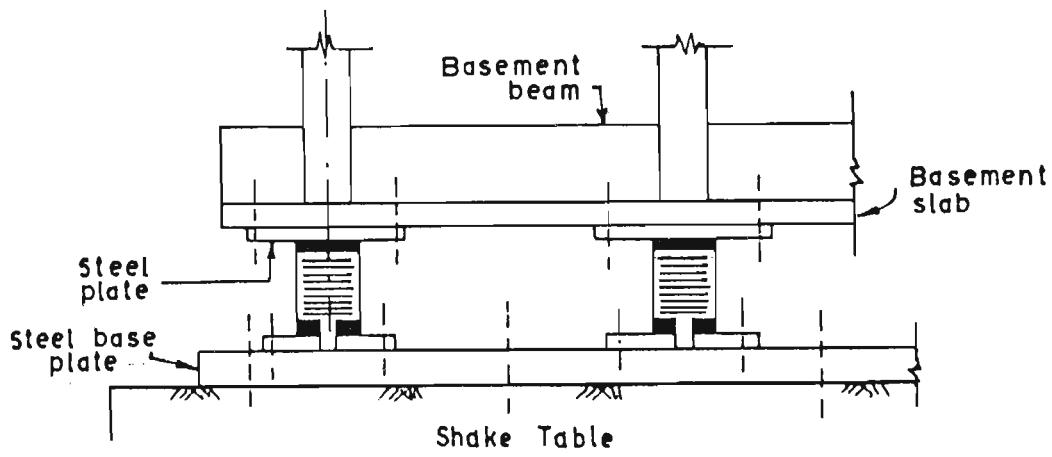
Fig.4.3 Connection Details of Isolation Bearing
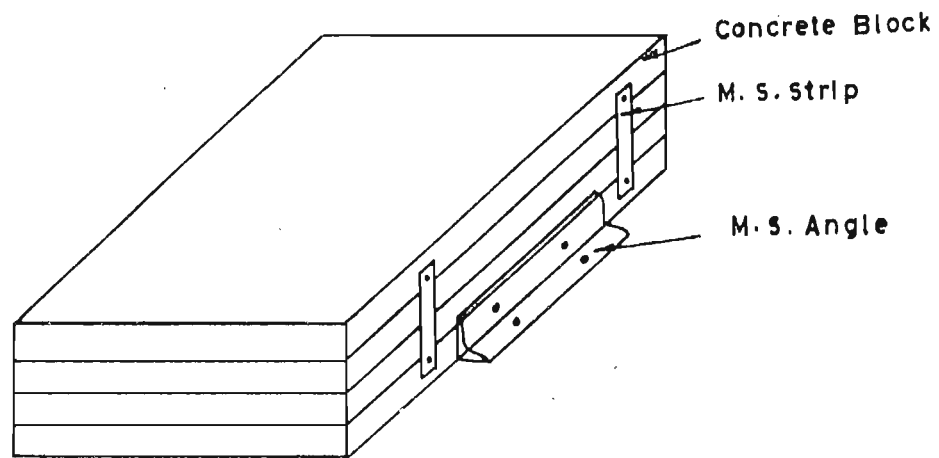
Fig.4.4 Connection Details of Concrete Blocks with Slab
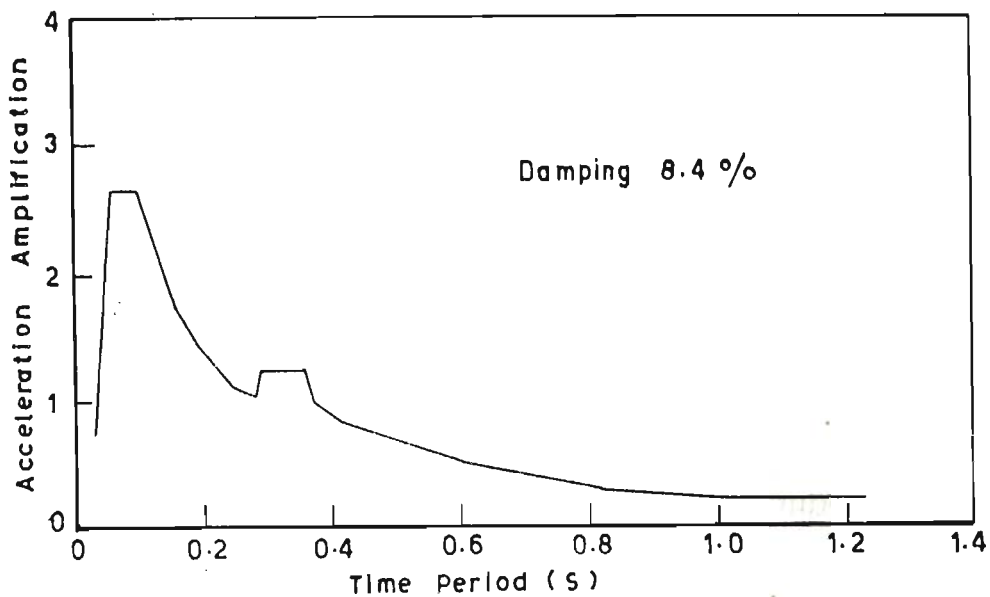
Fig.4.5 Time Scaled Average Spectra for Alluvial Soil
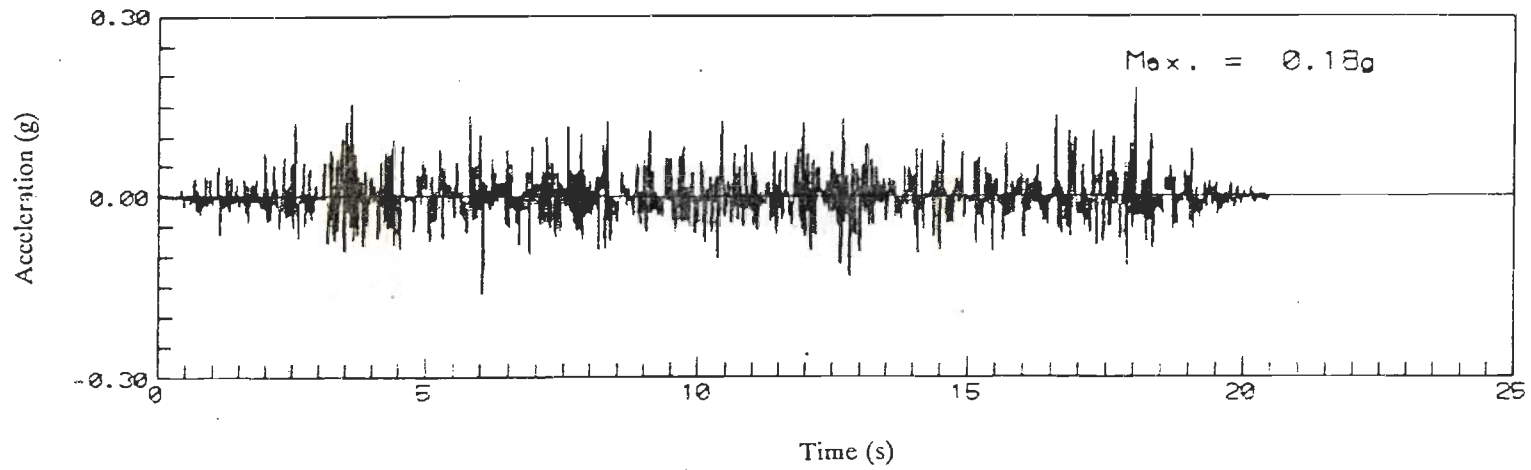
(a) Table Acceleration History
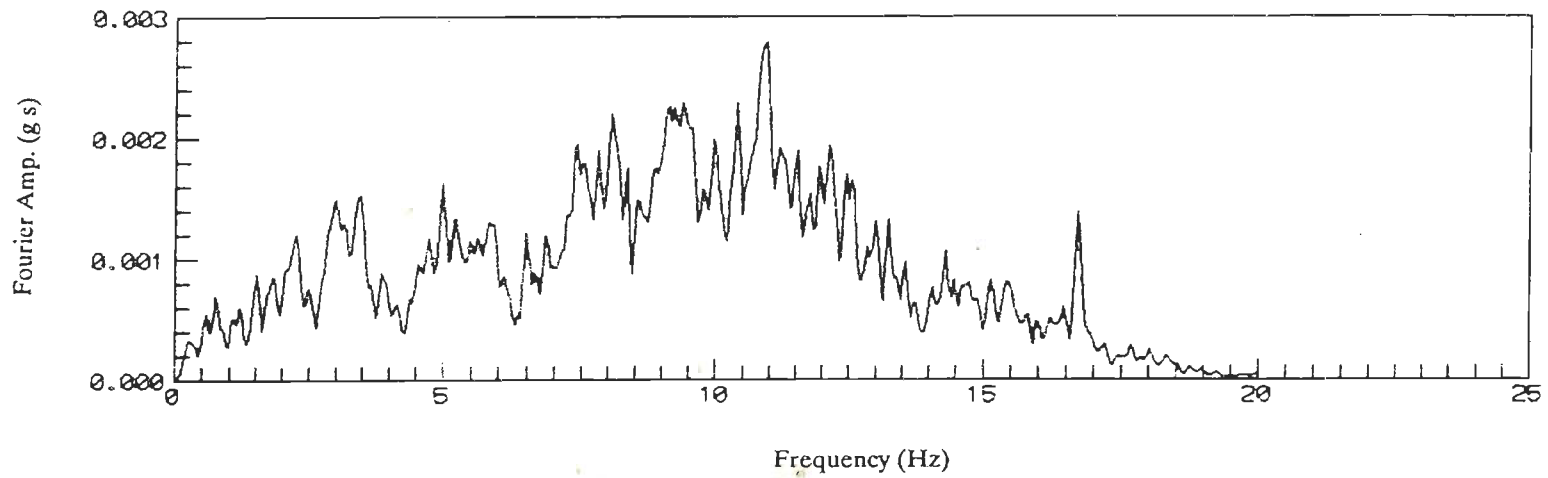
(b) Fourier Amplitude Spectra of Table Acceleration

Fig.4.6 Input Excitation Characteristics of Test Run-1

Max. = 0.23g

Acceleration (g)

0.30

0.00

-0.30

0   5   10   15   20   25

Time (s)

(a) Table Acceleration History

Fourier Amp. (g s)

0.003

0.002

0.001

0.000

0   5   10   15   20   25

Frequency (Hz)
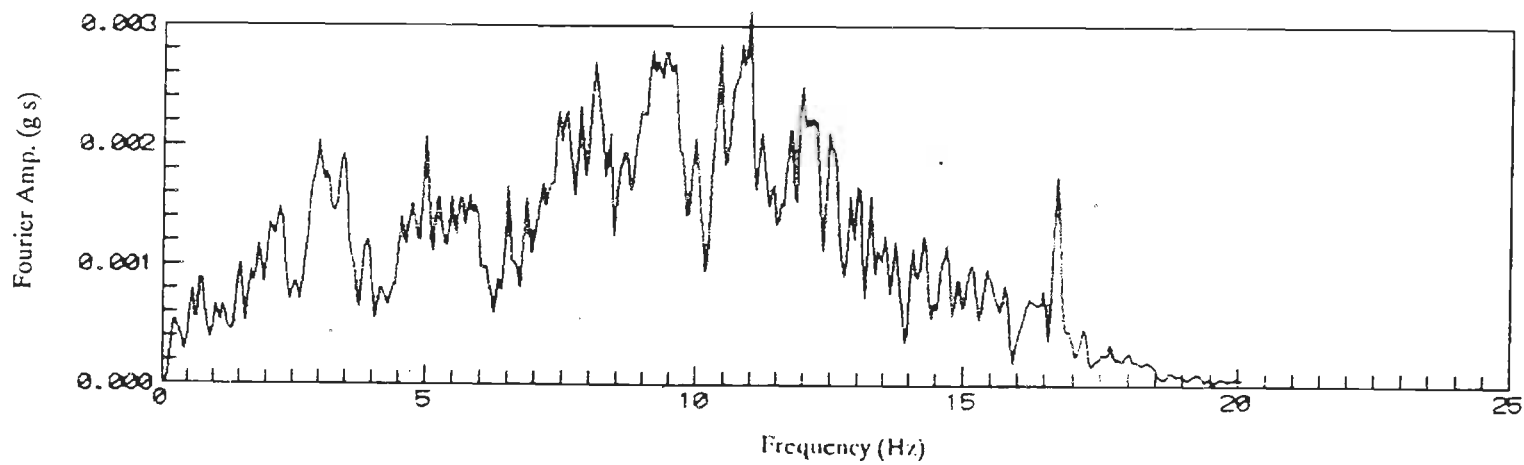
(b) Fourier Amplitude Spectra of Table Acceleration

Fig.4.7 Input Excitation Characteristics of Test Run-2
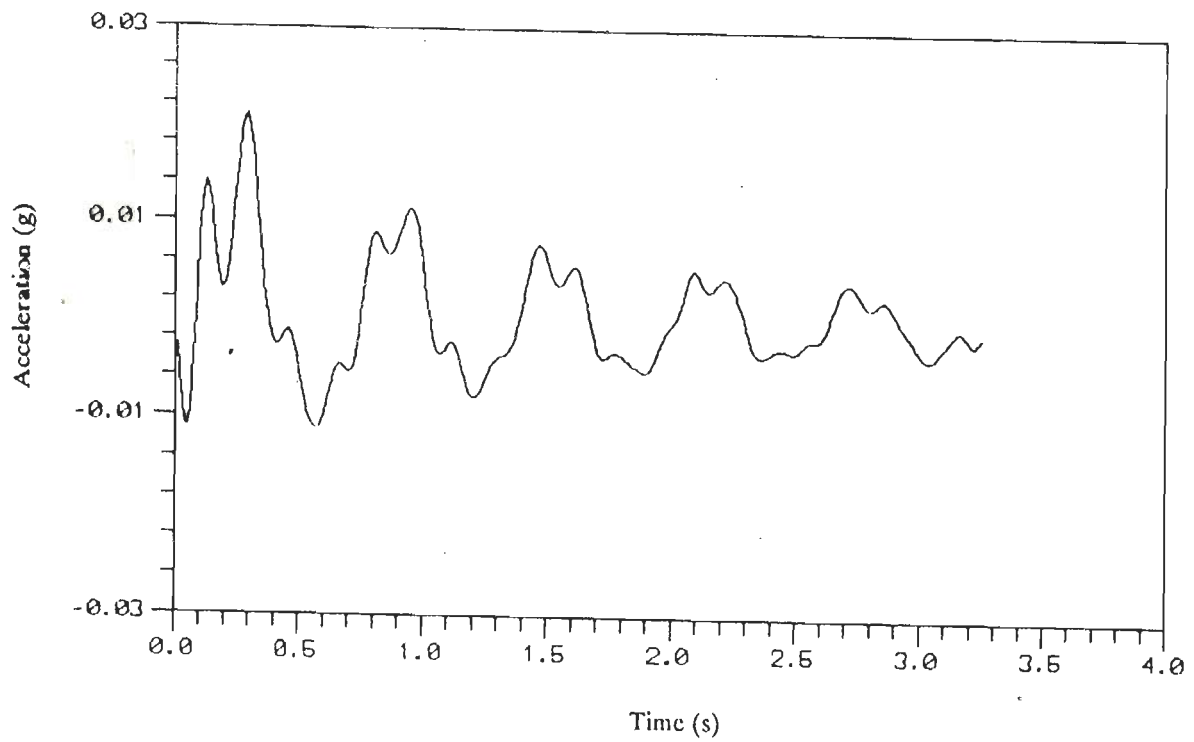
(a) Absolute Roof Acceleration Time History
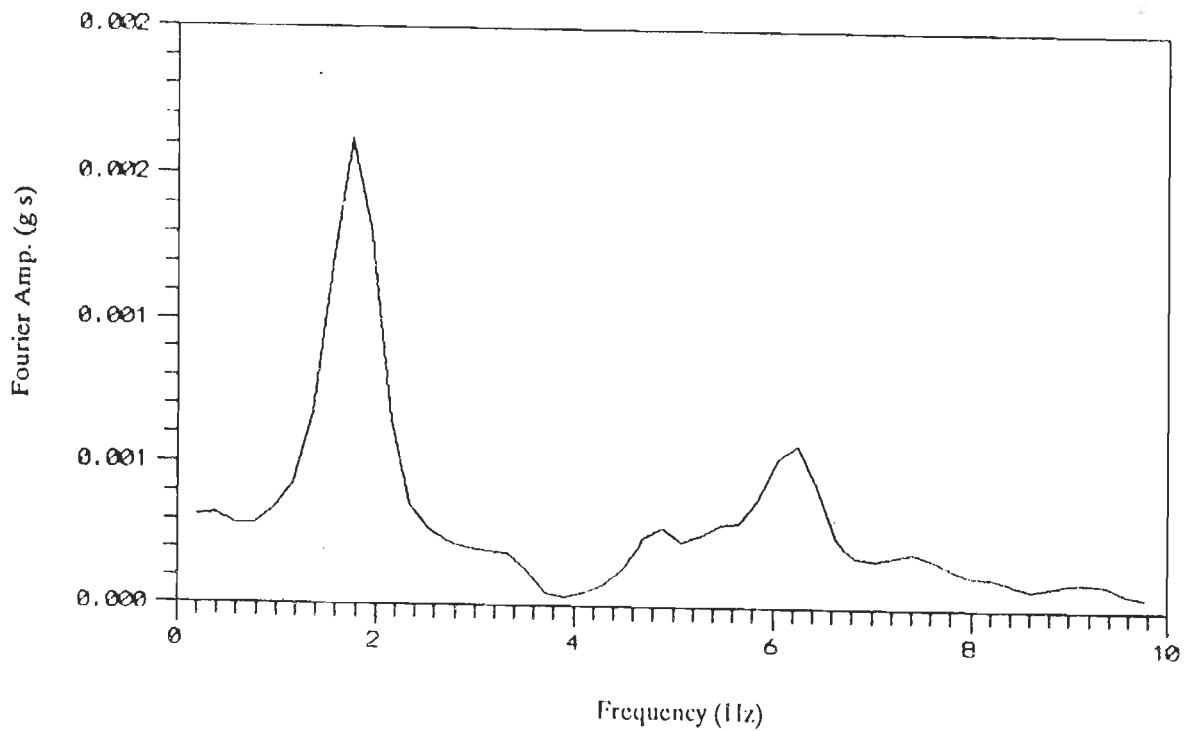
(b) Fourier Amplitude Spectra of Roof Acceleration

Fig.4.8 Measured Response of Free Vibration Test
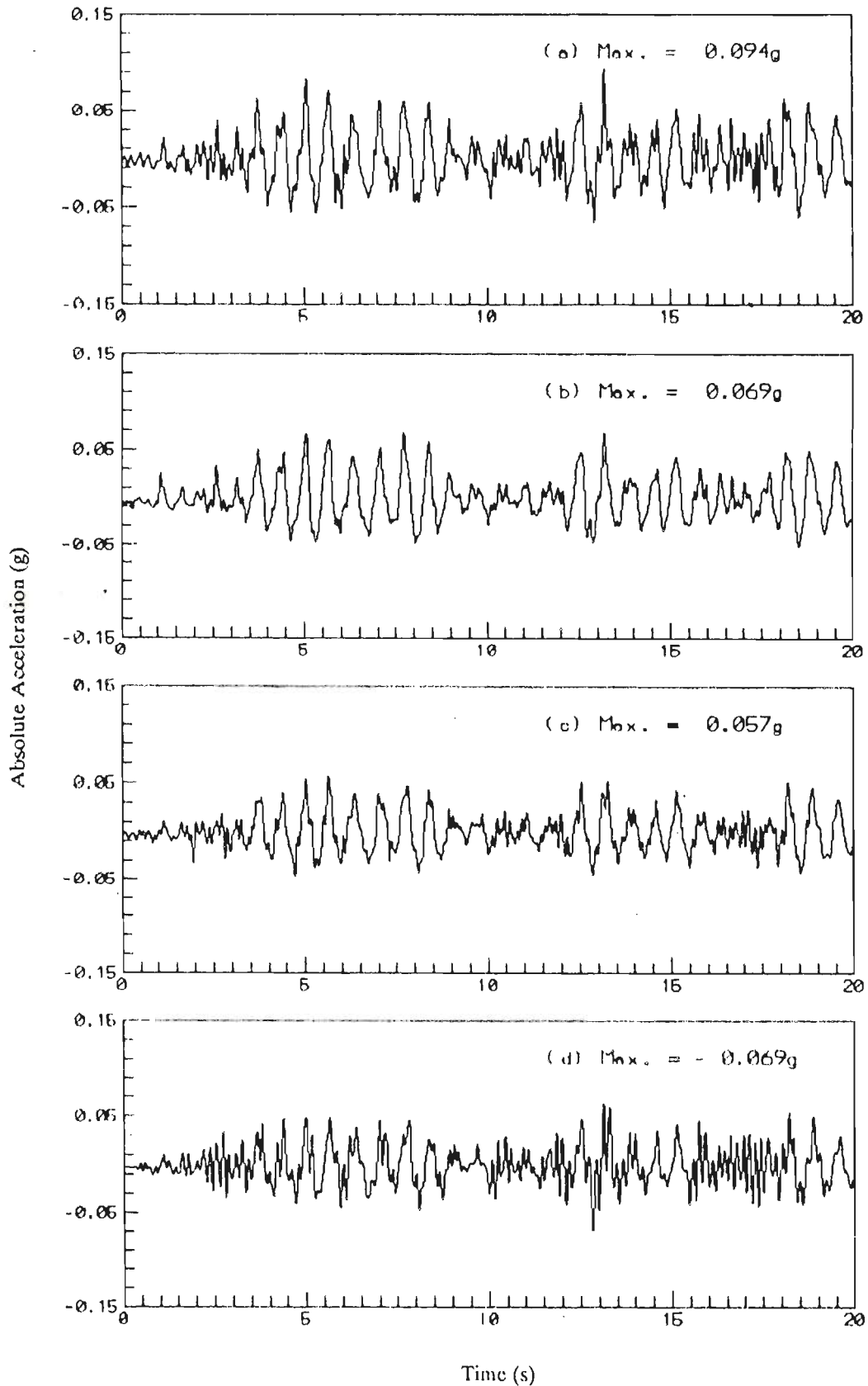
Fig.4.9 Measured Absolute Acceleration Histories of Test
Model in Test Run-1: (a) Roof, (b) Second floor,
(c) First floor and (d) Basement Level
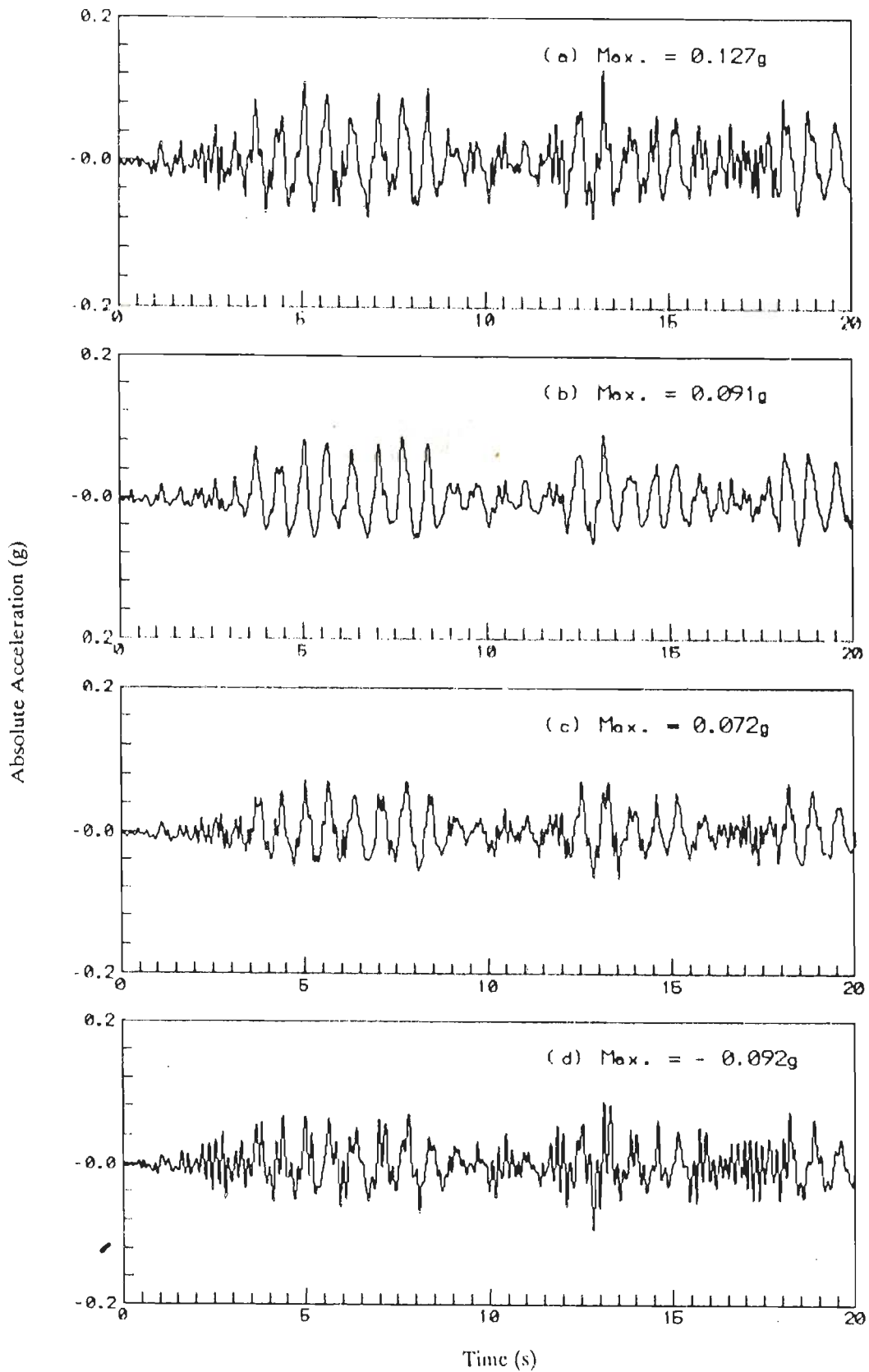
Fig.4.10 Measured Absolute Acceleration Histories of Test
Model in Test Run-2: (a) Roof, (b) Second floor,
(c) First floor and (d) Basement Level

70
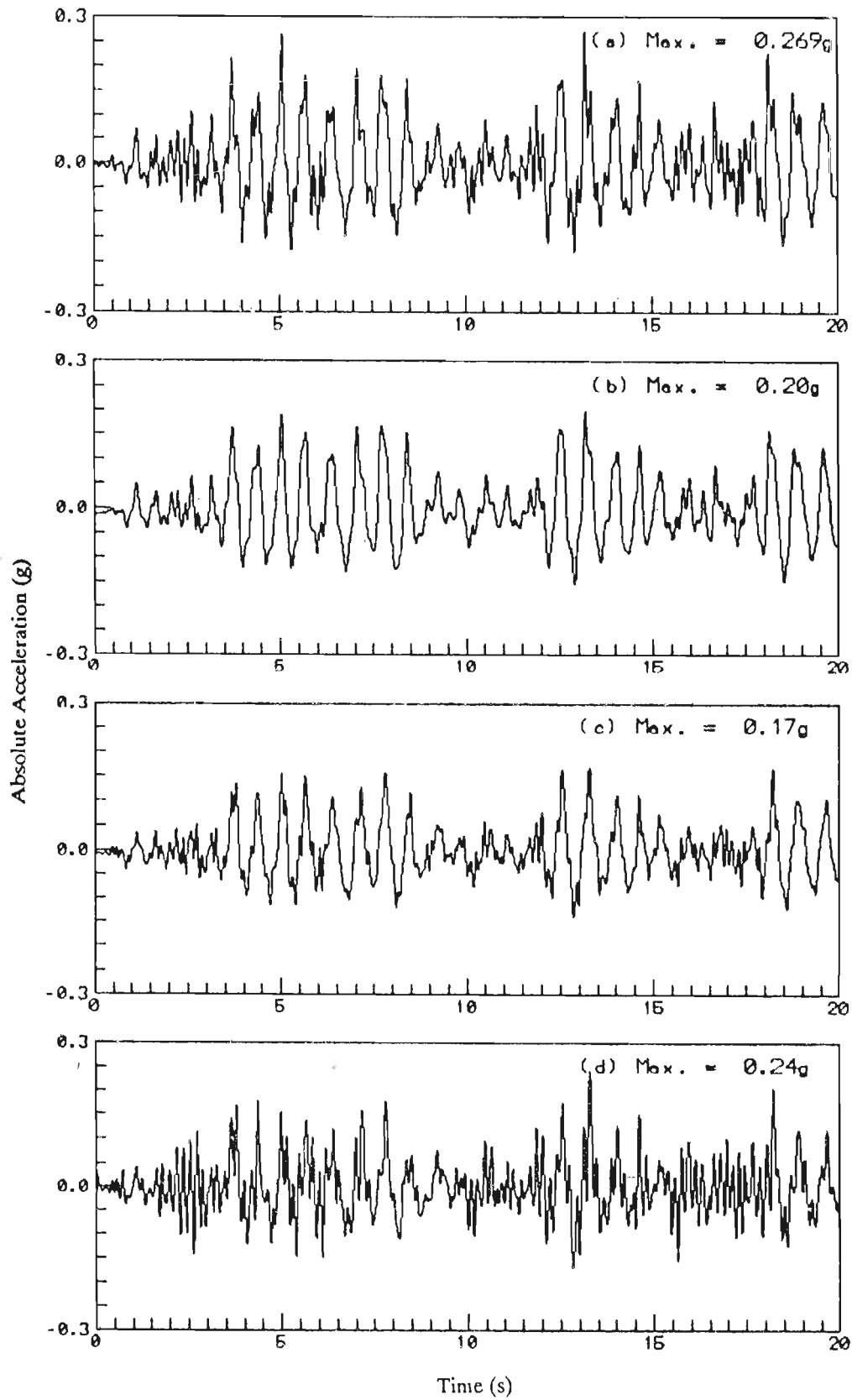
Fig.4.11 Measured Absolute Acceleration Histories of Test
Model in Test Run-3: (a) Roof, (b) Second floor,
(c) First floor and (d) Basement Level

71
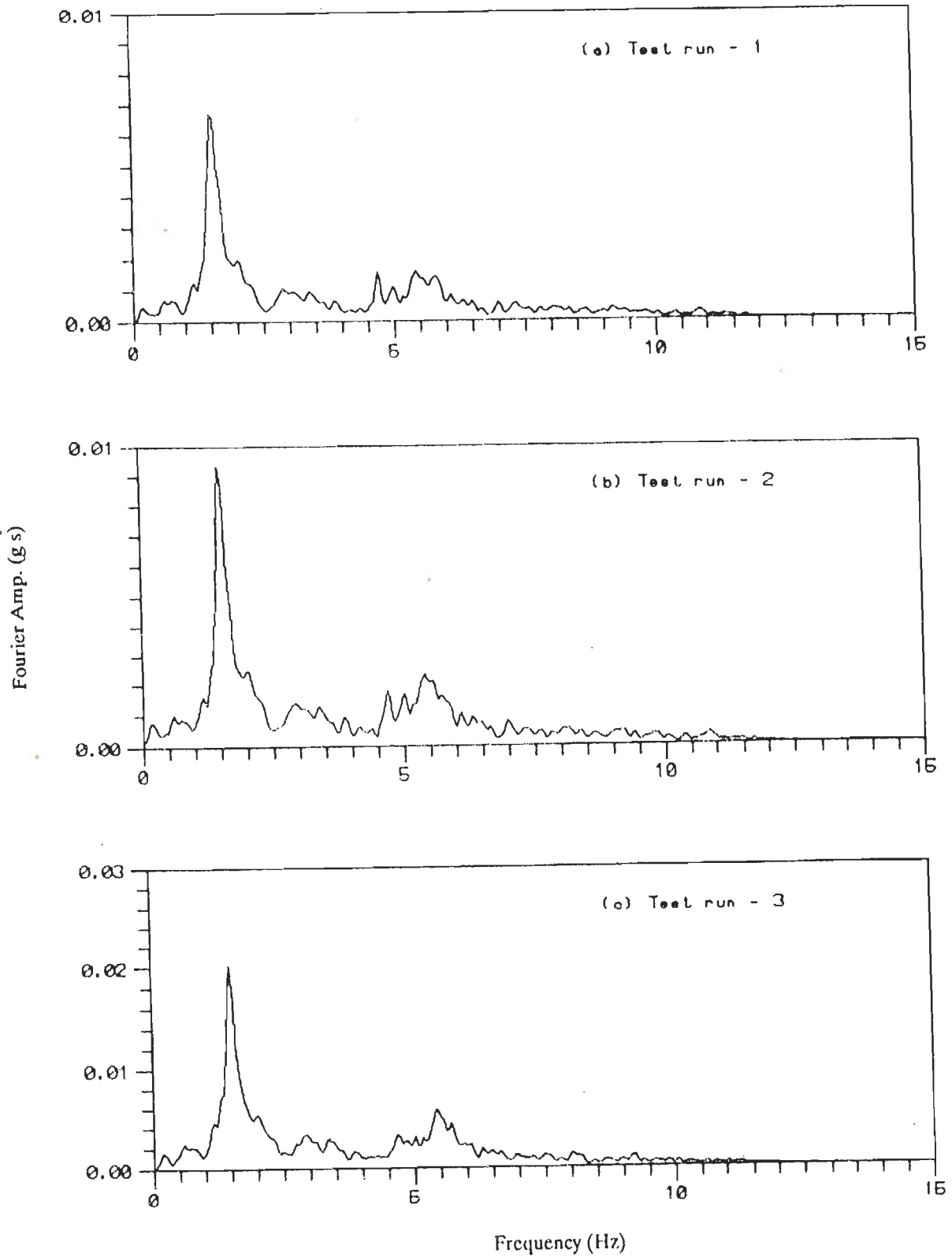
Fig.4.12 Fourier Amplitude Spectra of Roof Acceleration:
(a) Test Run-1, (b) Test Run-2 and (c) Test Run-3
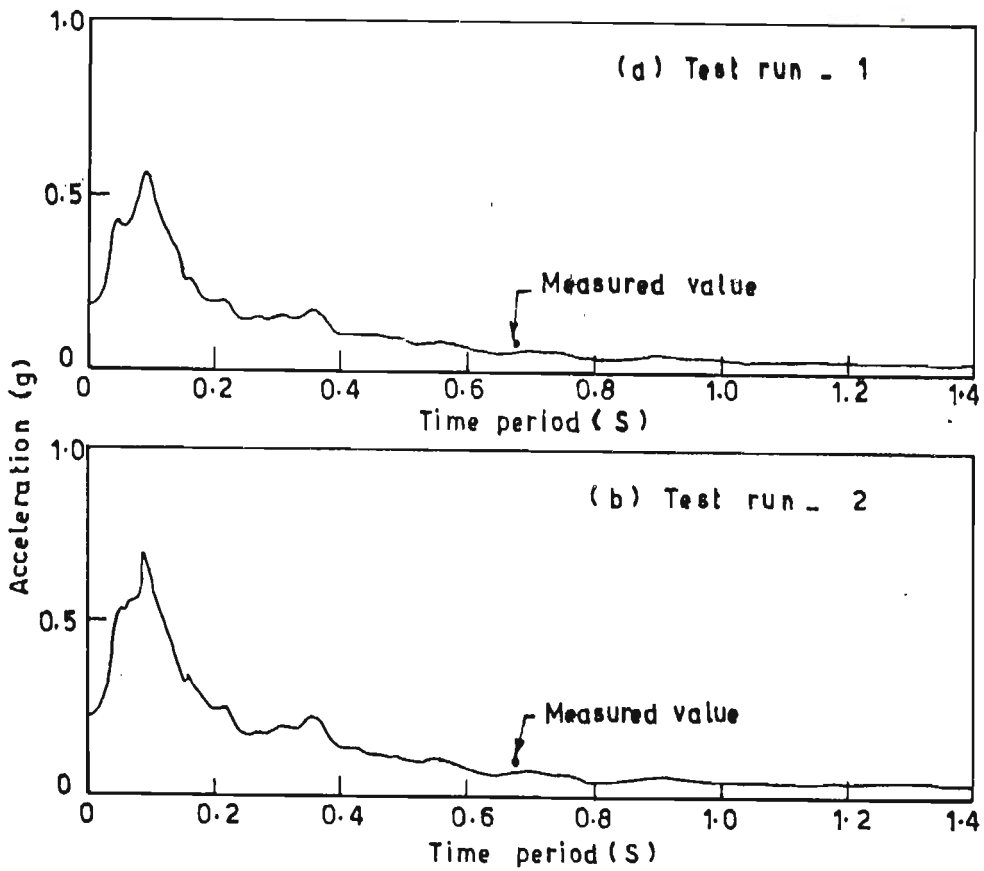
Fig.4.13 Linear Acceleration Response Spectra Obtained from Measured
Table Motion: (a) Test Run-1 and (b) Test Run-2
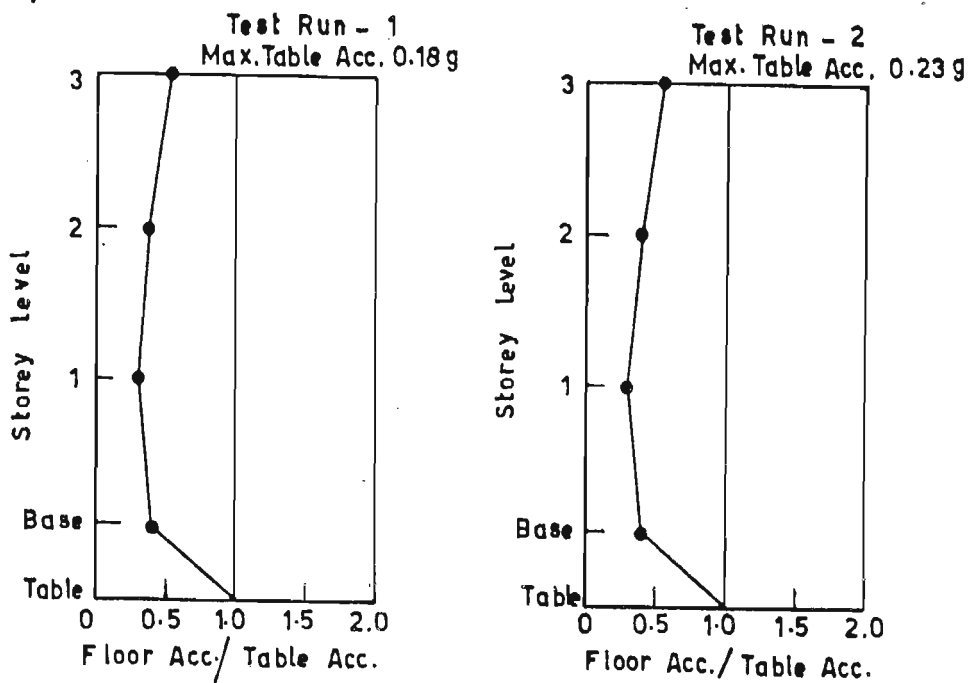
Fig.4.14 Amplification Envelop

73

CHAPTER-5

BASE ISOLATED BUILDINGS SUBJECTED TO UNIDIRECTIONAL MOTION

5.1 Introduction

In this chapter, the computed response of medium-rise reinforced concrete shear type buildings supported over either pure friction bearing (P-F), laminated rubber bearing (LRB), lead rubber bearing (LLRB) or sliding-elastomer bearing (EDF) isolation system, subjected to unidirectional seismic ground motions are studied. The computed response of isolated system subjected to general plane motion are presented in the Chapter-6.

The bi-linear hysteretic behaviour of LRB and LLRB are represented by equivalent linear stiffness and damping factor. Frictional behaviour of sliding isolation system is modelled by Coloumb's rigid plastic model. The governing equations of motion for friction based isolation system are highly non-linear and stiff. The criteria for stick-slip transition and vice versa are discussed in detail because these are crucial to the accuracy of the response analysis. The details of procedure adopted for avoiding difficulties in phase transition in Coloumb's model are presented. The superstructure is first idealized as a rigid body and then as flexible model (lumped mass model) to assess the effect of building flexibility on the overall response of the isolated system. To understand the effect of amplitude and frequency content of earthquake motion on the response of base isolated structure - Koyna (long.) accelerogram(1967) and El-Centro(NS) accelerogram (1940) are taken as the base excitation motion.

A unified solution algorithm for the analysis of medium-rise r.c. shear buildings supported over either - P-F bearing, LRB, LLRB or EDF isolation system has been developed. This solution algorithm is based on

Newmark's method in predictor-corrector form. This method of analysis is very direct and elegant which requires the solution of individual coupled equation in staggered fashion.

The peak absolute acceleration signifies the force that it experiences and is the main source of damage to the structure, the internal equipments and secondary systems. The peak relative base displacement is the most important parameter for the design of the life line connection to the ground. The deflection of the structure is directly proportional to the stresses and base shear in the columns. In this study, the peak absolute acceleration at the base and the roof levels, the maximum base displacement and the maximum structural deflection responses for selected base isolated systems are evaluated. Fourier amplitude spectra of absolute acceleration histories are obtained to determine predominant frequency of different base isolation systems. A comparative study of response of a building with different isolation systems have been made.

5.2 Equations of Motion

In this section, the equations governing the motion of base isolation systems and the criteria used for transition of motions for the frictional base isolators are discussed. A three storey shear building (Fig.5.1) will be considered for response calculation, although
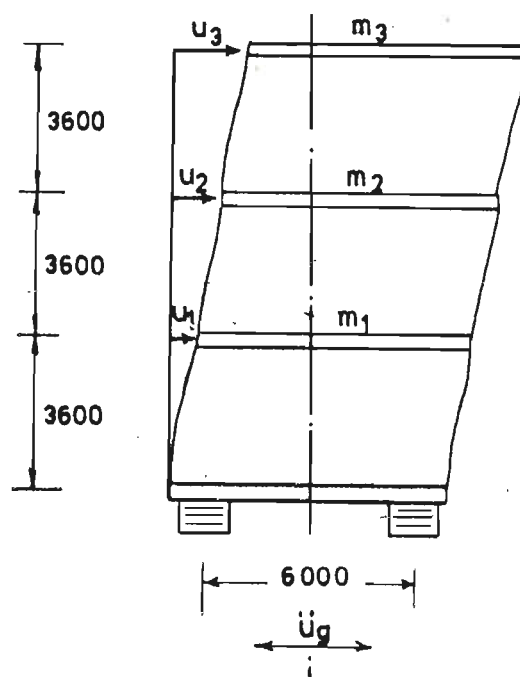
Fig.5.1 Structural Model of Three Storeyed
Base Isolated Building

the formulation is presented for general multi storey shear type buildings. In the rigid body model, the entire mass m_t of this system is included in the rigid block supported over isolation system. By applying Newton's second law of motion to the base isolated structure, the equations of motion are derived and the results for various base isolation system are described in the following sections.

5.2.1 Superstructure Idealized as Rigid Body Model

■ LRB/LLRB Isolation System: Figure 5.2 shows the schematic and free body diagrams of a rigid body supported over the LRB/Lead rubber isolation system.

(a) Schematic diagram   (b) Free body diagram

Fig.5.2 Schematic Diagram and Free Body Diagram of Rigid
Body Supported on LRB/LLRB

The governing equations of motion of the rigid body system is given as,

$$\ddot{u}_b + 2\,\zeta_{eq}\omega_{eq}\dot{u}_b + \omega_{eq}^2 u_b = -\ddot{u}_g \qquad \ldots\ldots(5.1)$$

where, u_b, $\dot{u}_b$ and $\ddot{u}_b$ are relative bearing displacement, velocity and acceleration with respect to the ground. The equivalent natural circular frequency of the bearing ω_{eq} and its equivalent damping ratio ζ_{eq} are defined as,

$$\omega_{eq}^2 = \frac{K_{eq}}{m_t} \quad \text{and} \quad 2\zeta_{eq}\omega_{eq} = \frac{C_{eq}}{m_t} \qquad \ldots\ldots(5.2)$$

76

Here, C_{eq} and K_{eq} are the equivalent damping and the equivalent horizontal shear stiffness of the bearing. For equivalent linearization of bilinear restoring force system of LRB/LLRB isolation system "Geometric Stiffness Method" presented by Jennings(1968) for elasto-plastic system is adopted. Figure 5.3 shows a typical bilinear hysteresis loop. Equivalent stiffness K_{eq} is given as,

$$K_{eq} = \frac{K_e \, u_{by} + K_p \, [u_{bmax} - u_{by}]}{u_{bmax}} \qquad \dots\dots (5.3)$$
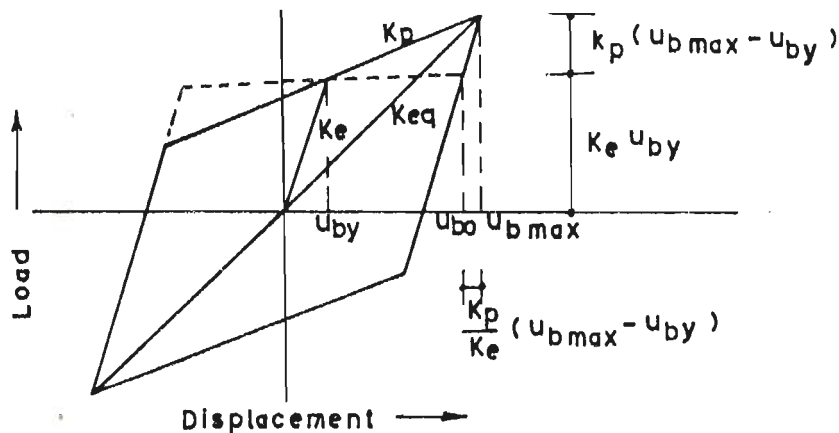
Fig.5.3 Bilinear Hysteresis Loop

$$= \frac{K_e + K_p \, (d_r - 1)}{d_r} \qquad \dots\dots (5.4)$$

where, $d_r = \dfrac{u_{bmax}}{u_{by}}$

in which, d_r is the ratio of maximum bearing displacement (u_{bmax}) and bearing displacement at yield point (u_{by}).

Equating, energies dissipated by equivalent linear and yielding isolation system results,

$$2\pi \, \zeta_{eq} K_{eq} \, u_{bmax}^2 = 4 \, K_e \, u_{by} \, [u_{bo} - u_{by}] \qquad \dots\dots (5.5)$$

where,

$$u_{bo} = u_{bmax} - \frac{K_p}{K_e} (u_{bmax} - u_{by}) \qquad \ldots \ldots (5.6)$$

Substituting, (5.4) and (5.6) in (5.5) and subsequent simplification gives,

$$\zeta_{eq} = \frac{2}{\pi} \frac{1 - \alpha}{1 + \alpha(d_r - 1)} \frac{(d_r - 1)}{d_r} \qquad \ldots \ldots (5.7)$$

where, α is the ratio of post yielding-stiffness (K_p) to pre yielding stiffness (K_e). K_p for both LRB and LLRB isolation system corresponds to a natural frequency of 0.5 Hz of the isolated structure. The ratio of K_e to K_p varies from 2.5 to 4 for LRB, while the same varies from 7 to 10 for LLRB.

■ **P-F Isolation System:**   Figure 5.4 shows the schematic and free body diagrams of a rigid body supported over P-F isolator.

(a) Schematic diagram   (b) Free body diagram
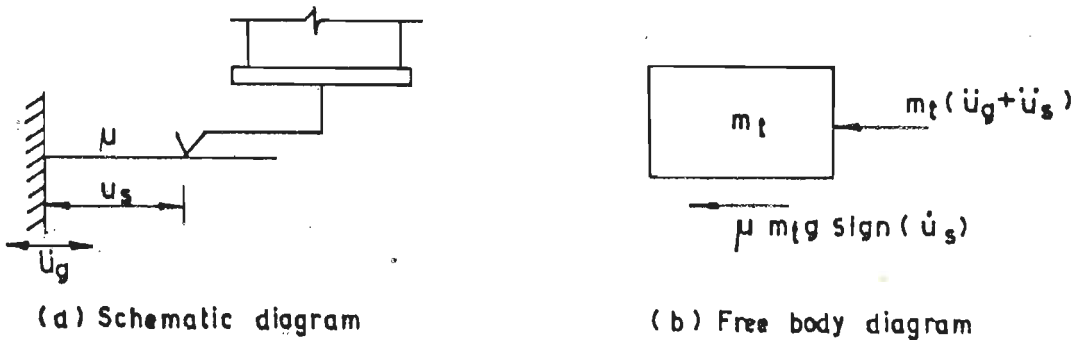
Fig.5.4 Schematic Diagram and Free Body Diagram of Rigid Body Supported on P-F Bearing

The governing equations of motion of the rigid body during the sliding phase is given as,

$$\ddot{u}_s + \mu g \; sign \; (\dot{u}_s) = - \ddot{u}_g \qquad \ldots \ldots (5.8)$$

where, u_s is the relative slip displacement between rigid body and the ground, $\ddot{u}_g$ is the horizontal ground acceleration, μ is the friction coefficient, g is the acceleration due to gravity, $sign(\dot{u}_s)$ is a function which is equal to +1 when u_s is positive, and -1 when u_s negative.

78

For the non-sliding phase governing equation become

$$\ddot{u}_s = \dot{u}_s = 0 \qquad \qquad \dots \dots (5.9)$$

For the non-sliding phase to continue, the force acting at the base of the structure must be less than equal to frictional resistance at the frictional interface i.e.

$$|m_t \ddot{u}_g| \leq \mu m_t g$$

$$\text{or, } |\ddot{u}_g| \leq \mu g \qquad \qquad \dots \dots (5.10)$$

must be satisfied, when L.H.S of the inequality (5.7) just exceeds R.H.S, sliding commences. In otherwords, at the initiation of sliding the frictional resistance and disturbing force are equal in magnitude but opposite in sign [Mostaghel and Tanbakuchi(1983)]. Therefore, in the first interval of sliding phase,

$$\text{sign}(\dot{u}_s) = - \frac{\ddot{u}_g}{|\ddot{u}_g|} \qquad \qquad \dots \dots (5.11)$$

In sliding phase, when $\dot{u}_s$ becomes equal to zero and simultaneously Eqn.(5.10) is satisfied, then structure sticks to the isolator.

■ EDF Isolation System: Figure 5.5 shows the schematic and free body diagrams of rigid body supported over EDF isolation system.

(a) Schematic diagram
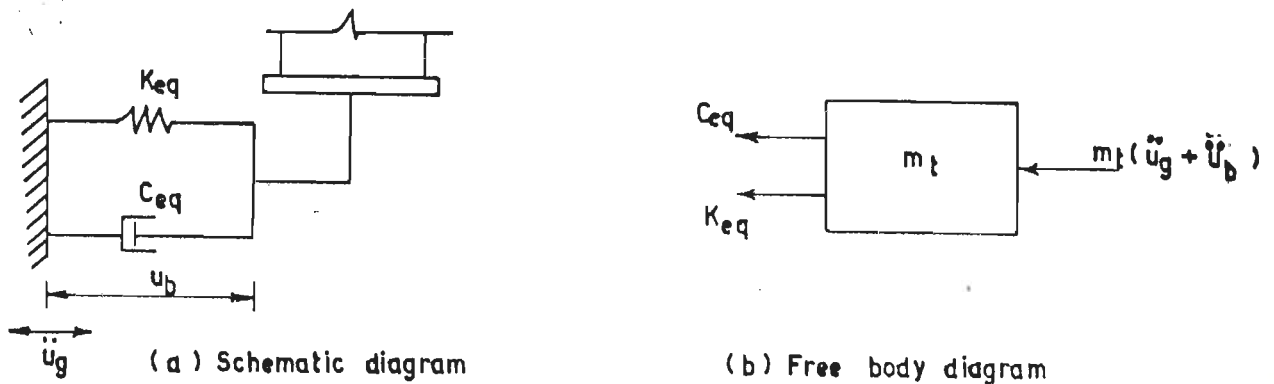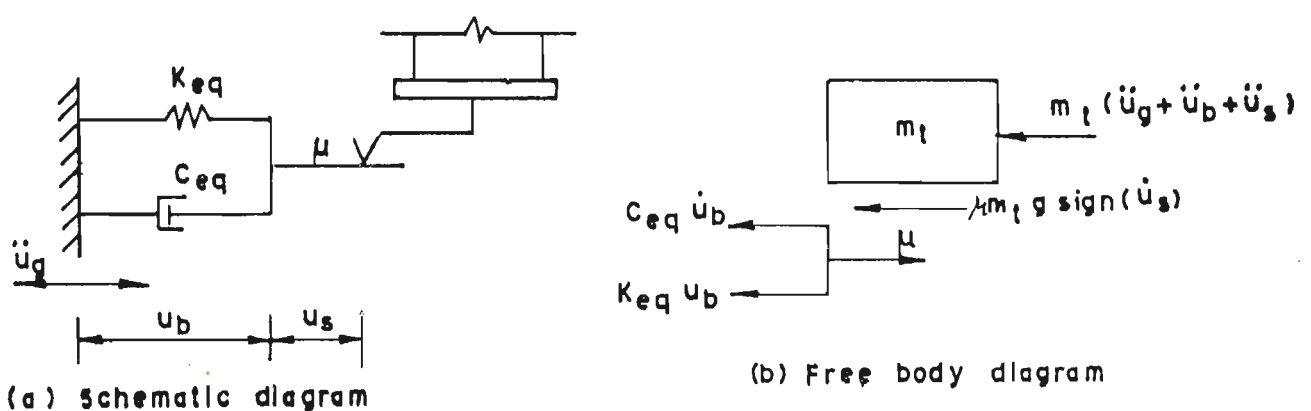
(b) Free body diagram

Fig.5.5 Schematic Diagram and Free Body Diagram of Rigid Body Supported on EDF Bearing

The governing equations of motion of rigid body supported over EDF isolation system in sliding phase are given as,

$$2\zeta_{eq}\omega_{eq}\dot{u}_b + \omega_{eq}^2 u_b = \mu g \; \text{sign} \; (\dot{u}_s) \qquad \ldots\ldots(5.12)$$

$$\ddot{u}_s + \mu g \; \text{sign}(\dot{u}_s) = -\ddot{u}_g - \ddot{u}_b \qquad \ldots\ldots(5.13)$$

where, u_b is the displacement in LRB and u_s is the slip displacement at the sliding interface.

In the Eqn.(5.12) inertia force experienced by LRB is neglected, since bearing mass is very small as compared to the base mass. It should be noted that here Eqn.(5.12) can not be integrated by Newmark's method due to absence of second order derivative terms in the left hand side of the same equation. Adding (5.12) and (5.13), and rearrangement results,

$$\ddot{u}_b + 2\zeta_{eq}\omega_{eq}\dot{u}_b + \omega_{eq}^2 u_b = -\ddot{u}_g - \ddot{u}_s \qquad \ldots\ldots(5.14)$$

In sliding phase, responses of rigid body and base isolator are evaluated by solving (5.13) and (5.14). The total displacement u_t is given as,

$$u_t = u_b + u_s \qquad \ldots\ldots(5.15)$$

In non-sliding phase governing equation becomes,

$$\ddot{u}_s = \dot{u}_s = 0 \qquad \ldots\ldots(5.16)$$

$$\ddot{u}_b + 2\zeta_{eq}\omega_{eq}\dot{u}_b + \omega_{eq}^2 u_b = -\ddot{u}_g \qquad \ldots\ldots(5.17)$$

For non-sliding phase to continue, the force acting at the base of the structure must be less than or equal to frictional resistance at the frictional interface i.e.

$$\left| m_t(\ddot{u}_g + \ddot{u}_b) \right| \leq \mu m_t g$$

or, $\left| \ddot{u}_g + \ddot{u}_b \right| \leq \mu g \qquad \ldots\ldots(5.18)$

must be satisfied. When L.H.S of the inequality (5.15) just exceeds R.H.S, sliding commences. In otherwords, at the initiation of sliding

the frictional resistance and disturbing force are equal in magnitude but opposite in sign. Therefore, in the first interval of sliding phase,

$$sign(\dot{u}_s) = - \frac{(\ddot{u}_g + \ddot{u}_b)}{|(\ddot{u}_g + \ddot{u}_b)|} \qquad \dots\dots(5.19)$$

In sliding phase, when $\dot{u}_s$ becomes equal to zero and simultaneously (5.18) is satisfied, then structure sticks to the isolator.

5.2.2 Structure Idealized as Flexible Model (Lumped Mass Model)

■ **LRB/LLRB Isolation System:** The governing equations of motion for lumped mass analytical model medium-rise shear building (Fig.5.2) supported over LRB/lead rubber bearing system are given as,

$$\ddot{u}_b + 2\zeta_{eq}\omega_{eq}\dot{u}_b + \omega_{eq}^2 u_b = -\ddot{u}_g - \sum_{i=1}^{N} \alpha_i \ddot{u}_i \qquad \dots\dots(5.20)$$

$$M\ddot{u} + C\dot{u} + Ku = -Mr(\ddot{u}_g + \ddot{u}_b) \qquad \dots\dots(5.21)$$

where, ζ_{eq} and ω_{eq} are the equivalent damping factor and equivalent angular natural frequency as defined in the Section 5.2.1, u_i is the relative displacement of each floor with respect to the base, K is the superstructure stiffness matrix for horizontal floor displacements relative to the base and this can be directly written. Thus, the stiffness matrix dimension is NxN, where N is the degrees of freedom. The superstructure mass matrix M is diagonal with the masses m_1, m_2, ... m_n respectively the masses attached at floor levels. The structural damping is assumed to be hysteretic, frequency independent with the matrix of equivalent viscous damping C specified in terms of the stiffness matrix as,

$$C = (2\zeta_{eq}/\omega)K \qquad \dots\dots(5.22)$$

where, ζ_{eq} is the material damping ratio, the circular frequency, ω is taken as equal to the first natural frequency of the building and r is earthquake influence coefficient vector [Clough and Penzien(1986)]. The mass ratio α_i is defined as,

$$\alpha_i = \frac{m_i}{m_t}, \qquad m_t = m_b + r^T M r$$

where, m_i is the mass of ith floor, m_b is the mass of the basement and m_t is the total mass.

■ **P-F Isolation System:**   The governing equations of motion for lumped mass analytical model of multistorey shear building supported on pure sliding isolation system during sliding phase are given as,

$$\ddot{u}_s + \mu g \, \text{sign}(\dot{u}_s) = -\ddot{u}_g - \sum_{i=1}^{N} \alpha_i \ddot{u}_i \qquad \qquad \ldots\ldots(5.23)$$

$$M \ddot{u} + C \dot{u} + K u = - M r (\ddot{u}_g + \ddot{u}_s) \qquad \qquad \ldots\ldots(5.24)$$

For the non sliding phase, governing equations of motion are

$$\ddot{u}_s = \dot{u}_s = 0 \qquad \qquad \ldots\ldots(5.25)$$

and the deformation of the structure is governed by Eqn.(5.24). For non-sliding phase to continue, the force acting at the base of the structure must be less than or equal to frictional resistance at the frictional interface i.e.

$$\sum_{i=1}^{N} m_i \ddot{u}_i + (\sum_{i=1}^{N} m_i + m_b) \ddot{u}_g \leq \mu m_t g$$

$$\text{or,} \ \sum_{i=1}^{N} m_i \ddot{u}_i + m_t \ddot{u}_g \leq \mu m_t g$$

$$\text{or,} \ \left| \ddot{u}_g + \sum_{i=1}^{N} \alpha_i \ddot{u}_i \right| \leq \mu g \qquad \qquad \ldots\ldots(5.26)$$

must be satisfied. When L.H.S. of the inequality (5.26) just exceeds R.H.S., sliding phase commences. In the first interval of sliding phase,

$$\text{sign}(\dot{u}_s) = - \frac{(\ddot{u}_g + \sum_{i=1}^{N} \alpha_i \ddot{u}_i)}{\left| \ddot{u}_g + \sum_{i=1}^{N} \alpha_i \ddot{u}_i \right|} \qquad \qquad \ldots\ldots(5.27)$$

In sliding phase, when $\dot{u}_s$ becomes equal to zero and simultaneously Eqn.(5.26) is satisfied, then structure sticks to the isolator.

■ **EDF Isolation System:**   The governing equations of motion for lumped mass analytical model of multistorey shear building supported over EDF isolation system are given as,

$$2\zeta_{eq}\omega_{eq}\dot{u}_b + \omega_{eq}^2 u_b = \mu g \; \text{sign} \; (\dot{u}_s) \qquad \ldots\ldots(5.28)$$

$$\ddot{u}_s + \mu g \; \text{sign}(\dot{u}_s) = -\ddot{u}_g - \ddot{u}_b - \sum_{i=1}^{N} \alpha_i \ddot{u}_i \qquad \ldots\ldots(5.29)$$

$$M\ddot{u} + C\dot{u} + Ku = -Mr(\ddot{u}_g + \ddot{u}_b + \ddot{u}_s) \qquad \ldots\ldots(5.30)$$

Adding (5.28) and (5.29), and rearrangement gives,

$$\ddot{u}_b + 2\zeta_{eq}\omega_{eq}\dot{u}_b + \omega_{eq}^2 u_b = -\ddot{u}_b - \ddot{u}_s - \sum_{i=1}^{N} \alpha_i \ddot{u}_i \qquad \ldots\ldots(5.31)$$

In sliding phase, responses of superstructure, base and base isolator are evaluated by solving (5.29), (5.30) and (5.31). In non-sliding phase governing equations of motion become,

$$\ddot{u}_s = \dot{u}_s = 0 \qquad \ldots\ldots(5.32)$$

$$\ddot{u}_b + 2\zeta_{eq}\omega_{eq}\dot{u}_b + \omega_{eq}^2 u_b = -\ddot{u}_g - \sum_{i=1}^{N} \alpha_i \ddot{u}_i \qquad \ldots\ldots(5.33)$$

$$M\ddot{u} + C\dot{u} + Ku = -Mr(\ddot{u}_g + \ddot{u}_b) \qquad \ldots\ldots(5.34)$$

For non-sliding phase to continue, the disturbing force acting at the base of the structure must be less than equal to the frictional resistance at the frictional couple .i.e

$$\left| \ddot{u}_g + \ddot{u}_b + \sum_{i=1}^{N} \alpha_i \ddot{u}_i \right| \le \mu g \qquad \ldots\ldots(5.35)$$

must be satisfied. When L.H.S of the inequality (5.35) just exceeds R.H.S, sliding phase just commences. In the first interval of sliding phase

$$\text{sign}(\dot{u}_s) = - \frac{(\ddot{u}_g + \ddot{u}_b + \sum_{i=1}^{N} \alpha_i \ddot{u}_i)}{|\ddot{u}_g + \ddot{u}_b + \sum_{i=1}^{N} \alpha_i \ddot{u}_i|} \qquad \dots\dots(5.36)$$

In sliding phase, when $\dot{u}_s$ becomes equals to zero and simultaneously Eqn.(5.35) is satisfied, then structure sticks to the isolator.

5.3 Method of Solution

An implicit-implicit partitioned Newmark's method in predictor-corrector form [Paul(1982), Zienkiewicz *et al.*(1988)] is used for direct integration of governing equations of motion. This method of analysis is very direct and elegant which requires the solution of individual coupled equations in staggered fashion. The complexity due to the presence of frictional interface in pure sliding system and sliding-elastomer system and transitions from non-sliding phase to sliding phase and vice-versa which makes the system of governing equations of motion highly non-linear and stiff respectively, can be solved by this method efficiently.

The algorithm for solution of equations of motion in sliding phase of the building supported over EDF isolator for rigid body idealization using Newmark's method in predictor-corrector form is shown below.

1. Initialize

$$u_b^{(1)} = 0, \qquad u_s^{(1)} = 0$$

$$\dot{u}_b^{(1)} = 0, \qquad \dot{u}_s^{(1)} = 0$$

$$\ddot{u}_b^{(1)} = 0, \qquad \ddot{u}_s^{(1)} = 0$$

$$n = 0$$

$$\text{sign}(\dot{u}_s) = - \frac{(\ddot{u}_g + \ddot{u}_b)}{|(\ddot{u}_g + \ddot{u}_b)|}$$

2. Set time step counter $n = n+1$

84

3. Begin predictor phase in which,

$$(u_b)^{(1)}_{n+1} = (\tilde{u}_b)_{n+1} = (u_b)_n + \Delta t (\dot{u}_b)_n + \Delta t^2 (1-2\beta)(\ddot{u}_b)_n / 2$$

$$(\dot{u}_b)^{(1)}_{n+1} = (\dot{\tilde{u}}_b)_{n+1} = (\dot{u}_b)_n + \Delta t (1-\gamma)(\ddot{u}_b)_n$$

$$(u_s)^{(1)}_{n+1} = (\tilde{u}_s)_{n+1} = (u_s)_n + \Delta t (\dot{u}_s)_n + \Delta t^2 (1-2\beta)(\ddot{u}_s)_n / 2$$

$$(\dot{u}_s)^{(1)}_{n+1} = (\dot{\tilde{u}}_s)_{n+1} = (\dot{u}_s)_n + \Delta t (1-\gamma)(\ddot{u}_s)_n$$

4. Set iteration counter i = 1 and assume the sliding acceleration $\ddot{u}_s = 0$

5. Evaluate residual forces using equation

$$\varphi^{(i)} = - \ddot{u}_g - (\ddot{u}_s)^{(i)}_{n+1} - (\ddot{u}_b)^{(i)}_{n+1} - 2\zeta\omega_{eq}(\dot{u}_b)^{(i)}_{n+1} - \omega^2_{eq}(u_b)^{(i)}_{n+1}$$

6. Form the effective stiffness matrix using the expression

$$K^* = 1/(\Delta t^2 \beta) + \gamma \, 2\zeta\omega_{eq}/(\Delta t \, \beta) + \omega^2_{eq}$$

or update K^* whenever Δt changes.

7. Solve

$$K^* \cdot \Delta(u_b)^{(i)} = \varphi^{(i)}$$

8 Enter corrector phase in which,

$$(u_b)^{(i+1)}_{n+1} = (u_b)^{(i)}_{n+1} + \Delta(u_b)^{(i)}$$

$$(\ddot{u}_b)^{(i+1)}_{n+1} = [(u_b)^{(i+1)}_{n+1} - (\tilde{u}_b)_{n+1}]/(\Delta t^2 \beta)$$

$$(\dot{u}_b)^{(i+1)}_{n+1} = (\dot{\tilde{u}}_b)^{(i)}_{n+1} + \gamma \, \Delta t (\ddot{u}_b)^{i+1}_{n+1}$$

$$(\ddot{u}_s)^{(i+1)}_{n+1} = - \ddot{u}_g - \ddot{u}_b - \mu g \, \text{sign}(\dot{u}_s)$$

$$(u_s)^{(i+1)}_{n+1} = (\tilde{u}_s)_{n+1} + \beta \, \Delta t^2 (\ddot{u}_s)^{(i+1)}_{n+1}$$

85

$$(\dot{u}_s)^{(i+1)}_{n+1} = (\tilde{\dot{u}}_s)^{(i)}_{n+1} + \gamma \, \Delta t (\ddot{u}_s)^{i+1}_{n+1}$$

9. Compute

$$\varepsilon_u = \frac{\sqrt{(u_b^2 + u_s^2)^{(i+1)}} - \sqrt{(u_b^2 + u_s^2)^{(i)}}}{\sqrt{(u_b^2 + u_s^2)^{(i+1)}}}$$

10. If $\varepsilon_u \geq$ tolerance, set $i = i+1$ and go to step-5, otherwise continue.

11. Set

$$(u_b)_{n+1} = (u_b)^{(i+1)}_{n+1}, \qquad (u_s)_{n+1} = (u_s)^{(i+1)}_{n+1}$$

$$(\dot{u}_b)_{n+1} = (\dot{u}_b)^{(i+1)}_{n+1}, \qquad (\dot{u}_s)_{n+1} = (\dot{u}_s)^{(i+1)}_{n+1}$$

$$(\ddot{u}_b)_{n+1} = (\ddot{u}_b)^{(i+1)}_{n+1}, \qquad (\ddot{u}_s)_{n+1} = (\ddot{u}_s)^{(i+1)}_{n+1}$$

$$\text{sign}(\dot{u}_s) = \frac{\dot{u}_s}{|\dot{u}_s|}$$

for use in the next time step, go to step-2.

The same algorithm can also be used for LRB/LLRB and P-F isolation system by assigning coefficient of friction at the sliding interface and stiffness of LRB/LLRB - a very large value respectively. This algorithm is then extended for lumped mass model for taking into account the structural flexibility.

Using predictor-corrector algorithm as described above, a FORTRAN - 77 program ISODYN-1D is developed for numerical solution of the equations of motion of structure supported over selected isolated systems. A time step of $\Delta t = 0.02$ to 0.1 sec is used in the non-sliding phase away from the transition points because further reduction of time step do not change calculated response noticeably. For accuracy of results in the transition zone and in the sliding phase finer time step of the range 0.002 to 0.0001 sec was used for response calculation and it was observed that step reduction beyond 0.0005 sec does not change computed response. Since sliding phase occurs for very small duration of time, a uniform fine time step was used in this phase. Further, at the

time interval in which phase change takes place, exact transition point is located (approximately) by linear interpolation (Fig.5.6). It is observed that the accuracy of analysis is increased by locating the transition points, but it is also noted that if time step considered is of the order of 0.0005 sec, then no noticeable change in response is achieved by locating exact transition point. Therefore, in this study a time step of 0.0005 sec is selected for numerical integration of equations of motion in transition zone and in sliding phase.
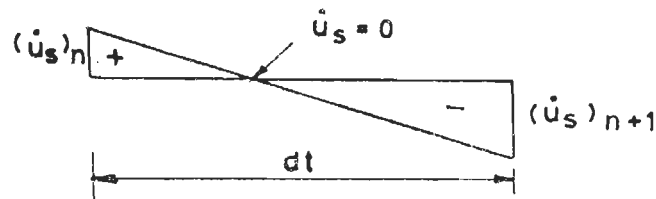
Fig.5.6 Location of Approximate Phase Transition Point

5.4 Validation of Analytical Model and Solution Algorithm

The validity of analytical model and solution algorithm used is demonstrated herein by comparison with analytical and experimental results obtained by Suzuki *et al.*(1992) from Shake Table tests of 1/3rd scale one mass model isolated by LRBs alongwith steel rod dampers. A band-fixed iron ingot weighing 13.3 t was supported on four numbers of isolators. The post yielding stiffness and damping ratio of LRB have been considered as 3.53 kN/cm and 0.035 respectively. The initial elastic stiffness of 16.4 kN/cm and yield strength of 3.9% have been considered for LRB in series with steel rod dampers. The ground motion considered was time scaled El-Centro N-S component (1940) with peak ground acceleration of 3.02 m/s^2. Figures 5.7 shows the measured and simulated displacement and acceleration response histories. Both measured and simulated responses are found to be in close agreement.

Three storeyed r.c. framed model (1/6th scale) weighing 63 kN was isolated by six numbers of model LRBs, for Shake Table Test in the

present study. The details of the experimental observations are provided in the preceding Chapter. The model LRBs designed in this study are exceptionally slender in shape unlike that of prototype bearing, because of relatively small load of the model. Experimental observations indicate the presence of rocking mode of vibration in the response of the test structure and this happens due to slender shape of the model bearing. Therefore, for simulation of response of the test structure, one additional degree of freedom is considered only at the rigid base and response are computed from the lumped mass model. Figure 5.8 shows both measured and simulated absolute roof acceleration histories of the test model and both are found to be in good agreement. Figure 5.9 shows the plots of frequency vs transfer function (ratio of FFTs of roof acceleration and table acceleration histories) for both measured and computed acceleration histories. Both measured and computed response indicate that fundamental period of the isolated structure is 1.5 Hz. Higher modes contribution are more in computed response as compared to that of measured response.

5.5 Results and Discussion

In this section, the response of both rigid body model and lumped mass model of a isolated three storey r.c. shear building subjected to two representative earthquake excitations, are evaluated by solution technique discussed in the preceding section. Performances of selected base isolation systems are studied. The three storey isolated building considered for analysis is geometrically similar to the test model (1/6 scale) used in experimental study. Plan and elevation of r.c. framed structure alongwith details of elements, are shown in Fig.5.10. Parameters of different isolation system are provided in the Table 5.1. The natural frequencies of the structure (fixed base) are as: ω_1 = 20.62 rad/sec, ω_2= 57.08 rad/sec and ω_3 = 87.07 rad/sec. The equivalent viscous damping ratio of 0.05 is taken in the first mode of vibration.

LRB, LLRB and EDF bearing are considered to have same geometry with same post yielding stiffness, which corresponds to a frequency of 0.5 Hz. The coefficient of friction in P-F bearing and EDF bearing is considered to be 0.1. This happened to be the mean coefficient of friction of Teflon/stainless steel sliding interface, which is widely used in friction based isolation systems developed in different parts of

the world. In the analysis, six numbers of bearings are considered for all four isolation systems with a bearing located under each column of the r.c. frame.

Table 5.1 Values of parameter used for various base isolators

Base Isolator	K_e (kN/mm) (1)	K_p (kN/mm) (2)	K_{eq} (kN/mm) (3)	f_{eq} (Hz) (4)	ζ_{eq} (5)	μ (6)
P-F	-	-	-	-	-	0.1
LRB	6.675	2.225	2.967	0.575	0.133	-
Lead Rubber	15.575	2.225	3.975	0.666	0.240	-
EDF	6.675	2.225	2.967	0.575	0.133	0.1

To understand the effects of amplitude and frequency contents - El-Centro(N-S) accelerogram(1940), and Koyna(long.) accelerogram(1967) are considered. The El-Centro(N-S) accelerogram has peak ground acceleration of 0.33g and has most of its frequency content between 1 Hz and 3 Hz. Koyna (Long.) accelerogram has peak ground acceleration of 0.63g and has most of its frequency content between 2.5 Hz to 8.5 Hz. The recorded acceleration are as such used and no effort has been made to normalize the accelerograms either with respect to peak ground acceleration or spectral intensity.

The responses of three storey shear building with various base isolators are evaluated. The instantaneous absolute base acceleration, the roof acceleration, the relative base displacement are computed and time history of these responses are plotted. Variation of the peak absolute base acceleration, roof acceleration, the peak relative base displacement, the peak roof displacement relative to base with different post yielding time period are evaluated for LRB, LLRB and EDF isolation systems. Further, to study the sensitivity of responses of EDF isolator to the coefficient of friction, variation of peak absolute base acceleration, the peak absolute roof acceleration, the peak absolute relative base displacement, peak absolute relative roof displacement with equivalent time period (corresponding to equivalent stiffness) of isolated structure for different values of μ are computed. The frequency decompositions for roof acceleration time histories for the base isolated structure and the fixed base one are examined.

5.5.1 Rigid Body Model: For the purpose of understanding the characteristic of selected isolation system clearly, effect of structural flexibility was not considered. Secondly, computed responses from rigid body model can be compared with the responses of more refined analytical model in connection with the development of simplified analytical model for practical design purpose.

Figures 5.11 and 5.12 show relative base displacement time histories of the rigid body supported over selected base isolation systems subjected to Koyna and El-Centro earthquake excitations. Base displacement time history of the P-F isolationsystem can be differentiated from that of the other isolation systems due to the presence of distinct characteristics in which sliding and non-sliding phase occurs alternately before returning finally to non-sliding phase. This system produces lowest base displacement amongst all isolation systems discussed in this study for both earthquake inputs. The displacement level in LLRB is less than that in LRB and this is due to the presence of lead core, which reduces the bearing displacement. Displacement in LRB of EDF bearing is less than that in LRB alone because slip occurs in the sliding interface but total displacement is comparable to that of LRB. In EDF bearing system, total base displacement oscillates around slip displacement. Comparison of Fig.5.11 with Fig.5.12 revealed that displacement level of all isolation systems studied, under Koyna excitation, are less than that under El-Centro excitation although peak ground acceleration of the former excitation is greater.

Figures 5.13 and 5.14 show absolute acceleration time histories of the rigid body supported on various base isolation systems subjected to Koyna and El-Centro excitations. Acceleration history of P-F isolation system contain high frequency components which are not present in the acceleration histories of other isolation system. Peak absolute acceleration of the structure is limited to μg irrespective of the types of ground motion. Acceleration histories of LRB and LLRB isolation systems are smooth as compared to that of P-F isolation system. Absolute acceleration histories of EDF isolation system are relatively smooth as compared to that of P-F isolator and also there is a limit on peak absolute acceleration transmitted to the structure irrespective of amplitude and frequency content of earthquake excitations. Comparison of

Fig.5.13 and Fig.5.14 revealed that acceleration level of LRB and LLRB under Koyna excitation are less than that under El-Centro excitation. Further, acceleration levels of friction based isolators are less sensitive to the amplitude and frequency content of earthquake excitations.

5.5.2 Lumped Mass Model: Figures 5.15 and 5.16 show relative base displacement time histories computed from lumped mass model with one dof per floor of three storey shear building subjected to Koyna and El-Centro earthquake excitations. Roof displacement histories in isolated building with LRB, LLRB and EDF bearing are nearly overlapping with respective base displacement histories. While roof displacement histories for P-F bearing is found to oscillate about base displacement histories, although displacement level in both cases are nearly same. Displacement at base level for P-F isolated system as obtained from this model is much higher than that obtained from rigid body model, although pattern of displacement histories are similar under both the excitations. Displacement at base level for LRB as obtained from this model is slightly lower than that obtained from rigid body model. For LLRB and EDF isolation system, computed base displacement from both the analytical model give almost same level. Slip displacement in EDF isolation system under Koyna excitation is nearly 2 mm when computed from this analytical model, where as it is only 0.2 mm when computed from rigid body model although sliding commences nearly at the same time in both the models.

Figures 5.17 and 5.18 show absolute base acceleration time histories of various isolated system studied, under Koyna and El-Centro excitations. It is seen from these figures that in P-F isolation system maximum level of base acceleration is not restricted to μg, and this happens due to flexibility of the structure above. In EDF isolation system, base acceleration is found to oscillate about μg acceleration level. Absolute acceleration response time histories for LRB and LLRB as obtained from this model are almost similar in pattern with slightly higher amplitude as compared to that obtained from the rigid body model.

Figures 5.19 and 5.20 show absolute roof acceleration time histories of structure supported over various isolation systems studied, subjected to Koyna and El-Centro excitations. Maximum acceleration

91

amplification takes place in case of P-F isolation system. This amplification is more in case of isolated system subjected to Koyna excitation than that subjected to El-centro excitation. This happens because Koyna accelerogram contains high frequency components and P-F isolation system can not filter out these components. This is not that prominent in case of EDF isolator under both these excitations. The level of acceleration amplification is very low in case of LRB and LLRB isolation system and acceleration time histories are smooth in case of these isolation system. Absolute roof acceleration histories for fixed base structure is also provided for the sake of comparison and it can be seen that maximum level of acceleration of all isolated structures are much lower than that of fixed base structure (F-B).

Figures 5.21 and 5.22 show the Fourier amplitude plot of absolute roof acceleration of building supported over various isolation system studied and fixed base structure. Fourier amplitude plot of roof acceleration with P-F isolation system show that energy containing frequencies are widely spread under both the earthquake inputs although two main peaks are seen at 3.75 Hz and 9.5 Hz. Fourier amplitude plot of roof acceleration for LRB isolated system shows that major peak occurs at 0.55 Hz under both the excitations and amplitude of this peak is higher for El-Centro excitation than that with Koyna excitation but there is second prominent peak at 9.5 Hz under Koyna excitation. For LLRB the major peak occurs at 0.6 Hz for both the inputs and Fourier amplitude at this frequency is less than that in the LRB but high frequency amplitudes are higher in this case. For EDF bearing there are three distinct peaks at 0.6 Hz, 4.25 Hz and 9.5 Hz. For Koyna excitation Fourier amplitude is larger at second frequency. The high frequency components are contributed by the small sliding phase of the motion although high frequency responses are less when compared with P-F isolation system. For F-B structure the main peak occurs at 3.3 Hz, which happened to be its lowest natural frequency.

Figures 5.23 and 5.24 show the variation of the structure isolated by EDF isolation system against equivalent time period of the isolated structure for different values of coefficient of friction under Koyna and El-Centro excitations respectively. In the practical range of equivalent time period (2.5 sec to 4.0 sec) the responses are not sensitive to the variation of coefficient of friction, when the isolated

structure is subjected to Koyna earthquake. Further, the responses are slightly sensitive to the variation of coefficient of friction, when the same structure is subjected to the El-Centro earthquake excitation.
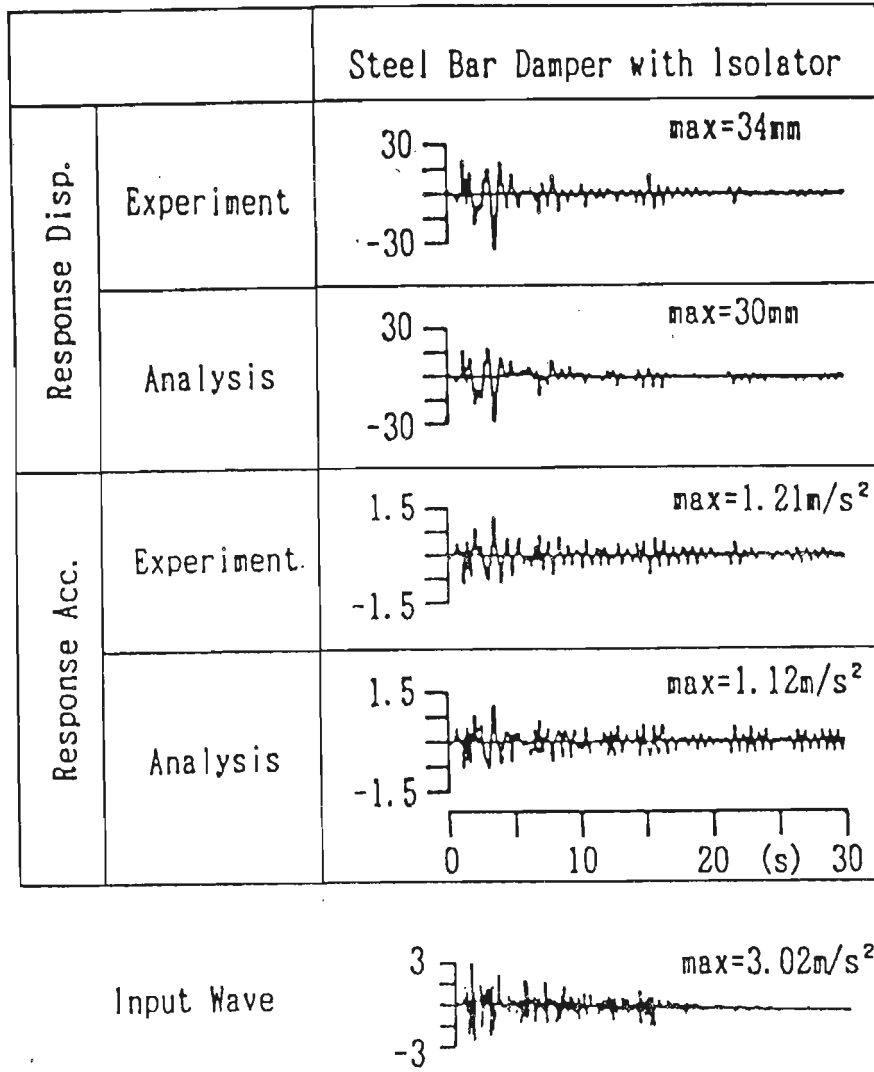
Figures 5.25 nd 5.26 a comparison of show the variation of responses of building supported over three different isolation system with post yielding period T_p under Koyna and El-Centro excitations respectively. In practical range of isolated period (1.5 sec to 2.5 sec) the behaviour of LRB and EDF isolation system are very close to one another under Koyna excitations and this is because of the fact that very little slip takes place in the latter bearing. Base displacement spectra for LLRB is lying at lower level than that of the LRB and EDF isolation system, while the base acceleration, roof acceleration and roof deflection spectra of the same are lying at higher level when compared with that of the other isolated systems under Koyna excitation. Behaviour of EDF bearing under El-Centro excitation is quite different from that of LRB and this is because of the fact that substantial amount of slip takes place in this bearing which provides additional safety. Level of maximum base acceleration, maximum roof acceleration and maximum roof deflection are least for EDF bearing, while maximum total base displacement is on the higher side in the practical range of isolated period. The level of responses for LLRB are similar also under El-Centro excitation.

5.6 Concluding Remarks

In this chapter, behaviour of a three storeyed r.c. shear frame building supported over P-F system, LRB, LLRB and EDF isolator subjected to Koyna (Long.) and El-Centro (N-S) accelerogram have been studied. The bilinear hysteretic behaviour of LRB and LLRB have been idealized by equivalent linear stiffness and damping factor, while frictional behaviour of sliding systems have beenidealized by Coulomb's rigid plastic model. Responses of the building have been obtained by idealizing the building as (1) rigid body model (2) lumped mass model with one dof per floor. On the basis of the detailed analysis of responses and discussion made in the previous section following conclusions are drawn:

o   Analytical responses obtained from analytical model and solution algorithm presented in this Chapter are in good agreement with the analytical and experimental responses reported in literature.

o   Base displacement histories obtained from rigid body model for LRB, LLRB and EDF bearing give quite good estimate as compared to that obtained from lumped mass model. For P-F isolation system the pattern of displacement histories obtained from rigid body model is same as that obtained from lumped mass model but level of displacements are different. Base acceleration histories of structure obtained from rigid body model give lower level of acceleration as compared to that obtained from the second analytical model.

o   In the responses of structure isolated by this system, energy containing frequencies are widely spread, because P-F isolation system can not filter out high frequency components of earthquake motion.

o   LRB system results smooth acceleration response histories and it is because of the fact that it filter out high frequency components effectively.

o   Presence of lead core in the LLRB reduces bearing displacement but the contribution of higher modes to the response of the structure increases.

o   EDF isolation system results lowest level of acceleration transmitted to the structures but higher mode contributions increases slightly due to small amount of slip in the sliding interface. Displacement in LRB of this system is lower but total displacement is found to be more than that in LRB alone.

o   For Koyna type of high frequency accelerogram EDF bearing behaves as LRB in the practical range of T_p but it provides additional safety for El-Centro types of motions.

o   EDF isolation system is not sensitive to the coefficient friction under Koyna type of earthquake excitations, while the same is slightly sensitive to the same under the El-Centro types of motion in the practical range of time period T_{eq} .
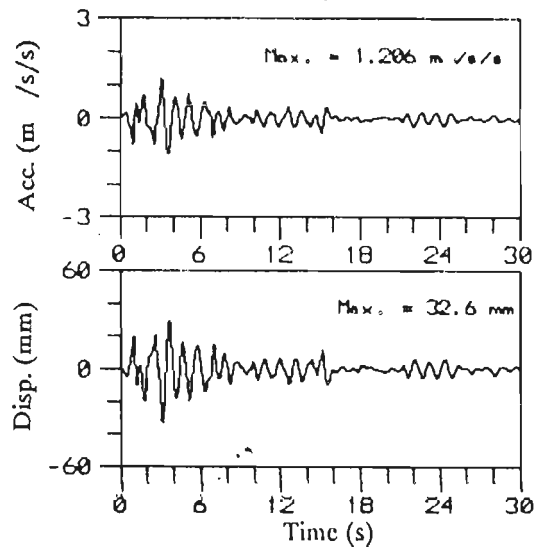
94

(a)

		Steel Bar Damper with Isolator
Response Disp.	Experiment	30 / -30 max=34mm
	Analysis	30 / -30 max=30mm
Response Acc.	Experiment	1.5 / -1.5 max=1.21m/s²
	Analysis	1.5 / -1.5 max=1.12m/s²

0　　10　　20 (s) 30

Input Wave   3 / -3   max=3.02m/s²

(b)

Max. = 1.206 m/s/s

Max. = 32.6 mm

Time (s)

Fig.5.7 Response of 1/3rd Scale Model Isolated by LRB with
　　　Steel Bar Damper: (a) Measured and Computed Response
　　　obtained by Suzuki et al.(1992) and (b) Computed
　　　Response of Present Study　　95

(a)

Max. = 0.127g

Absolute Acceleration (g)

Time (s)

(a)

Transfer Function

Frequency (Hz)

(b)

Max. = 0.138g

Absolute Acceleration (g)

Time (s)

(b)

Transfer Function
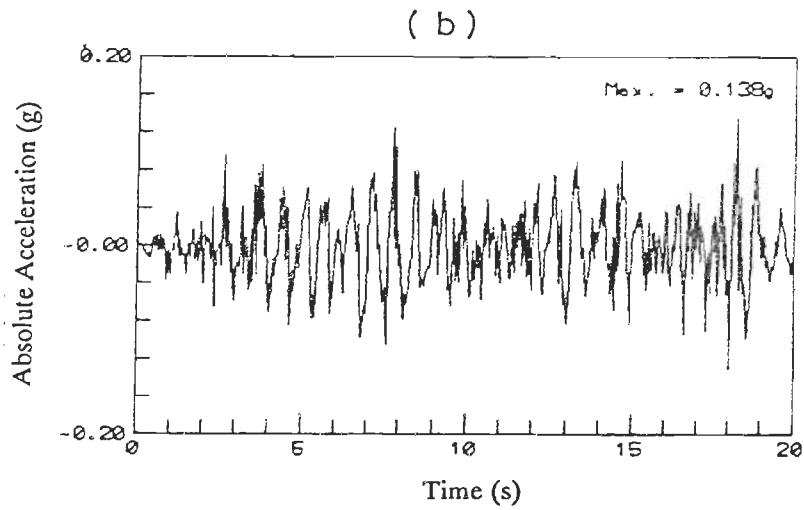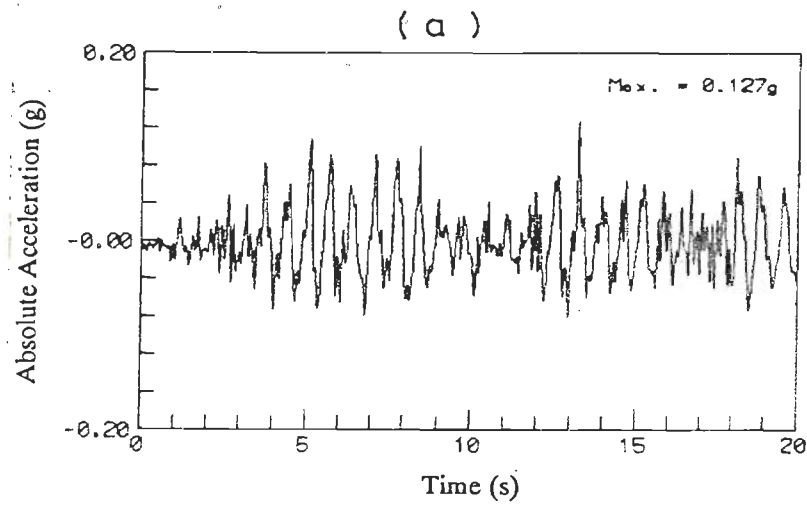
Frequency (Hz)

Fig.5.8 Absolute Roof Acceleration Histories
of 1/6th Scale Model: (a) Experimental
and (b) Simulated
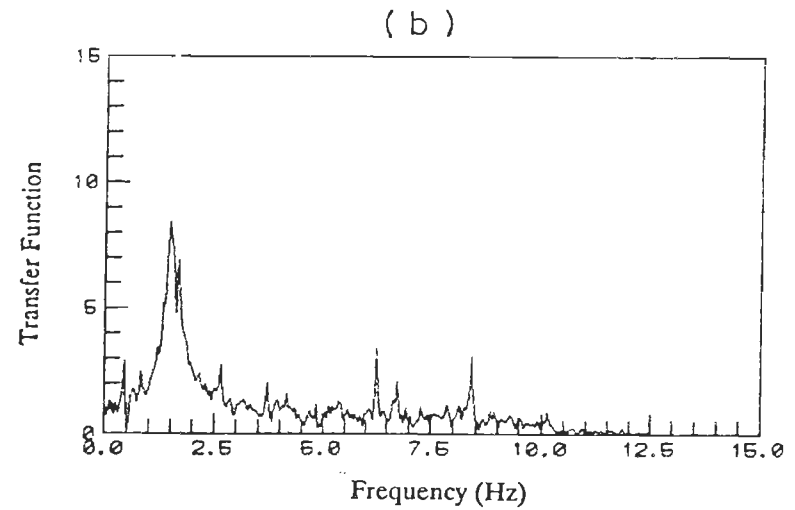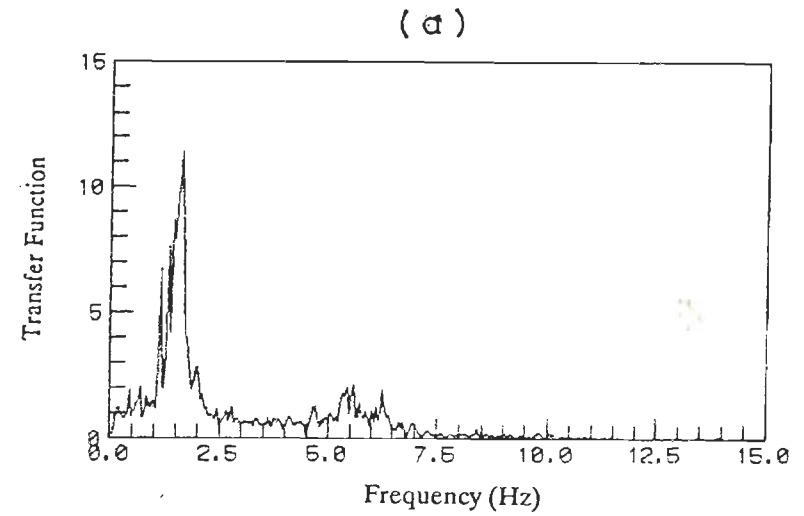
Fig.5.9 Transfer Function vs Frequency Plot
of 1/6th Scale Model: (a) Experimental
and (b) Simulated

Plan

Elevation

500 KN

575 KN

575 KN

575 KN

3600

3600

3600

6000

6000

6000

6000

6000

2 - 20 Ø

150

450

420

mid span

7 - 20 Ø

420
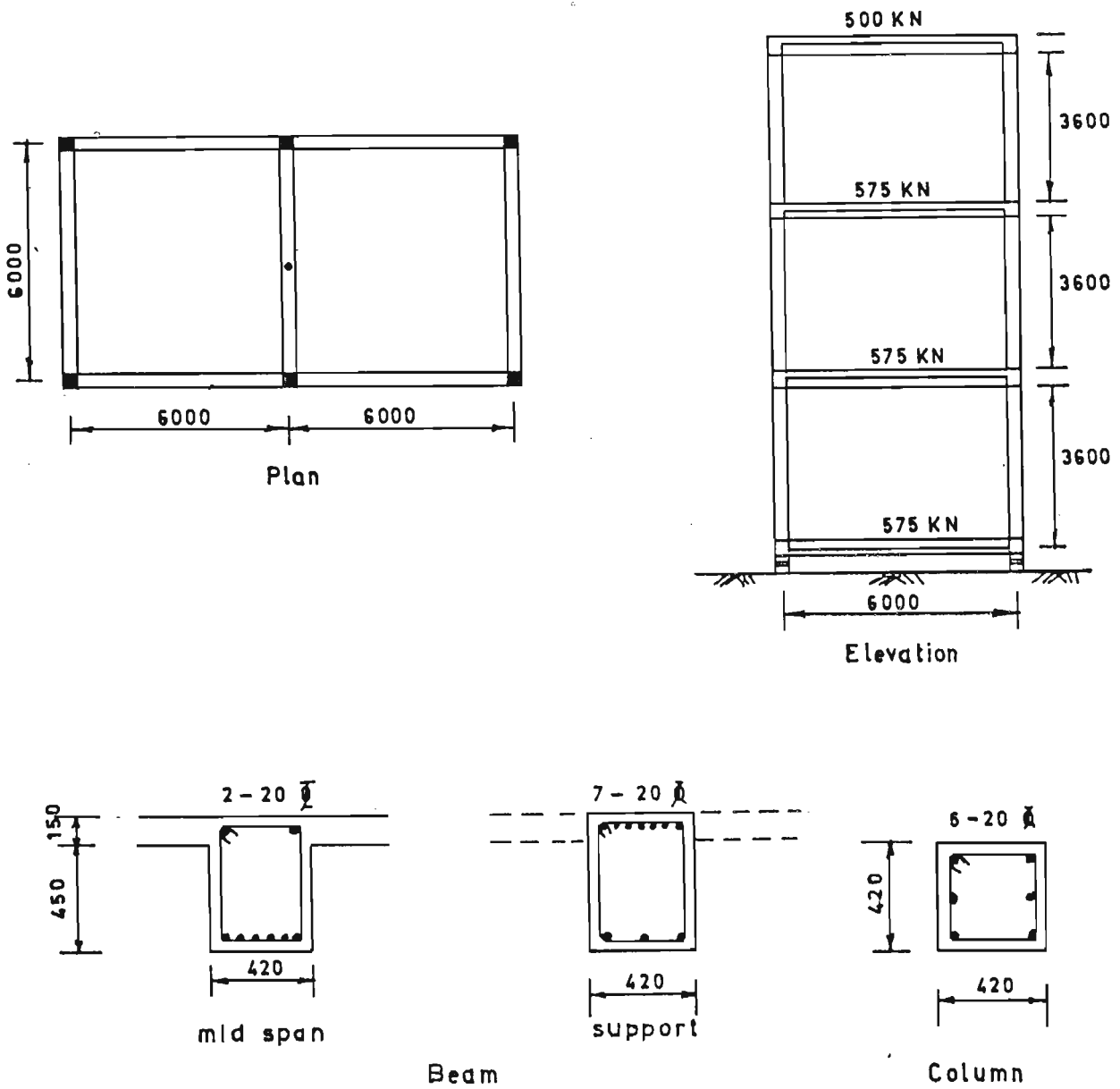
support

Beam

6 - 20 Ø

420

420

Column

Fig.5.10 Details of the Three Storeyed R.C. Building
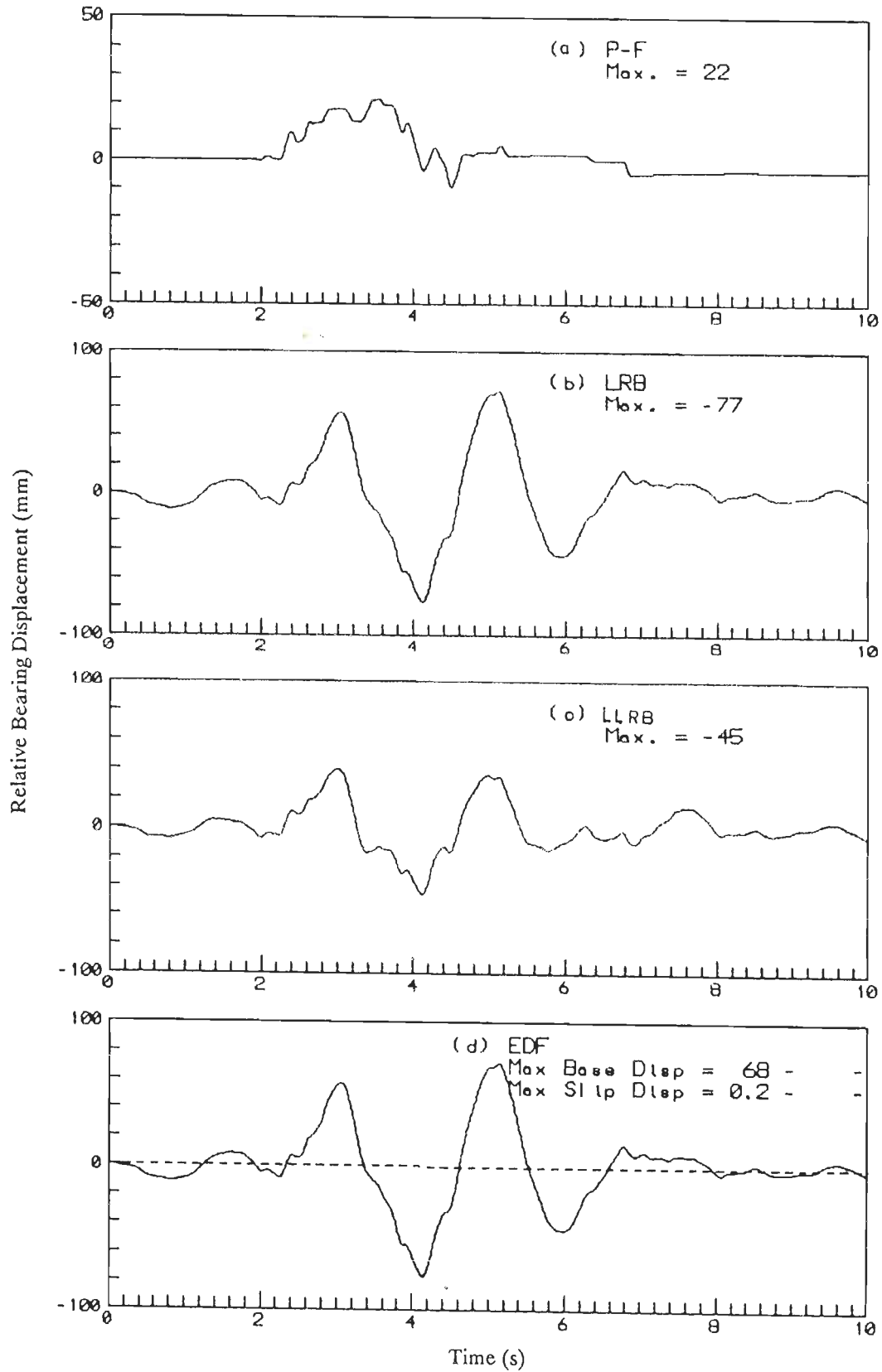
Rigid Body Model

Fig.5.11 Bearing Displacement History for Different Base Isolation
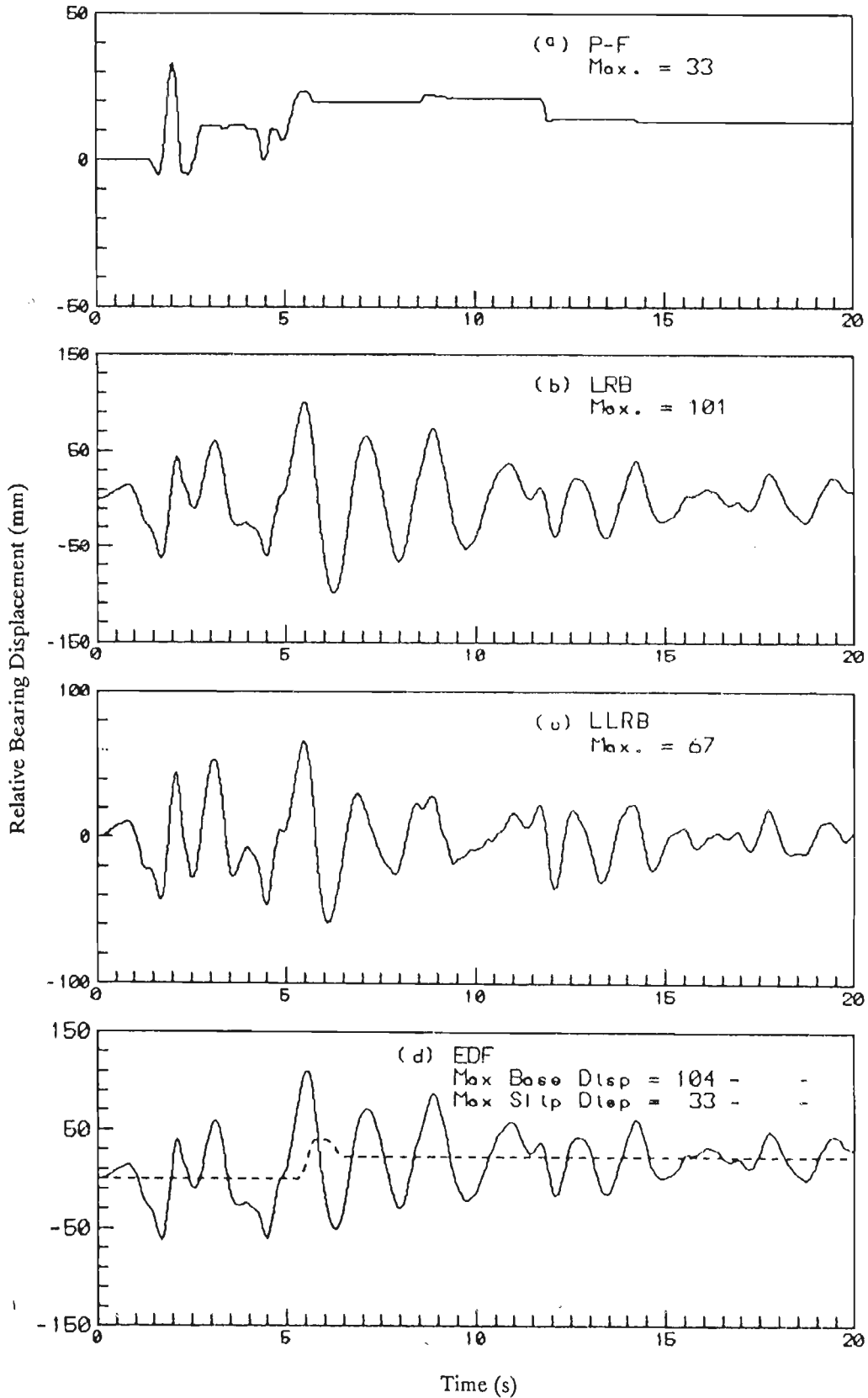Systems Subjected to Koyna (L) Earthquake

Rigid Body Model

Fig.5.12 Bearing Displacement History for Different Base Isolation
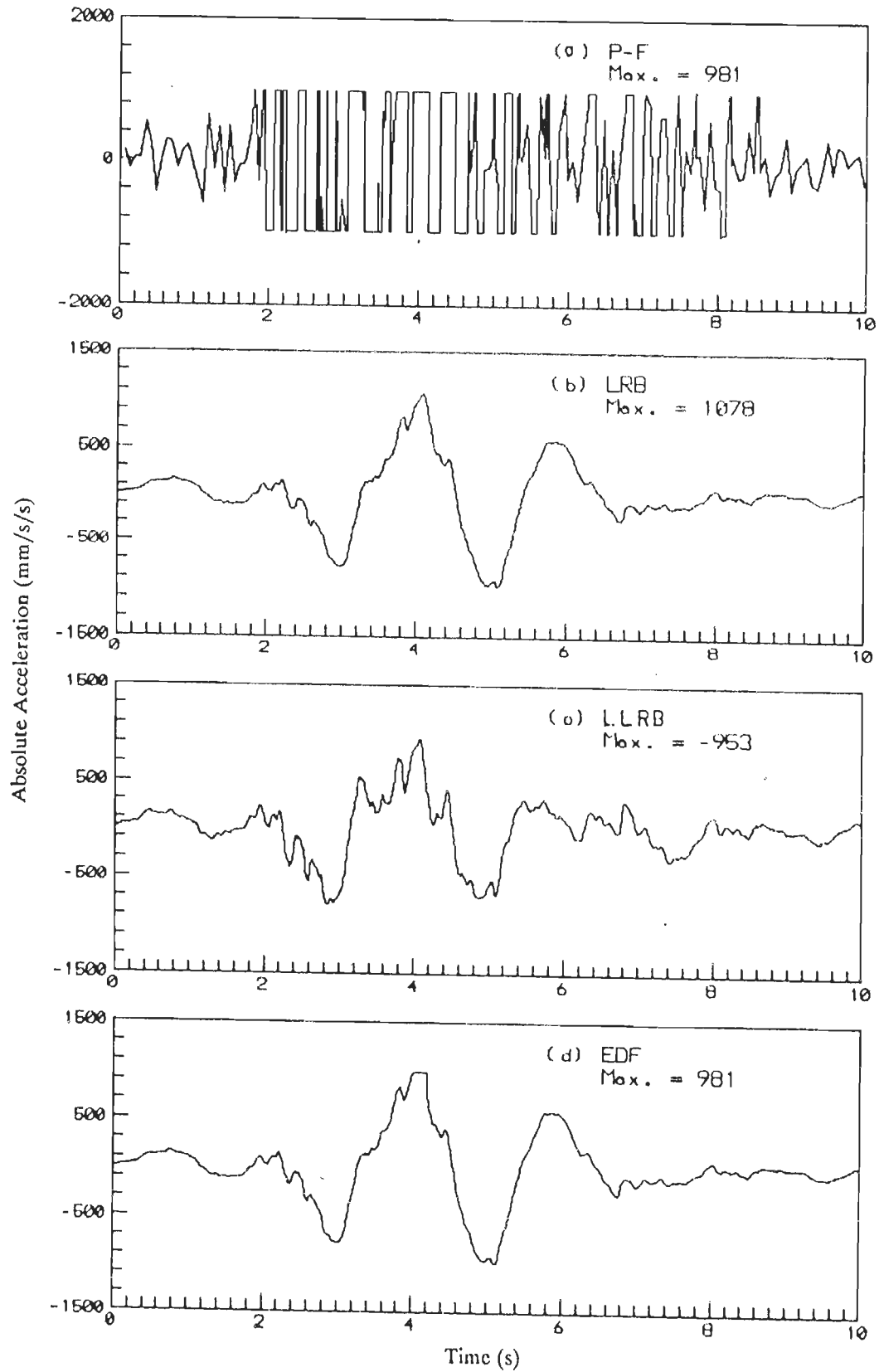Systems Subjected to El-Centro (N-S) Earthquake

99

Fig.5.13 Absolute Acceleration History of Rigid body for Different
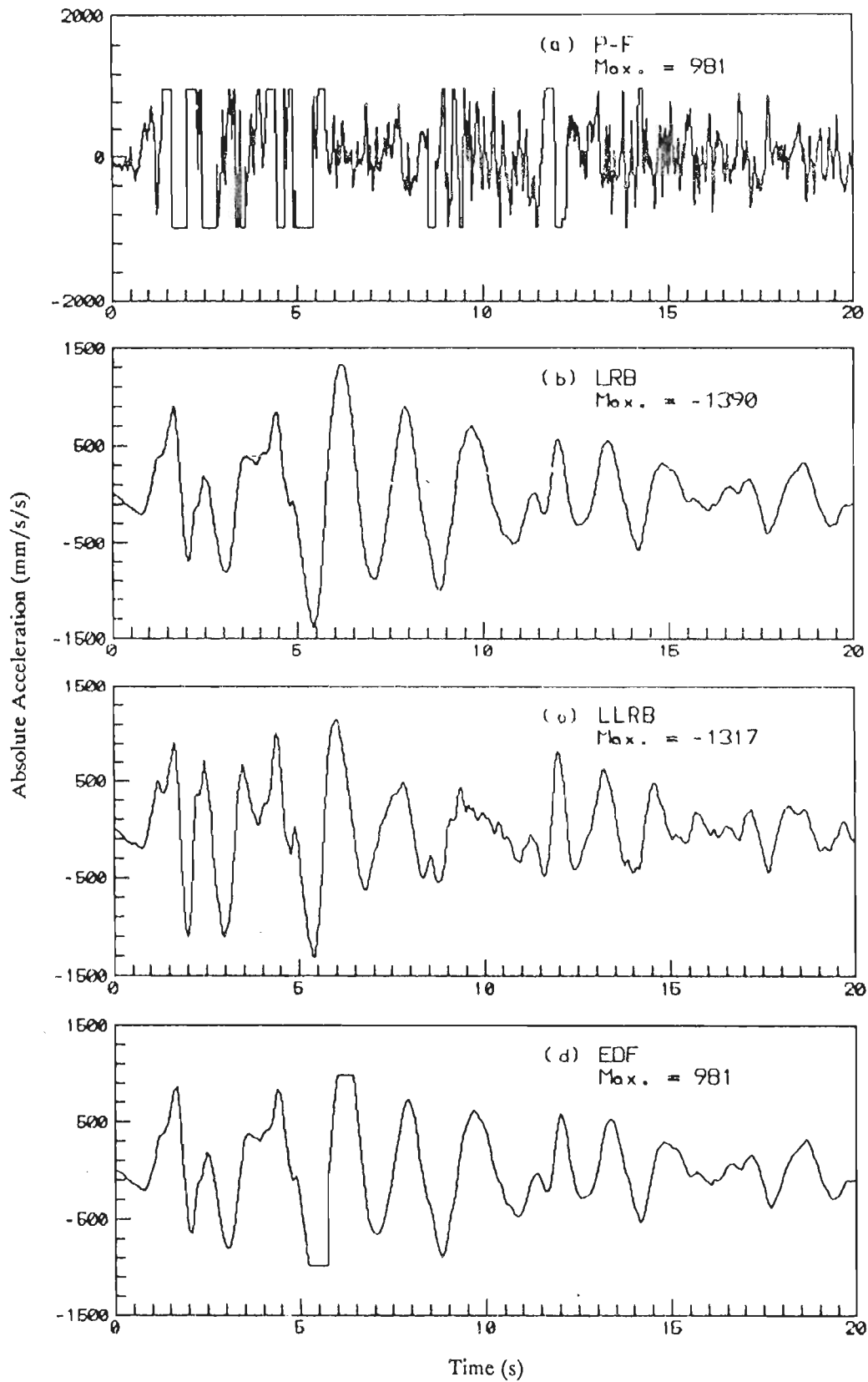Base Isolation Systems Subjected to Koyna (L) Earthquake

Fig.5.14 Absolute Acceleration History of Rigid body for Different Base
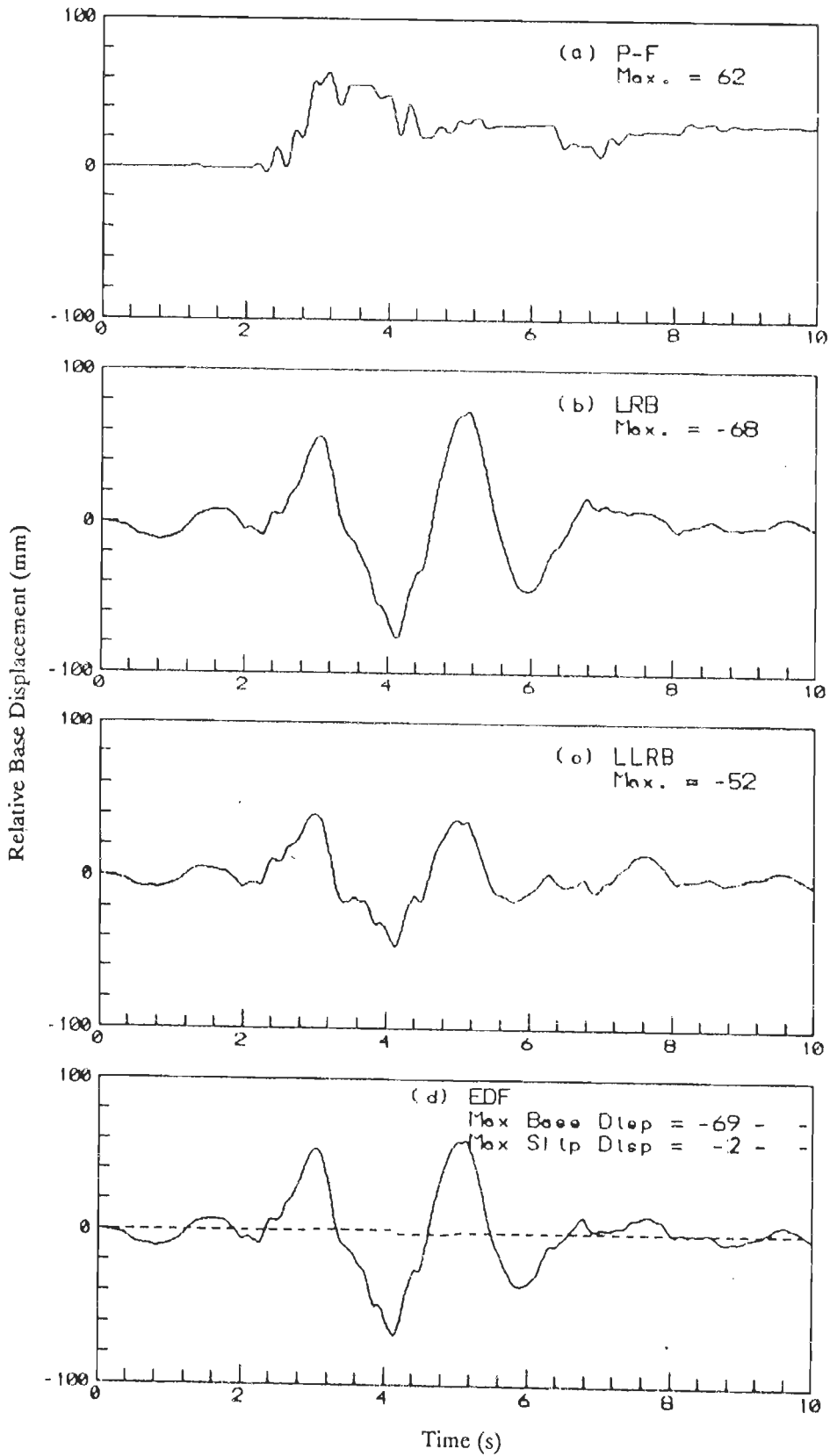Isolation Systems Subjected to El-Centro (N-S) Earthquake

Lumped Mass Model

Fig.5.15 Base Displacement History for Different Base Isolation
Systems Subjected to Koyna (L) Earthquake

102

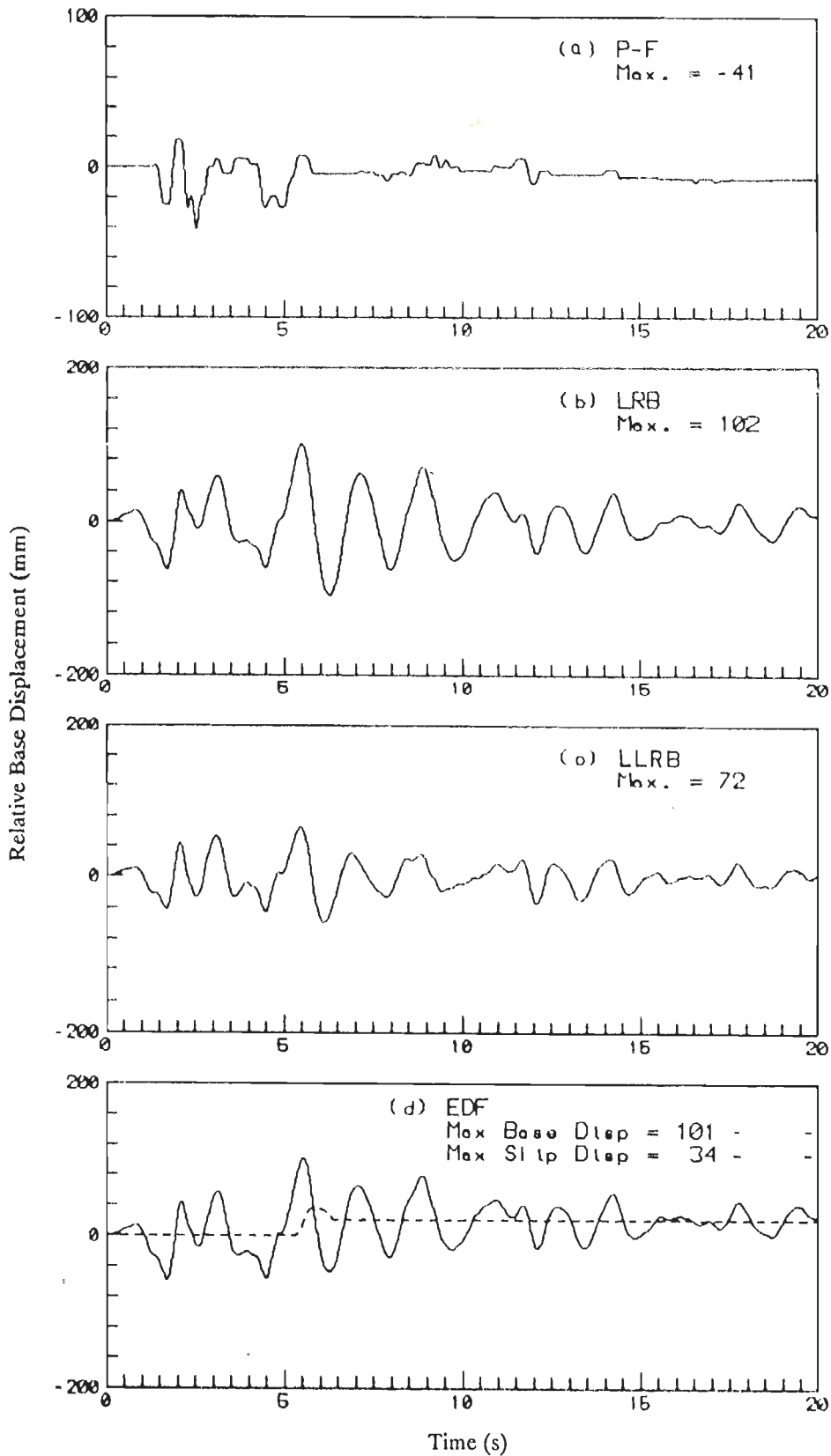Fig.5.16 Base Displacement History for Different Base Isolation
Systems Subjected to El-Centro (N-S) Earthquake

Fig.5.17 Absolute Base Acceleration History for Different Base
Isolation Systems Subjected to Koyna (L) Earthquake

Fig.5.18 Absolute Base Acceleration History for Different Base
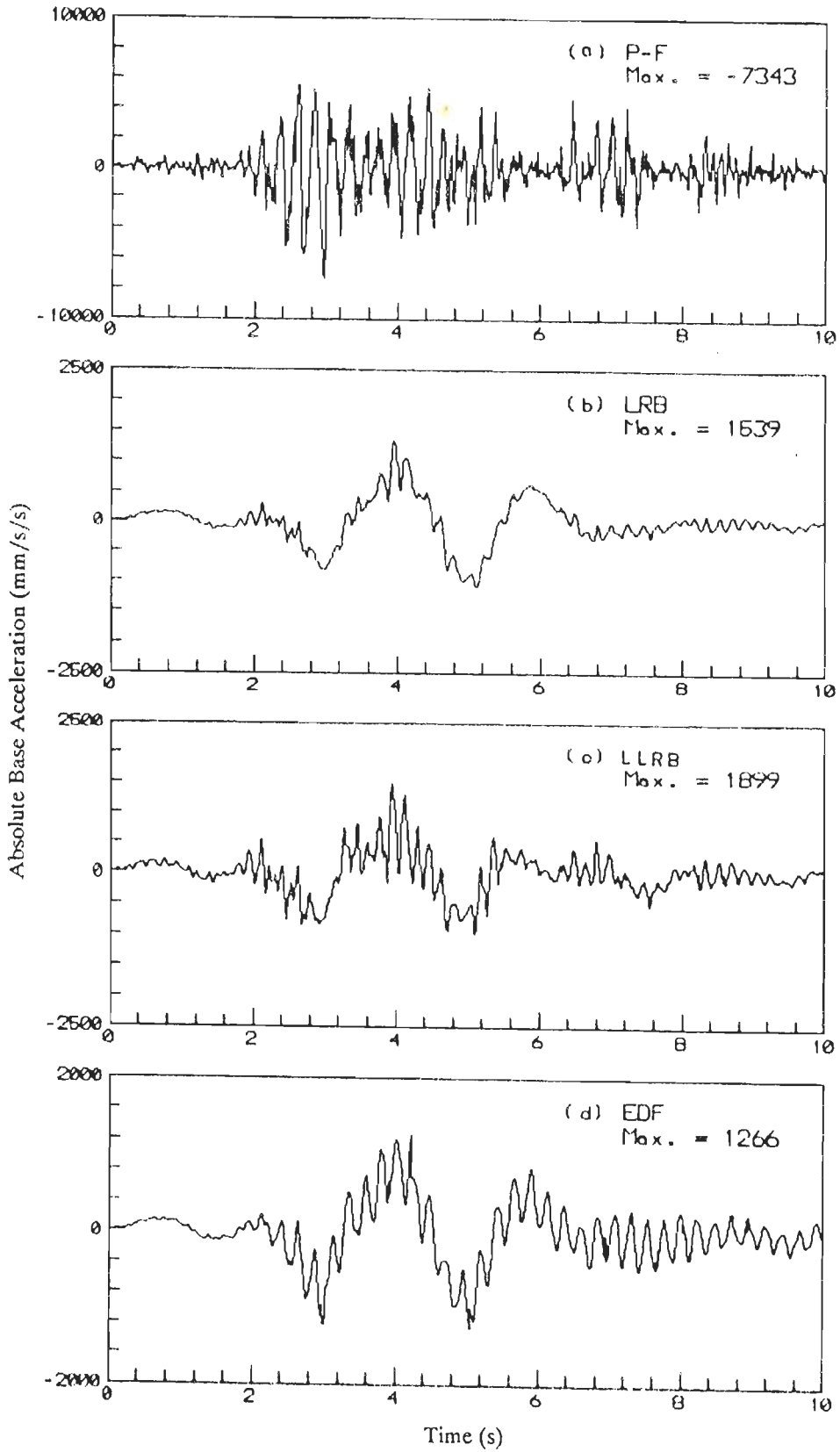Isolation Systems Subjected to El-Centro (N-S) Earthquake
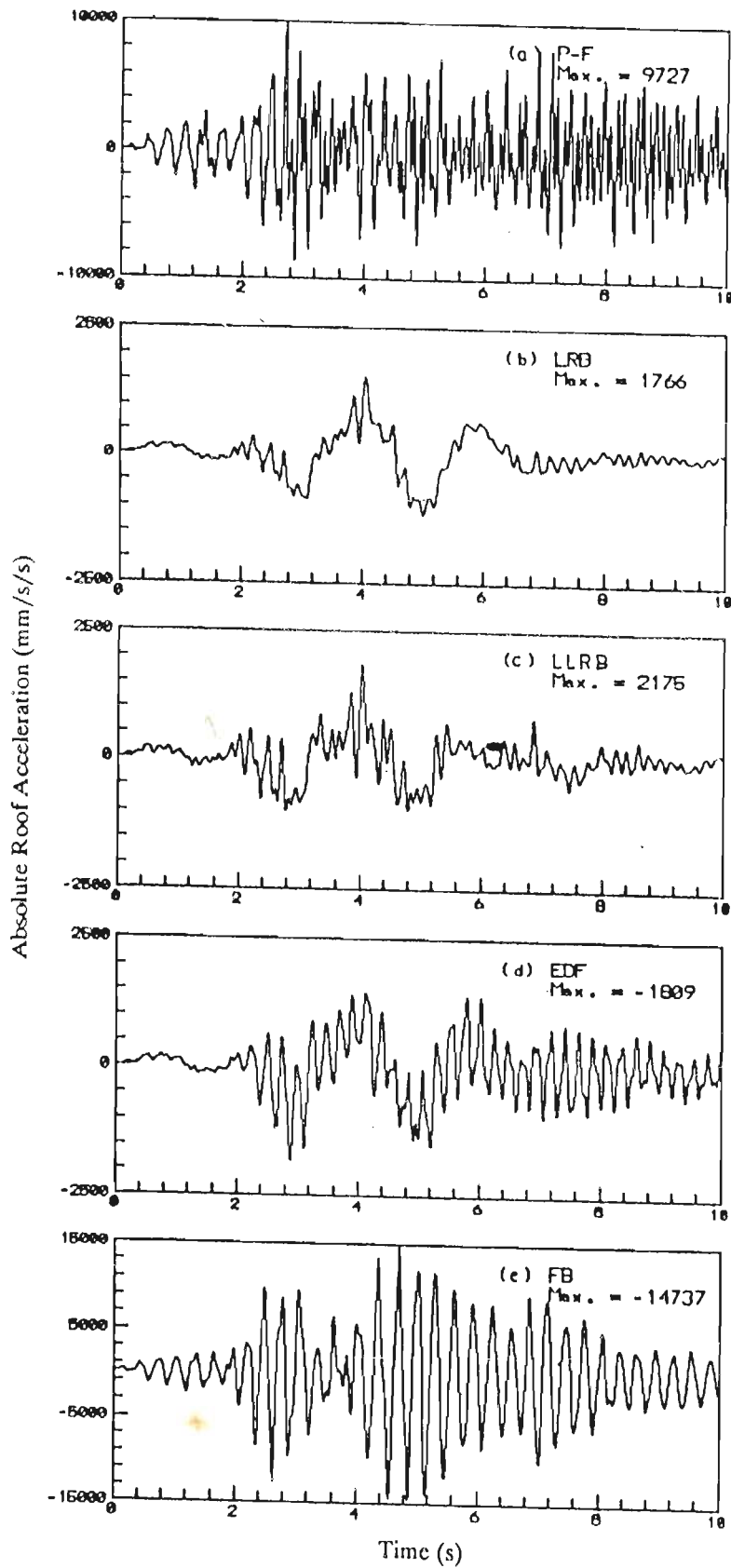
Fig.5.19 Absolute Roof Acceleration History for Different Base
Isolation Systems Subjected to Koyna (L) Earthquake

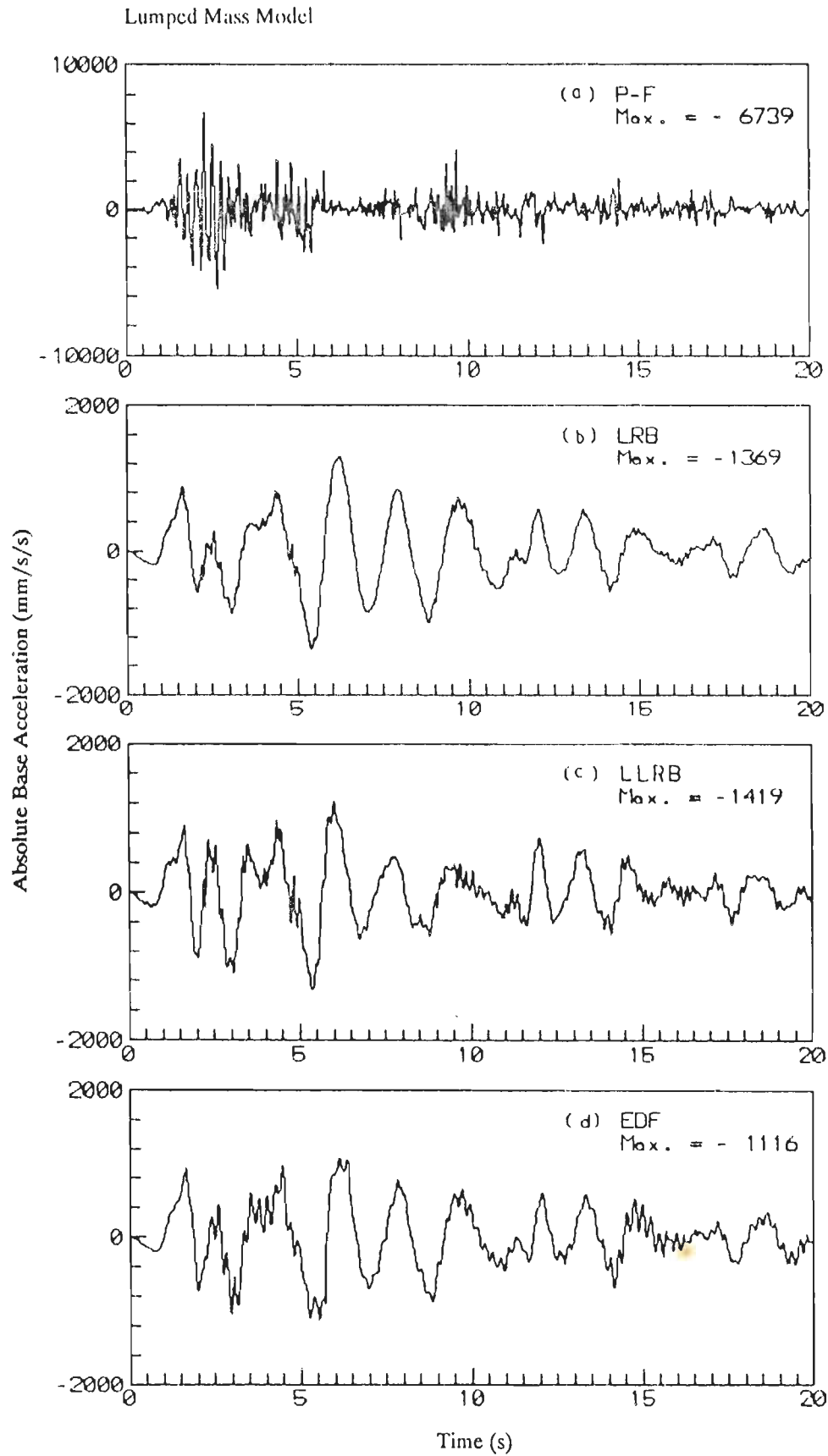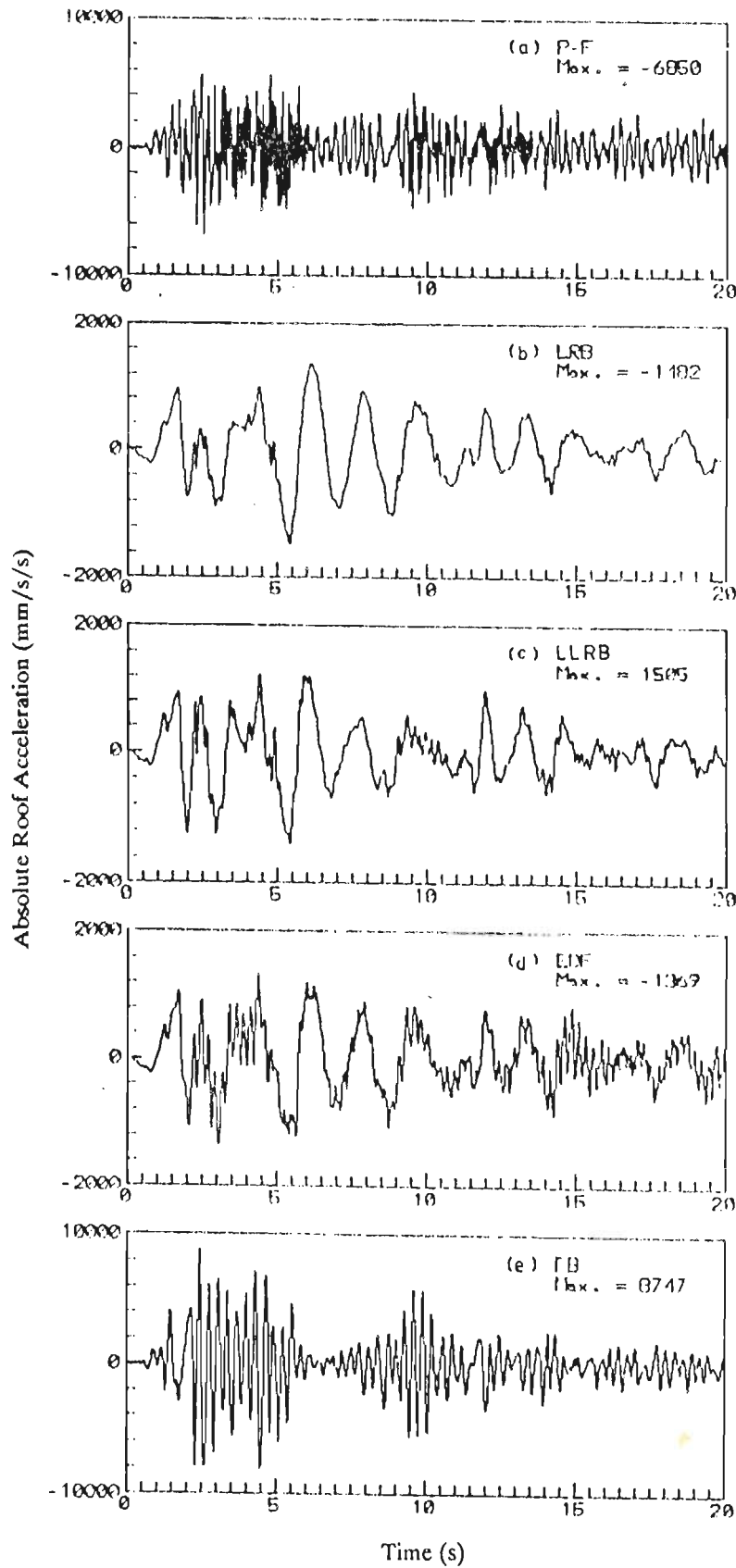Fig.5.20 Absolute Roof Acceleration History for Different Base Isolation Systems Subjected to El-Centro (N-S) Earthquake
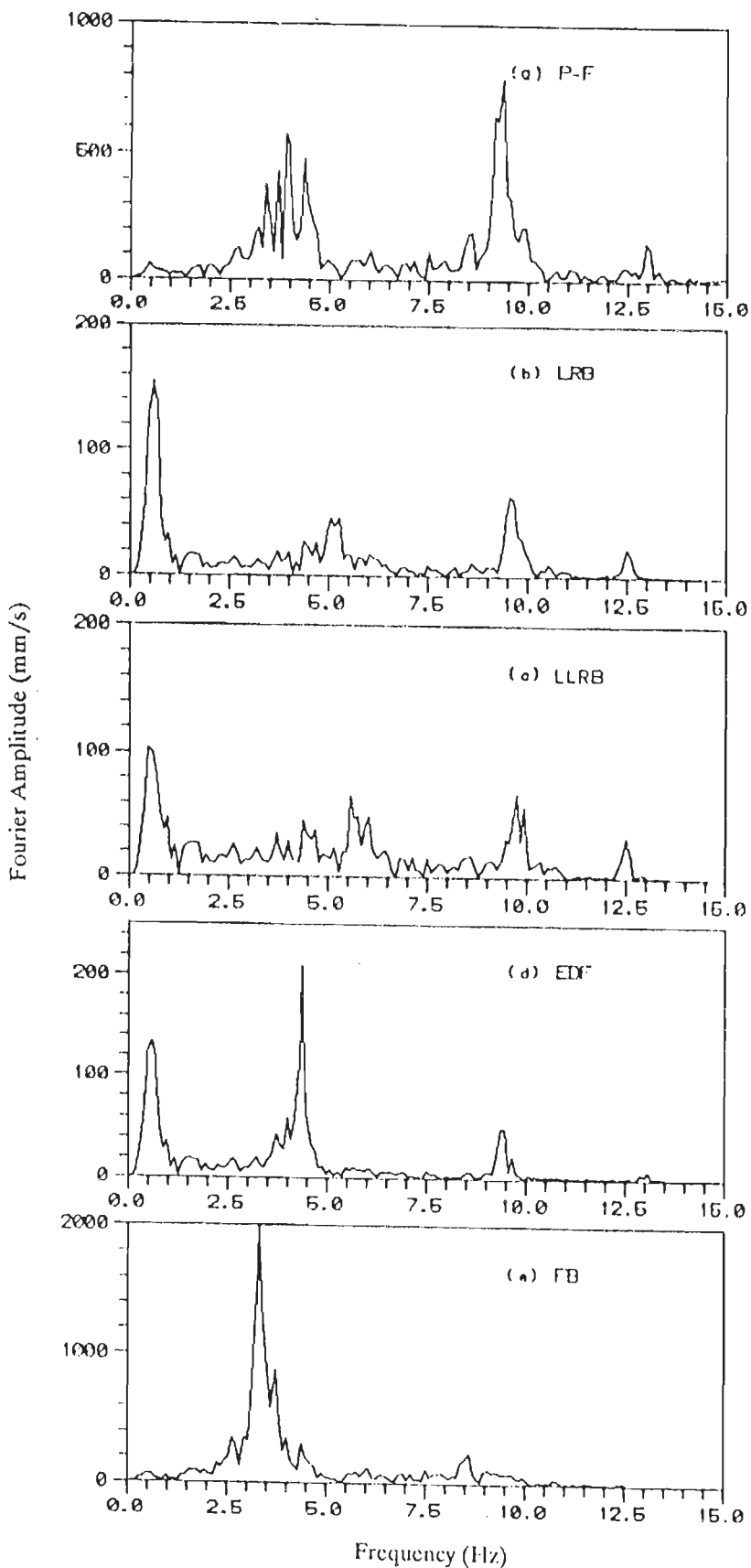
Fig.5.21 Fourier Amplitude Spectra of Roof Acceleration for Different Isolation Systems and Fixed Base Structure Subjected to Koyna (L) Earthquake
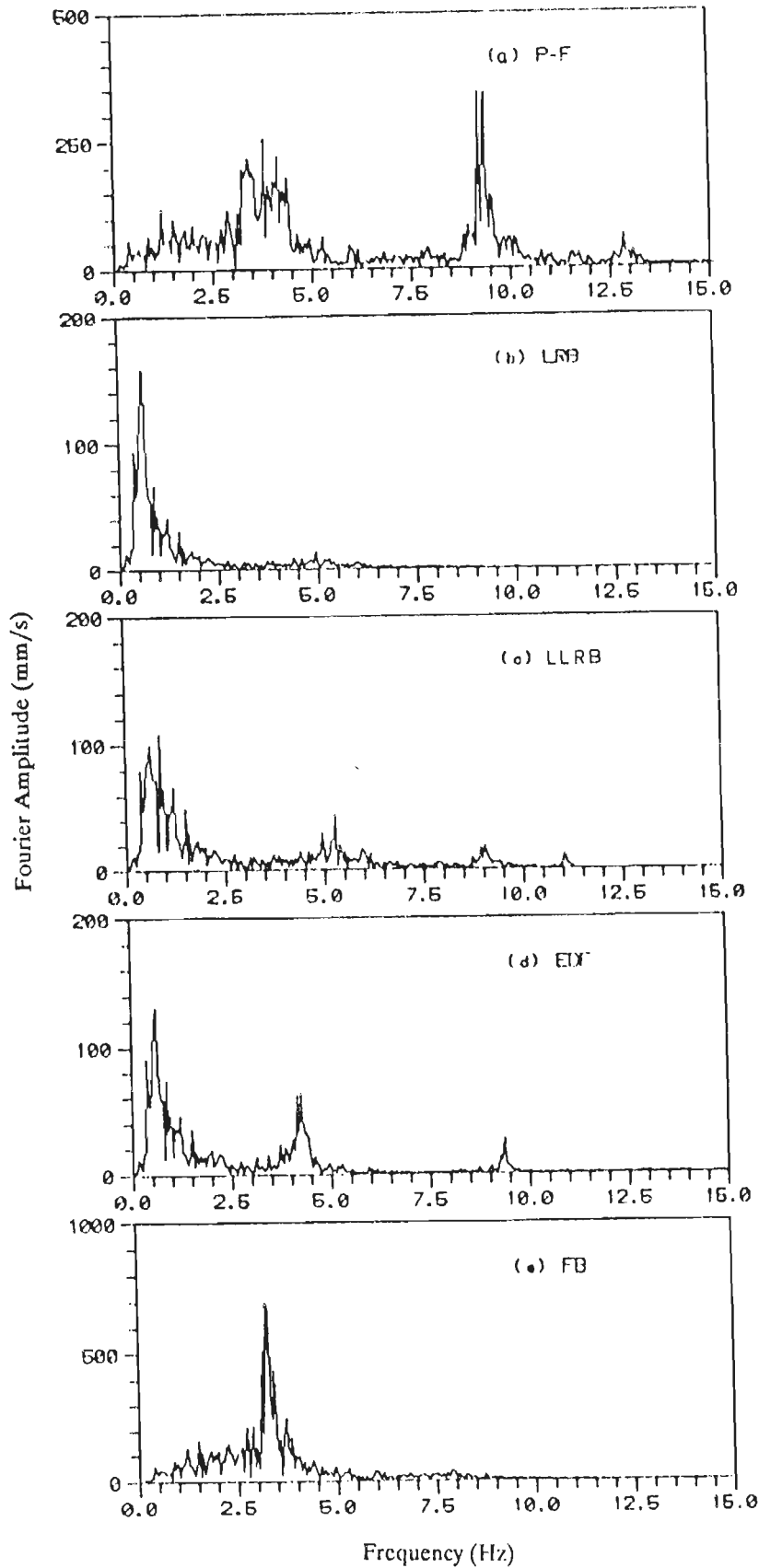
Fig.5.22 Fourier Amplitude Spectra of Roof Acceleration for Different Isolation Systems and Fixed Base Structure Subjected to El-Centro (N-S) Earthquake

Lumped Mass Model
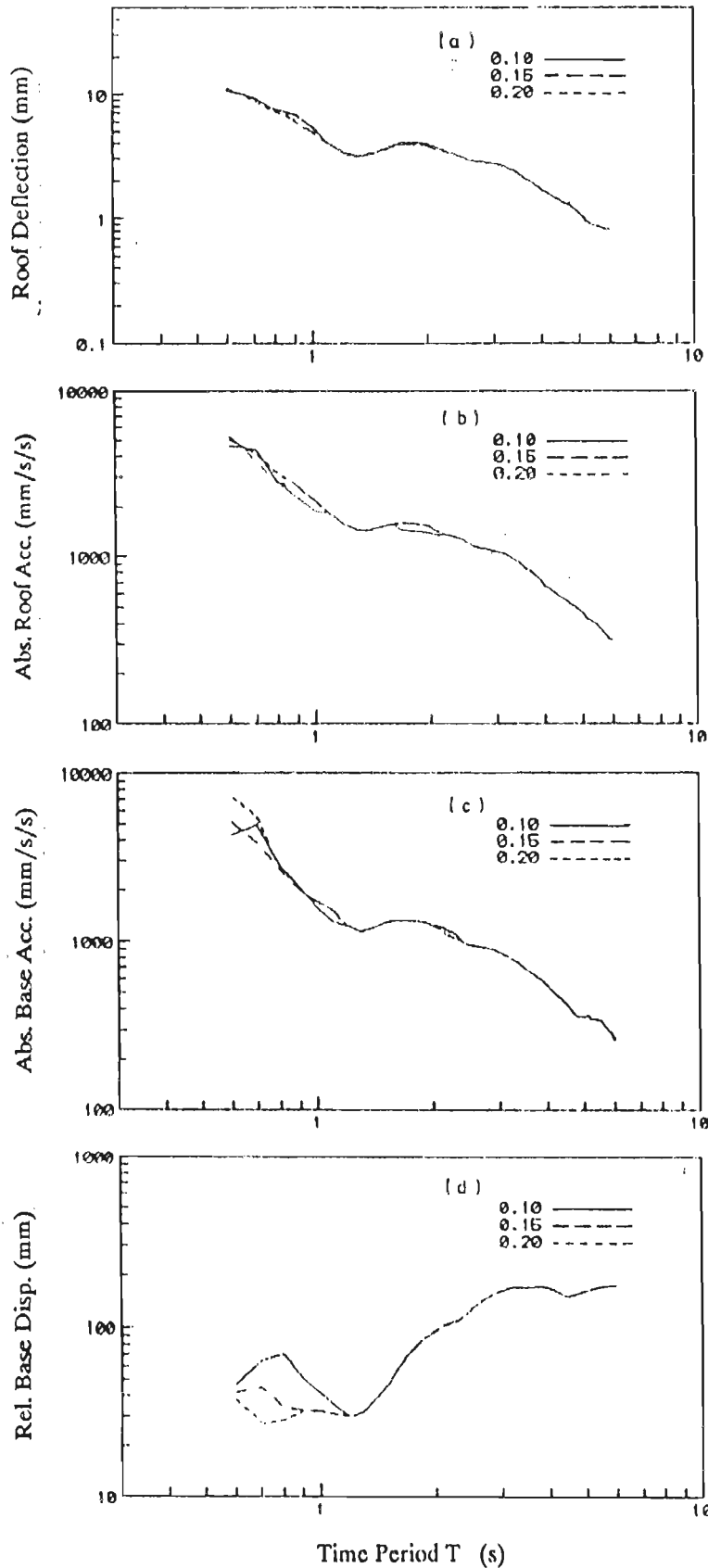
Fig.5.23 Variation of Response of Structure Isolated by EDF System
with Teq Subjected to Koyna (L) Earthquake: (a) Relative
Roof Deflection, (b) Absolute Roof Acceleration, (c) Absolute
Base Acceleration and (d) Relative Base Displacement

110

Lumped Mass Model

Fig.5.24 Variation of Response of Structure Isolated by EDF System with T_{eq} Subjected to El-Centro (N-S) Earthquake: (a) Relative Roof Deflection, (b) Absolute Roof Acceleration, (c) Absolute Base Acceleration and (d) Relative Base Displacement

Lumped Mass Model

Fig.5.25 Variation of Response of Structure Isolated by LRB, LLRB and
EDF System with T_D Subjected to Koyna (L) Earthquake: (a)
Relative Roof Deflection, (b) Absolute Roof Acceleration, (c)
Absolute Base Acceleration and (d) Relative Base Displacement

Fig.5.26 Variation of Response of Structure Isolated by LRB, LLRB and EDF System with T_D Subjected to El-Centro (N-S) Earthquake: (a) Relative Roof Deflection, (b) Absolute Roof Acceleration, (c) Absolute Base Acceleration and (d) Relative Base Displacement

CHAPTER-6

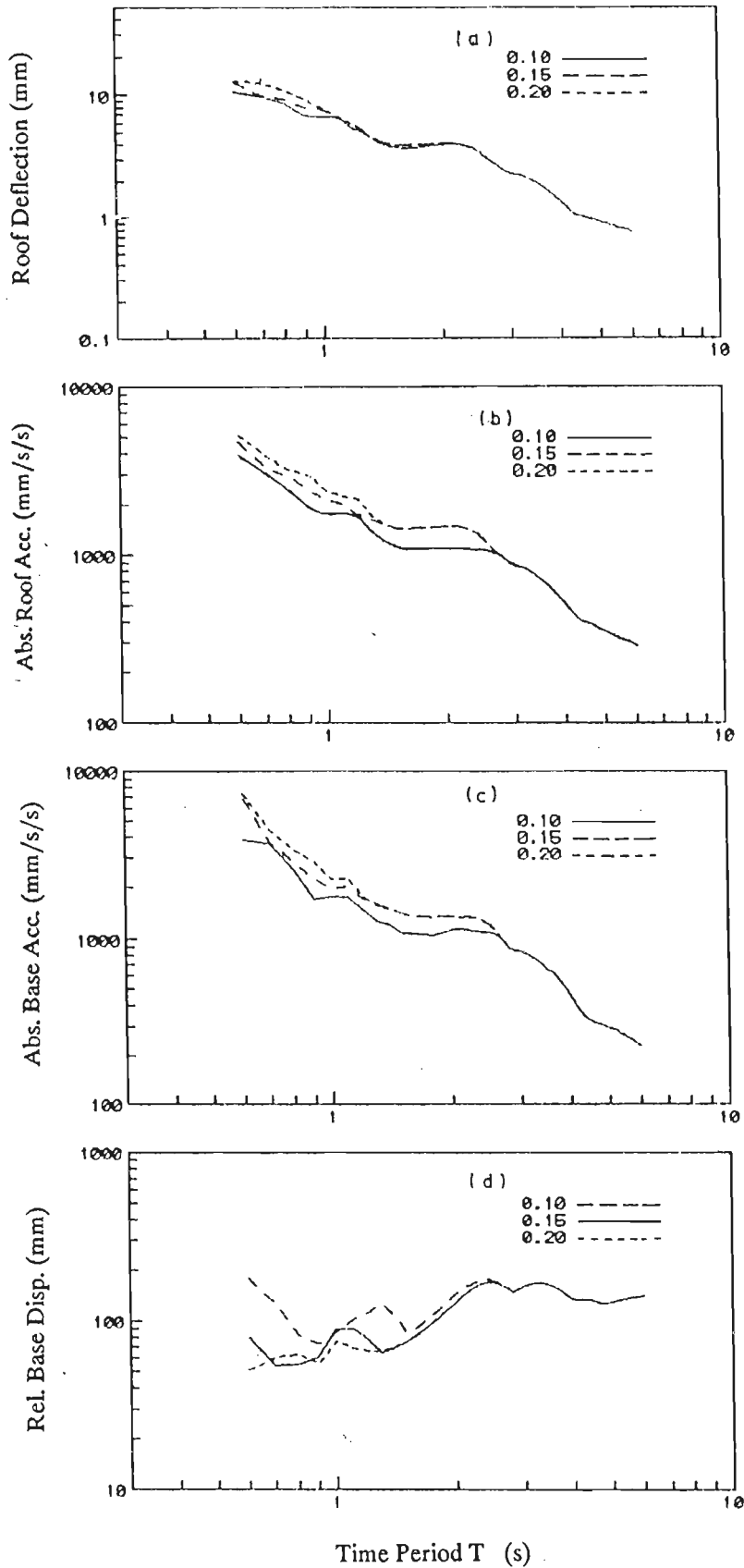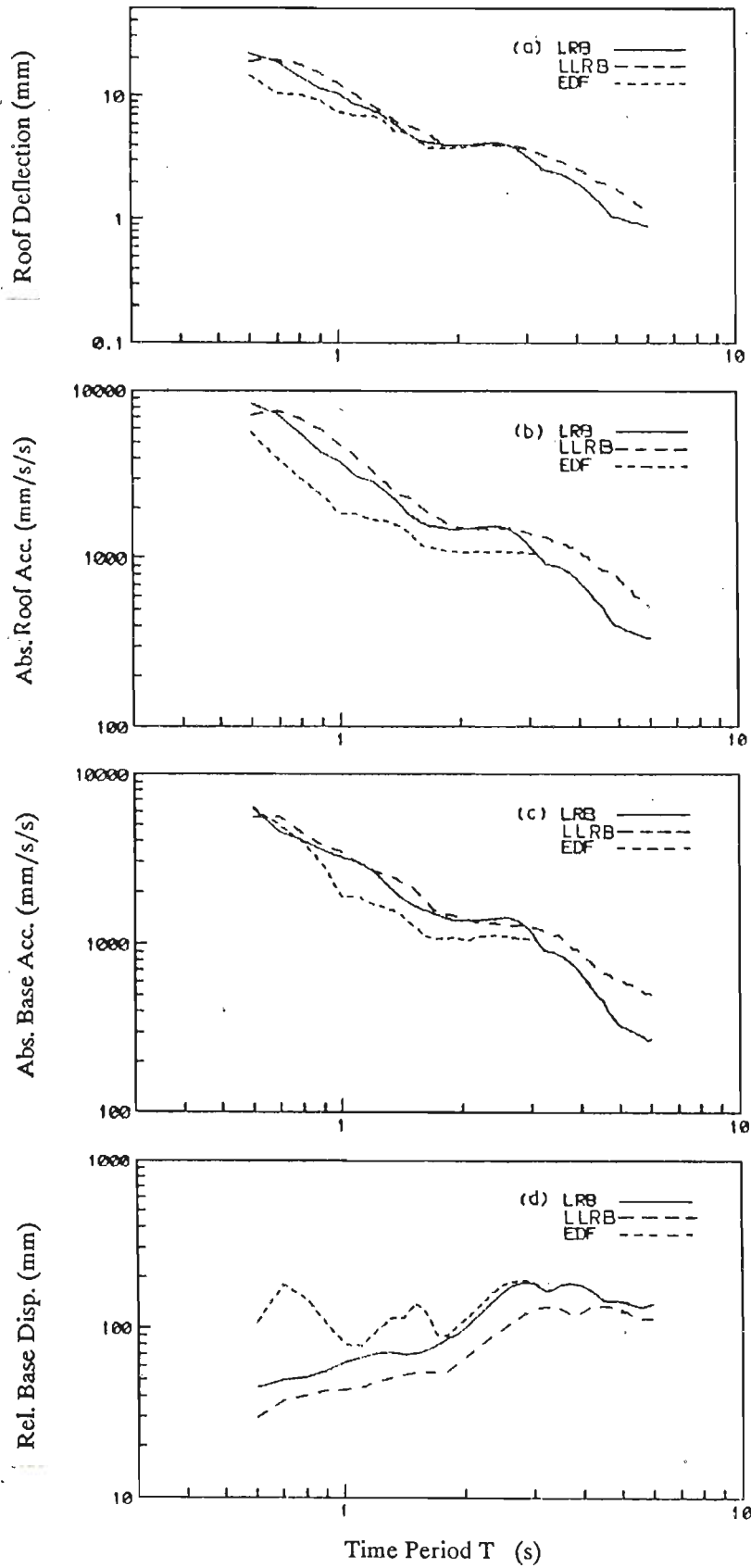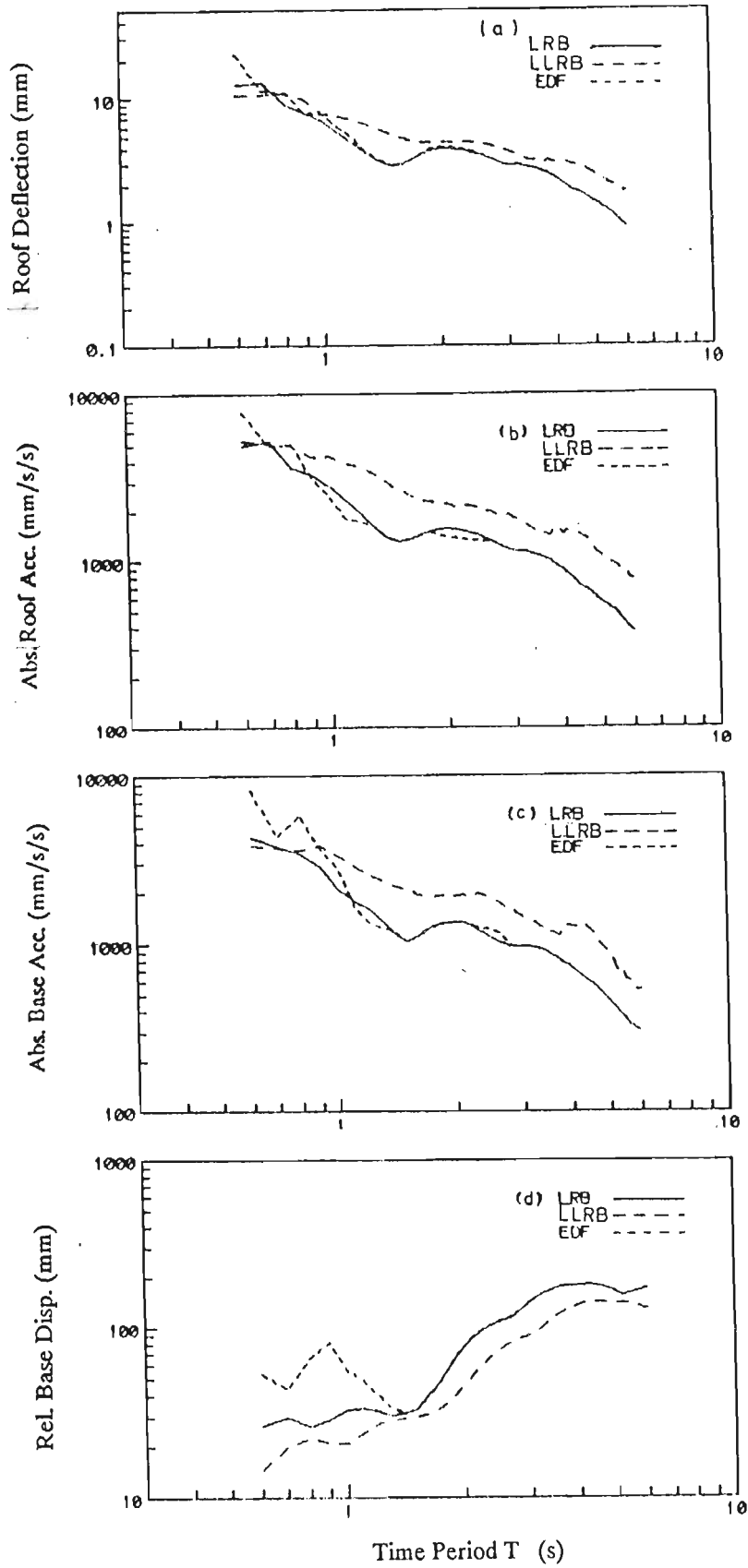# BASE ISOLATED BUILDINGS SUBJECTED TO GENERAL PLANE MOTION

6.1 Introduction

In this chapter, the response of medium-rise r.c. shear type buildings supported over either P-F bearing, LRB, LLRB or EDF isolation system subjected to general plane motion are studied. The floors and basement slab of the building are assumed to be infinitely rigid in plane. The superstructure of the building is idealized as an elastic 3-D model with 3 dof per floor. The isolation bearings are modelled taking into account their non-linear characteristics.

Seismic isolation systems developed so far, comprise of mainly, LRBs that can be represented by models with bilinear characteristics or sliding bearings that can be represented by models with rigid plastic characteristics. When isolated structure experiences multidirectional motion due to asymmetry in the structure and/or due to multidirectional excitation, it becomes very difficult to compute the response by conventional models. In the present study, a hysteretic model proposed by Bouc(1967), and subsequently developed by Wen(1976) will be used. Hysteretic force in the LRB and LLRB was computed by expression proposed by Wen(1980). While that in sliding isolation systems were computed using modified visco-plastic model developed by Constantinou et al. (1990). This model is based on extensive series of tests on teflon/stainless steel sliding interface. Teflon undergoes a small elastic shear deformation (0.1 mm to 0.2 mm) before sliding commences at the interface. Although, this model can not reproduce rigid plastic behaviour, the small shear deformation of the teflon renders a finite but high elastic stiffness to the hysteretic loop, which can be reproduced by the hysteretic model.

A unified solution algorithm have been developed for computation of response of structure isolated by various isolation systems, subjected to general plane motion. This solution algorithm is based on Newmark's method in predictor-corrector form. The forces mobilized in the non-linear elements of different isolation system are computed from close form solution of stiff differential equation of hysteretic model. The analytical model and the solution algorithm have been implemented in the computer program ISODYN-3D. Comparison with experimental results and results from other numerical schemes are presented to verify the accuracy of simple solution algorithm developed in the present study.

6.2 Non-linear Hysteretic Model of Isolation Systems

Relative bearing displacement and velocity in X and Y directions with respect to ground are designated by u_{b1} , u_{b3} and $\dot{u}_{b1}$, $\dot{u}_{b3}$ respectively. The isolation bearings are considered to be rigid in the vertical direction. Therefore, the instantaneous direction of displacement 'θ_b' and velocity '$\dot{U}_b$' are given by

$$\theta_b = \tan^{-1}\left(\frac{\dot{u}_{b3}}{\dot{u}_{b1}} \right) \qquad \dots\dots(6.1)$$

$$\dot{U}_b = (\dot{u}_{b1}^2 + \dot{u}_{b3}^2)^{1/2} \qquad \dots\dots(6.2)$$

The direction of the resultant force at the bearing is opposite to the direction of motion. The forces mobilized in the non-linear elements of different isolation systems considered in the present study, are given as follows:

6.2.1 Sliding System: Forces mobilized in the sliding interface in two orthogonal direction are expressed as

$$f_1 = \mu_s W z_1 \qquad \dots\dots(6.3a)$$

$$f_2 = 0. \qquad \dots\dots(6.3b)$$

$$f_3 = \mu_s W z_3 \qquad \dots\dots(6.3c)$$

where, W is the total load at the frictional interface, z_1 and z_3 are hysteretic dimensionless constants in X and Y directions respectively and μ_s is the coefficient of sliding friction, which depends on bearing pressure and instantaneous sliding velocity at the sliding interface.

Equation (6.3) is identical to Coulombs's friction force model discussed in the preceding chapter. Here, sign function is replaced by z and it takes values of ± 1 during sliding (yielding) phase. During non-sliding (elastic) phase, the absolute value of z is less than unity.

Constantinou et al.(1990) modelled the coefficient of sliding friction on the basis of extensive experimental work by the following expression

$$\mu_s = \mu_{max} - \Delta\mu \; exp(-a'|\dot{U}_b|)$$ .....(6.4)

where, μ_{max} is the maximum coefficient of friction at large velocity of sliding, $\Delta\mu$ is difference between μ_{max} and sliding value at very low velocity and a' is a constant which takes care of variation of bearing pressure at sliding interface.

6.2.2 Laminated Rubber Bearing: Hysteretic component of restoring force developed in laminated rubber bearing is expressed as

$$f = (1-\alpha) \; Y \; K_e z$$ .....(6.5)

where, K_e is the initial stiffness matrix (3x3) of LRB considering 3 dof of the base, Y is the yield displacement of the bearing, α is the ratio of post yielding to pre yielding stiffnesses and z is the 3x1 vector of hysteretic dimensionless constant.

In addition to this, non-hysteretic component of stiffness provided by rubber/elastomer has also been taken into account. The contribution of torsional moment which develops at the bearing, due to the total torque exerted to the superstructure supported by bearings is insignificant [Constantinou Mokha(1989)]. Therefore, z_2 is considered to be equal to zero.

6.2.3 Lead Rubber Bearing:

Restoring force provided by lead core in the LLRB are expressed as

$$f_1 = \alpha \frac{F_y}{Y} u_{b1} + (1-\alpha) F_y z_1 \qquad \ldots\ldots(6.6a)$$

$$f_2 = 0. \qquad \ldots\ldots(6.6b)$$

$$f_3 = \alpha \frac{F_y}{Y} u_{b3} + (1-\alpha) F_y z_3 \qquad \ldots\ldots(6.6c)$$

where, F_y is the yield force in lead core, Y is the yield displacement, α is ratio of post yielding to pre yielding stiffnesses and z_1 and z_3 are hysteretic dimensionless constants in X and Y directions respectively.

In addition to this, non-hysteretic component of stiffness provided by rubber/elastomer has also been taken into account, while its hysteretic part is neglected as it is very small compared to that provided by the lead core.

The dimensionless hysteretic constants z_1 and z_3 can be calculated from the following coupled differential equations [Park et al.(1986)]

$$Y\dot{z}_1 + \gamma' |\dot{u}_{b1}z_1|z_1 + \beta' \dot{u}_{b1}z_1^2 + \gamma' |\dot{u}_{b3}z_3|z_1 + \beta' \dot{u}_{b3}z_1z_3 - A\dot{u}_{b1} = 0 \quad \ldots(6.7a)$$

$$Y\dot{z}_3 + \gamma' |\dot{u}_{b3}z_3|z_3 + \beta' \dot{u}_{b3}z_3^2 + \gamma' |\dot{u}_{b1}z_1|z_3 + \beta' \dot{u}_{b1}z_1z_3 - A\dot{u}_{b3} = 0 \quad \ldots(6.7b)$$

where, γ', β' and A are the dimensionless constants which govern the general shape of the hysteresis loop and Y represents a displacement quantity. Constantinou and Adane(1987) have shown that when A = 1 and $\beta' + \gamma' = 1$, the model of Eqn.(6.7) reduces to a model of viscoplasticity and in this case Y represents the yield displacement.

The Eqns.(6.7a) and (6.7b) are extension of the one dimensional hysteretic restoring force. The hysteretic behaviour represented by Eqns.(6.7a) and (6.7b) can be illustrated by Fig.6.1(a), which has shown a simple displacement path. In this case the variables in Eqns.(6.7a) and (6.7b) are expressed as

$$z_1 = z \cos\theta_b, \ z_3 = z \sin\theta_b, \ u_{b1} = U_b\cos\theta_b \ \text{and} \ u_{b3} = U_b\sin\theta_b \quad \ldots\ldots(6.8)$$
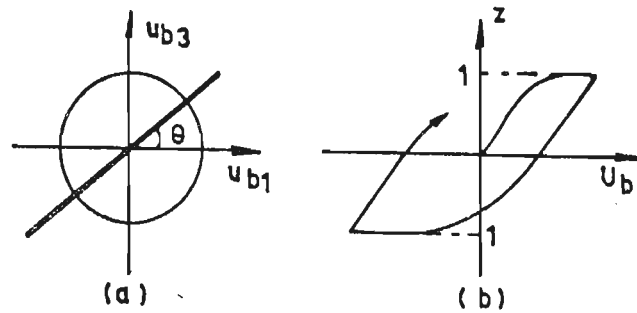
Fig.6.1 Hysteretic Behaviour under Linear Path [Park et al.(1986)]:
(a) Linear Displacement Path and (b) Hysteretic Behaviour

In which U_b and z are resultant uniaxial displacement and hysteretic dimensionless constant respectively. Substituting Eqn.(6.8) into (6.7) and subsequent simplification results following equation.

$$\gamma \dot{z} + \gamma' |\dot{U}_b z| z + \beta' \dot{U}_b z^2 - A \dot{U}_b = 0 \qquad \ldots \ldots (6.9)$$

The hysteretic property prescribed by the above formulation is shown in Fig.6.1(b). Considering the signs of $\dot{U}_b$ and z in Eqn.(6.9) are the same, the equation simplifies to the following form.

$$\frac{dz}{dt} + z^2 \left(\frac{\dot{U}_b}{\gamma} \right) - \frac{\dot{U}_b}{\gamma} = 0 \qquad \ldots \ldots (6.10)$$

The explicit solution of the Eqn.(6.10) is given by Kamke(1959) as

$$z = \tanh \left[\frac{\dot{U}_b}{\gamma} \right] \qquad \ldots \ldots (6.11)$$

In the present study, hysteretic dimensionless constant z is calculated from Eqn.(6.11) and then z_1 and z_3 with proper sign are calculated using Eqn.(6.8) and these values are used in turn to compute hysteretic component of restoring force using Eqn.(6.3) to (6.6).

The hysteretic dimensionless constant z_1 for unidirectional response in X-direction can be computed from Eqn.(6.9) by replacing z and $\dot{U}_b$ by z_1 and $\dot{u}_{b1}$ respectively.

6.3 Verification of Hysteretic Model

For verification of hysteretic model discussed in the preceding section, simulated hysteretic loops are compared with the experimental results obtained from both uniaxial test of present study and uniaxial and biaxial tests carried out by other investigators. The slope of the tangent at zero displacement of experimental hysteresis loop (K_t) was considered as post yielding stiffness K_p for LRB and LLRB isolation system. For simulation of hysteretic behaviour of LRB, the ratio of post yielding stiffness to pre yielding stiffness α of the order of 0.25 to 0.4 and the ratio of maximum displacement and yielding displacement (d_r) in the bearing of the order of 5 to 7 are found to be appropriate.

Experimental and simulated loops of model LRB obtained in the present study from uniaxial shear test are shown in Fig.6.2. The maximum shear strain during this test is restricted to 55 %, because this is the expected maximum strain level during earthquake simulator testing of base isolated test model for a vertical load of 20 kN. For the simulation of the hysteretic behaviour, the value of α and d_r are considered to be 0.333 and 6 respectively. Figure 6.2 shows that simulated loop is in good agreement with experimental loop.

Hysteretic behaviour of LLRB is simulated considering α equal to 0.1 to 0.14 and yielding shear force as 5 to 6 % of vertical load over bearing. Figure 6.3 depicts hysteresis loop for LLRB obtained by Robinson *et al.*(1982) from uniaxial shear test and simulated loop for 110 mm maximum horizontal displacement and a vertical load of 3.15 MN. This bearing was used for base isolation of William Clayton Building situated in Wellington, New Zealand. The simulated loop is found to match the experimental loop closely.

Figure 6.4 shows hysteresis loops of high damping LRB obtained by Aiken *et al.*(1989) from horizontal shear test subjected to uniaxial sinusoidal input and simulated loop for 100% maximum strain and a vertical load of 31.455 kN. In this case, α is taken equal to 0.285 as the initial stiffness is more in high damping LRB as compared simple LRB and d_r is taken equal to 6. The simulated loop is in good agreement with that obtained from the experiment.

Hysteretic behaviour of a frictional system is shown in Fig.6.5 in which frictional force-displacement relation as observed by Mokha *et al.* (1990) from testing of Teflon/stainless steel interface and simulated behaviour under unidirectional sinusoidal input are presented. The frequency of sinusoidal input was 0.16 Hz with a amplitude of 1 in. For simulation of hysteretic behaviour, Y is equal to 0.001 in, a' is equal to 0.6 sec/in, μ_{max} is equal to 11.93% and $\Delta\mu$ is equal to 9.27% are considered. Both simulated and experimental force-displacement loop are in good agreement.

Yasaka *et al.*(1988b) carried out biaxial tests on 1/7 th scale steel bar damper of 17 mm diameter and effective height of 100 mm. The steel damper had a lateral elastic stiffness of 2.53 kN/mm, yield force of 2.806 kN, yield displacement of 1.11 mm and α is equal to 0.023. The bidirectional motion is given by

$$u_{b1} = u_m \sin \omega t \qquad \qquad \dots\dots(6.12a)$$
$$u_{b3} = u_m \sin 2\omega t \qquad \qquad \dots\dots(6.12b)$$

in which $\omega = 1.57$ rad/sec. Figure 6.6 shows that the simulated hysteresis loops in X and Y directions with u_m equal to 14.65 and 29.3 mm are found to be in good agreement with corresponding experimental hysteresis loops in X and Y directions.

Figure 6.7 shows the bi-axial hysteretic behaviour of Teflon/ stainless steel interfaces - both simulated and experimental observation of Test-3 and Test-6 performed by Mokha *et al.*(1993) in X and Y directions. The out of phase sinusoidal excitations represented by Eqn.(6.12) are considered as input in X and Y directions. For simulation of hysteretic behaviour: $\Delta\mu = 0.0811$; $\mu_{max} = 0.12$; a'= 0.4 sec/in in the direction parallel to lay and $\Delta\mu = 0.094$; $\mu_{max} = 0.14$; a'= 0.454 sec/in in the direction perpendicular to lay are considered. The bearing pressure in the interface was 500 psi. In the Test-3, peak displacements in X and Y directions are 1.791 in and 1.728 in respectively with a frequency of 0.5 rad/sec, while in Test-6, peak displacements in X and Y directions are 1.779 in and 1.728 in respectively with a frequency of 2.22 rad/sec. Both simulated loops and experimental loops in X and Y directions are found to be in good agreement. Further, comparison of shape of the hysteresis loop in Figure 6.5 and shape of the hysteresis

'loop (X - dir) in Figure 6.7 show that biaxial interaction is significant.

6.4 Equation of Motion

In this study, the superstructure is assumed to be a three dimensional multi-storey elastic shear frame with three dof per floor. This three dof are two translational motion in X and Y directions respectively and a rotation about Z axis. Figure 6.8 shows the structural model of a three storey shear frame building. The three dof are associated with the centre of mass of each floor and the base. The floors and the base are assumed to be infinitely rigid in its plane. The centre of mass of all the floors and the base are assumed to be on the same vertical axis. The asymmetry in floor plan (if any) is identical for all the floors.

The governing equations of motion of elastic superstructure for 3-D model of isolated multi-storey shear building are expressed as

$$M \ddot{u} + C \dot{u} + K u = - M R \ddot{u}_{bt} \qquad \dots (6.13)$$

where, M, C and K are mass matrix, damping matrix and stiffness matrix of size NxN of the superstructure, defined as in Kan and Chopra(1977), N is three times number of the floors, and R is the matrix of size Nx3 of earthquake influence coefficient [Clough and Penzien(1986)]. Here, $\ddot{u}$, $\dot{u}$ and u represent the floor acceleration, velocity and displacement vectors (Nx1) relative to the base, $\ddot{u}_{bt}$ is the absolute base acceleration.

The equations of motion of the base for P-F bearing, LRB and LLRB isolation systems are given as

$$M_b \ddot{u}_b + C_b \dot{u}_b + K_b u_b + f = - M_b \ddot{u}_g - R^T M \ddot{u} \qquad \dots (6.14)$$

where, M_b is the diagonal mass matrix (3x3) and each of the diagonal elements is having a value of m_t, C_b is the damping matrix (3x3) of viscous isolation elements, K_b is the resultant stiffness matrix (3x3) of non-hysteretic part of isolation elements and f is the vector (3x1) containing hysteretic part of restoring force of isolation system. $\ddot{u}_b$,

$\ddot{u}_b$, and u_b represent the base acceleration, velocity and displacement vectors (3x1) relative to the ground. The absolute base acceleration $\ddot{u}_{bt}$ is given by

$$\ddot{u}_{bt} = \ddot{u}_g + \ddot{u}_b \qquad \dots\dots(6.15)$$

The equations of motion of the base for EDF isolation system are given as:

$$M_b \ddot{u}_b + C_b \dot{u}_b + K_b u_b = - M_b (\ddot{u}_g + \ddot{u}_s) - R^T M \ddot{u} \qquad \dots\dots(6.16)$$

$$\ddot{u}_s = - \ddot{u}_g - \ddot{u}_b - \frac{1}{m_t} f - \frac{1}{m_t} \left(R^T M \ddot{u} \right) \qquad \dots\dots(6.17)$$

where, $\ddot{u}_b$, $\dot{u}_b$, and u_b are the acceleration, velocity and displacement vectors (3x1) of the LRB in EDF isolation system and $\ddot{u}_s$, $\dot{u}_s$ and u_s are the sliding acceleration, velocity and displacement vectors (3x1) of the isolation system. Here, f is the vector (3x1) containing forces mobilized in the frictional interface. Hysteretic part of restoring force in LRB is not considered. The absolute base acceleration $\ddot{u}_{bt}$ is given as:

$$\ddot{u}_{bt} = \ddot{u}_g + \ddot{u}_b + \ddot{u}_s \qquad \dots\dots(6.18)$$

Here, $m_t = m_b + \sum_{i=1}^{nf} m_i$

6.5 Method of Solution

The implicit-implicit partitioned Newmark's method in predictor-corrector form is used again for direct integration of individual coupled equations of motion in staggered fashion [Paul(1982), Zienkiewicz et al.(1988)]. The solution of differential equations governing the behaviour of non-linear isolation elements, which are essentially very stiff, are obtained by using Kamke's solution in close form as discussed in the Section 6.2. The algorithm for solution of governing equations of motion of 3-D elastic shear frame supported over pure friction, LRB and lead rubber isolation system is shown below:

122

1. Initialize

$$u_b^{(1)} = 0, \qquad u^{(1)} = 0$$

$$\dot{u}_b^{(1)} = 0, \qquad \dot{u}^{(1)} = 0$$

$$\ddot{u}_b^{(1)} = 0, \qquad \ddot{u}^{(1)} = 0$$

$$n = 0$$

2. Set time step counter $n = n + 1$

3. Begin predictor phase in which,

$$(u_b)_{n+1}^{(1)} = (\tilde{u}_b)_{n+1} = (u_b)_n + \Delta t (\dot{u}_b)_n + \Delta t^2 (1-2\beta)(\ddot{u}_b)_n / 2$$

$$(\dot{u}_b)_{n+1}^{(1)} = (\tilde{\dot{u}}_b)_{n+1} = (\dot{u}_b)_n + \Delta t (1-\gamma)(\ddot{u}_b)_n$$

$$(u)_{n+1}^{(1)} = (\tilde{u})_{n+1} = (u)_n + \Delta t (\dot{u})_n + \Delta t^2 (1-2\beta)(\ddot{u})_n / 2$$

$$(\dot{u})_{n+1}^{(1)} = (\tilde{\dot{u}})_{n+1} = (\dot{u})_n + \Delta t (1-\gamma)(\ddot{u})_n$$

4. Set iteration counter $i = 1$ and assume $f = 0$ in $i = 1$

5. Evaluate residual forces using equation

$$\phi_b^{(1)} = - M_b (\ddot{u}_b)_{n+1}^{(1)} - C_b (\dot{u}_b)_{n+1}^{(1)} - K_b (u_b)_{n+1}^{(1)} - f^{(1)} - M_b (\ddot{u}_g)_{n+1} - R^T M \ddot{u}_{n+1}^{(1)}$$

6. Form the effective isolator stiffness matrix using the expression

$$K_b^* = 1/(\Delta t^2 \beta) M_b + \gamma/(\Delta t \ \beta) C_b + K_b$$

or update K_b^* if Δt changes.

7. Solve

$$K_b^* \ \Delta(u_b)^{(1)} = \phi_b^{(1)}$$

8. Enter corrector phase for responses of basement in which,

$$(u_b)_{n+1}^{(i+1)} = (u_b)_{n+1}^{(i)} + \Delta(u_b)^{(i)}$$

$$(\ddot{u}_b)_{n+1}^{(i+1)} = [(u_b)_{n+1}^{(i+1)} - (\tilde{u}_b)_{n+1}]/(\Delta t^2 \beta)$$

$$(\dot{u}_b)_{n+1}^{(i+1)} = (\tilde{\dot{u}}_b)_{n+1}^{(i)} + \gamma \Delta t (\ddot{u}_b)_{n+1}^{i+1}$$

9. Compute $(\ddot{u}_{bt})_{n+1}^{(i+1)}$ using Eqn.(6.15)

10. Evaluate the residual forces for superstructure from Eqn.(6.13)

$$\phi_s = - M \ddot{u}_{n+1}^{(i)} - C \dot{u}_{n+1}^{(i)} - K u_{n+1}^{(i)} - M R (\ddot{u}_{bt})_{n+1}^{(i+1)}$$

11. Form the effective superstructure stiffness matrix using the expression

$$K^* = 1/(\Delta t^2 \beta) M + \gamma/(\Delta t \beta) C + K$$

or, update K^* if Δt changes

12. Solve

$$K^* \Delta u^{(i)} = \phi_s^{(i)}$$

13 Enter corrector phase for responses of super-structure in which

$$(u)_{n+1}^{(i+1)} = (u)_{n+1}^{(i)} + \Delta(u)^{(i)}$$

$$(\ddot{u})_{n+1}^{(i+1)} = [(u)_{n+1}^{(i+1)} - (\tilde{u})_{n+1}]/(\Delta t^2 \beta)$$

$$(\dot{u})_{n+1}^{(i+1)} = (\tilde{\dot{u}})_{n+1}^{(i)} + \gamma \Delta t (\ddot{u})_{n+1}^{(i+1)}$$

14. Calculate non-linear forces developed in the isolation system from Eqn.(6.3) for P-F and EDF isolators, Eqn.(6.5) for LRB, Eqn.(6.6) for LLRB.

124

15. Compute

$$\varepsilon_u = \frac{\| u_b + u \|^{(i+1)} - \| u_b + u \|^{(i)}}{\| u_b + u \|^{(i+1)}}$$

16. If $\varepsilon_u \geq$ tolerance, set $i = i+1$ and go to step-5, otherwise continue.

17. Set

$$(u_b)_{n+1} = (u_b)_{n+1}^{(i+1)}, \qquad (u)_{n+1} = (u)_{n+1}^{(i+1)}$$

$$(\dot{u}_b)_{n+1} = (\dot{u}_b)_{n+1}^{(i+1)}, \qquad (\dot{u})_{n+1} = (\dot{u})_{n+1}^{(i+1)}$$

$$(\ddot{u}_b)_{n+1} = (\ddot{u}_b)_{n+1}^{(i+1)}, \qquad (\ddot{u})_{n+1} = (\ddot{u})_{n+1}^{(i+1)}$$

for use in the next time step, go to step-2.

The same algorithm can also be extended for 3-D elastic shear frame building supported over EDF isolation system.

Using the predictor-corrector algorithm as described above, a FORTRAN-77 program ISODYN-3D is developed for numerical solution of the equation of motion of the structure supported over selected isolation system, subjected to bidirectional earthquake excitations. A time step $\Delta t = 0.01$ sec is used for response calculation of LRB and LLRB isolated system. For friction based isolation system a time step $\Delta t = 0.002$ sec is used for response calculation of isolated structure. Further reduction of time step size in both cases resulted no noticeable change in the computed response.

6.6 Validation of Analytical Model

The validity of the analytical model and the solution algorithm used in ISODYN-3D is demonstrated by comparing the analytical response of a single storey asymmetric structure supported over sliding isolation alongwith helical springs acting in parallel, as obtained by Nagarajaiah et al.(1990) and the results of the present study. The structure has equal base dimensions of 12,192 mm (L) and is supported on four corner columns having a height of 4,572 mm. The total weight of the structure was considered to be 2,135 kN. The weight of floor and base of the

structure was considered to be equal. The weight of floor and base slab has been distributed non-uniformly. Centre of mass of both floor and basement of the structure have been assumed to be on same vertical axis. Eccentricities e_x = e_y = 0.1 L of the centre of stiffness of the superstructure from the centre of mass were considered. The uncoupled translational period (T_s) of the superstructure was considered to be 0.3 sec in both X and Y directions. The uncoupled torsional period (T_θ) of the superstructure was considered as $0.58T_s$. Damping ratio of 0.02 of critical was used for the superstructure in all modes. Four sliding Teflon disc bearing under a pressure of 6.9 MPa were used. For this condition, the bearing properties are μ_{max} = 0.12, $\Delta\mu$ = 0.093 and a' = 0.0234 sec/mm. The helical springs were designed to provide a rigid body mode period, T_p, of 3 sec. The ground motion considered was El-Centro earthquake with N-S component in X-direction and E-W component in Y-direction. Figure 6.9 shows the comparison of base displacement response in both X and Y directions. The peak ground displacement (PGD) of 108.96 mm was used for normalizing the displacement response. This comparison shows good agreement between response computed by Nagarajaiah et al.(1990) with the present study.

Nagarajaiah et al.(1991) computed response of similar structure supported over LLRBs. Eccentricities e_x = e_y = 0.1 L of the centre of stiffness of the superstructure from the centre of mass were considered. The uncoupled translational period (T_s) of the superstructure was considered to be 0.3 sec in both X and Y directions. The uncoupled torsional period (T_θ) of superstructure was considered to be equal to T_s. Damping ratio of 0.02 of critical was used for the superstructure in all modes. Four LLRBs were placed below the columns for seismic isolation. The properties of bearings were the initial elastic stiffness of 3.12 kN/mm, the post yielding stiffness of 0.48 kN/mm and the yield strength of 29.36 kN. The ground motion considered was El-Centro earthquake with N-S component in X-direction and E-W component in Y-direction. Figure 6.10 shows the comparison of base displacement response in both X and Y directions obtained in the present study and that obtained by Nagarajaiah et al.(1991). The peak ground displacement (PGD) of 108.96 mm was used for normalizing the displacement response. This comparison shows good agreement between response computed from both studies.

6.7 Results and Discussions

In this section, the response of 3-D model of a three storey r.c. shear building subjected to Koyna Earthquake with Longitudinal component in X-direction and transverse component in Y-direction, are computed based on solution technique/algorithm discussed in the preceding section. Performances of selected base isolation systems are studied. Details of the r.c. framed structure considered in this section is same as that considered in the Chapter-5 (Fig.5.10). Bearing parameters in both X and Y directions are considered to be same for all isolation systems studied and these are same as listed in Table 5.1.

Figures 6.11(a) and (b) show relative base displacement histories and absolute acceleration histories in X and Y directions, of the isolated structure supported on P-F isolator subjected to bidirectional Koyna earthquake motion. Figure 6.12 shows relative base displacement history, absolute roof acceleration history and Fourier amplitude spectra of absolute roof acceleration in X-direction of the structure isolated by P-F bearing subjected to only longitudinal component of Koyna earthquake. Comparison of displacement and acceleration histories as shown in Figs.6.11 and 6.12 in X-direction shows that substantial biaxial interaction exists in the response in both the directions. Comparison of Figs.5.21(a) and 6.12(c) shows that modelling friction by Coulomb's rigid plastic model excites more higher modes than that induced by visco-plastic modelling. In visco-plastic model, small amount of yielding at the sliding interface has been considered before initiation of the sliding phase and also there is no discontinuity in the force-displacement hysteresis loop. Thus, in visco-plastic model transition from sliding to non-sliding and vice-versa are smooth as compared to Coulomb's model and it is for this reason higher modes contributions are less in the former modelling of friction. Comparison of Fig.5.15(a) and 6.12(a) shows that pattern of displacement histories are similar for both the modelling, while the level of displacement is higher in the rigid plastic model.

Figures 6.13(a) and (b) show relative base displacement histories and absolute acceleration histories in X and Y directions, of the isolated structure supported on LRB system subjected to bidirectional Koyna earthquake motion. Figure 6.14 shows relative base displacement

history, absolute roof acceleration history and Fourier amplitude spectra of absolute roof acceleration in X-direction of the isolated structure isolated by LRB subjected to longitudinal component of Koyna earthquake. Comparison of displacement and acceleration histories shows that the effects of biaxial interaction is also considerable for LRB isolation system as shown in Figs.6.13 and 6.14. Comparison of Figs.5.21(b) and 6.14(c) shows that modelling of force-displacement characteristic of LRB by non-linear model proposed by Wen(1980) excites more higher mode contribution than that in equivalent linear model. In equivalent linear model, equivalent stiffness (K_{eq}) considered for analysis is much lower than the pre-yielding stiffness of the bearing, while in non-linear hysteretic model, high pre-yielding stiffness of the bearing has been taken into account and this high initial stiffness increases higher modes contributions and at the same time decreases lower modes contributions in the response of the isolated structure. Figures 5.15(b) and 6.14(a) show that the pattern of displacement histories are similar and also level of displacements differs only by small margin.

Figures 6.15(a) and (b) show relative base displacement histories and absolute acceleration histories in X and Y directions, of the isolated structure supported on LLRB subjected to bidirectional Koyna earthquake motion. Figures 6.16(a) and (b) show relative base displacement histories and absolute acceleration histories in X and Y directions, of the isolated structure supported on EDF isolation system subjected to bidirectional Koyna earthquake motion. For LLRB and EDF isolation system, effects of biaxial interaction are also considerable and variation of response with different modelling of isolation system are similar to that of LRB.

6.8 Concluding Remarks

In this chapter, response of three storeyed r.c. shear frame building isolated by P-F bearing, LRB, LLRB and EDF isolator subjected to Koyna earthquake with logitudinal component in X-direction and transverse component in Y-direction, have been studied. The force-displacement characteristics of the isolation systems have been modelled by non-linear hysteretic model. Response of the building have been obtained by idealizing superstructure as 3-D model having 3 dof per

floor. On the basis of the detailed analysis of response and discussion made in the previous sections following conclusions are drawn:

o   Simulated shear force-displacement hysteresis loops of different isolation systems obtained by solution developed in this chapter are in close agreement with the experimental force-displacement loops reported in the literature.

o   Response of the base isolated structure subjected to general plane motion, obtained from solution algorithm developed in this chapter are in good agreement with that obtained from more complex numerical studies reported in the literature.

o   Effects of biaxial interaction on the response of isolated structure are significant for P-F bearing and its effects are considerable for LRB based isolation systems.

o   Modelling of force-displacement characteristics of pure friction bearing by visco-plastic model results in reduction of contribution of higher modes in the response of isolated structure as compared to that of Coulomb's rigid plastic model.

o   Modelling of force-displacement characteristics of LRB by non-linear hysteretic model increases higher mode contributions and decreases lower mode contributions in the response of isolated structure as compared to that of equivalent linear analysis. Similar behaviour is also observed for LLRB and EDF isolator.
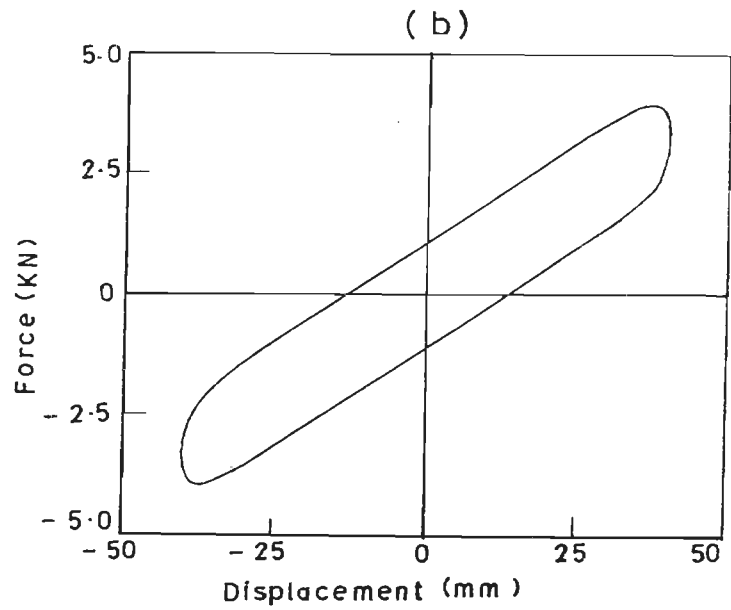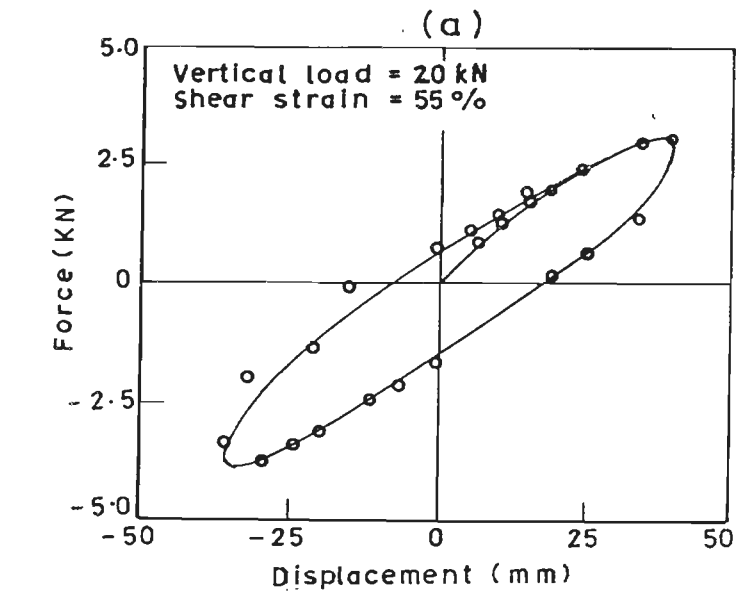
Fig.6.2 Shear Force-Displacement Characteristics
for Laminated Rubber Bearing Model: (a)
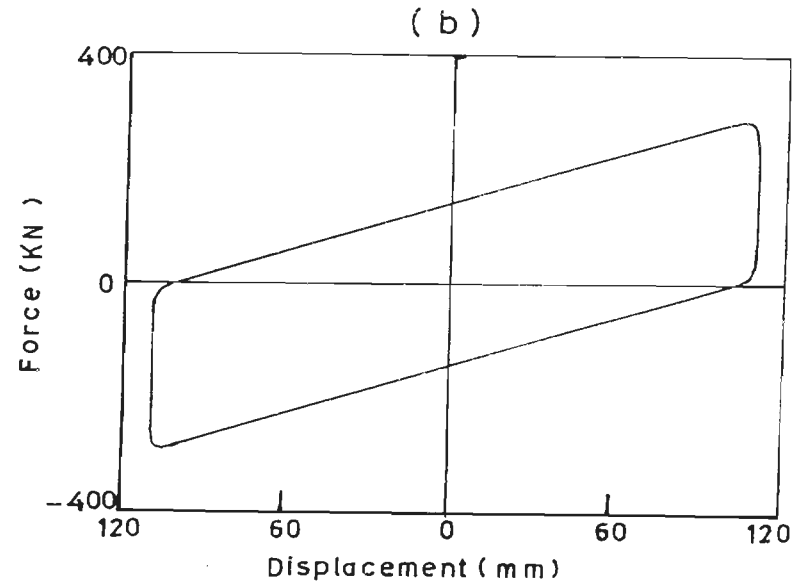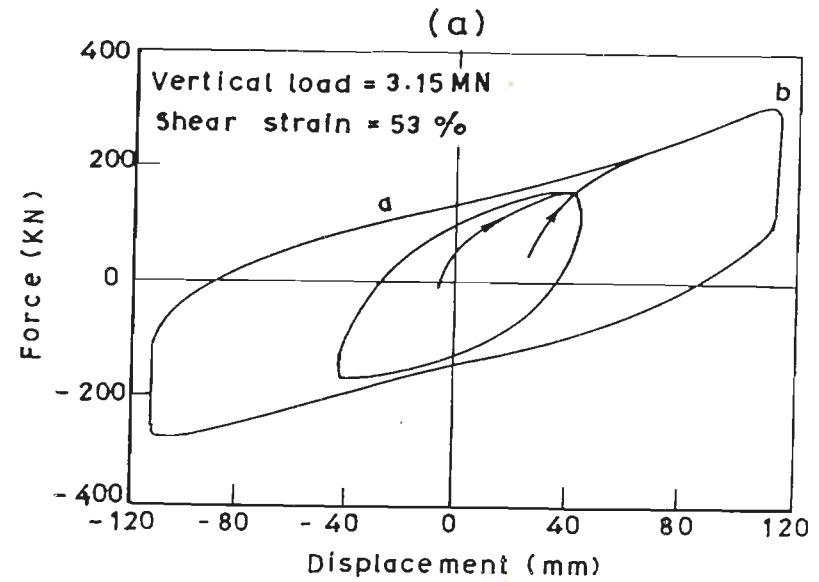Experimental and (b) Simulated

Fig.6.3 Shear Force-Displacement Characteristics
for Lead Rubber Bearing: (a) Experimental
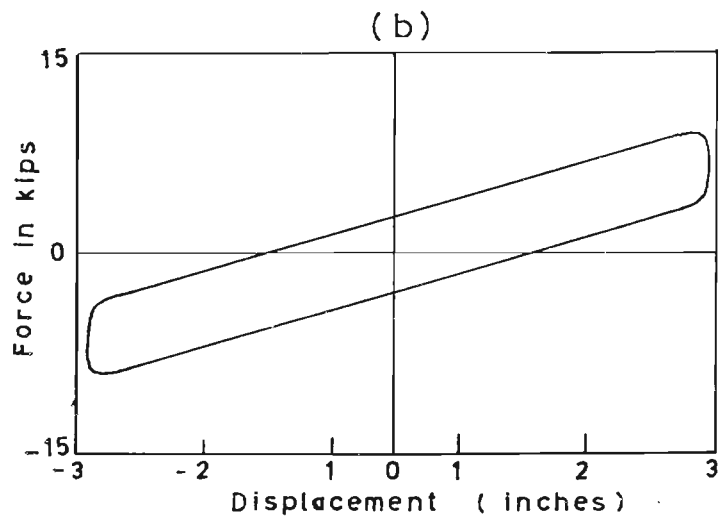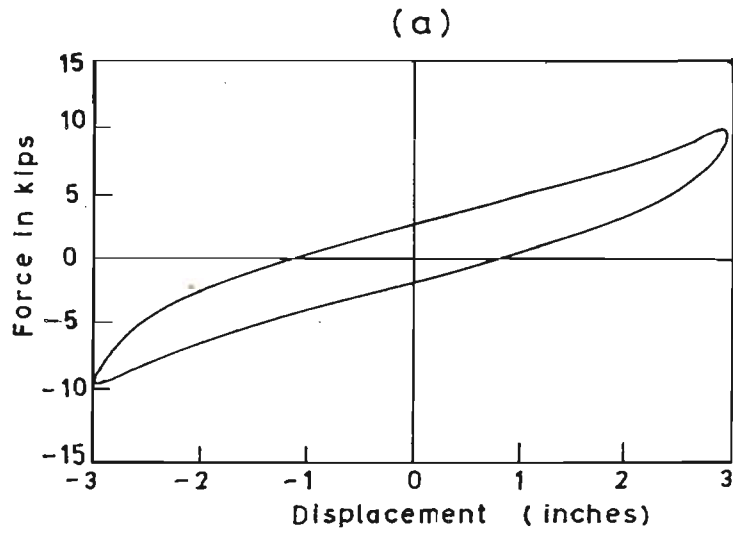[Robinson (1982)] and (b) Simulated

Fig.6.4 Shear Force-Displacement Characteristics
for High Damping LRB: (a) Experimental
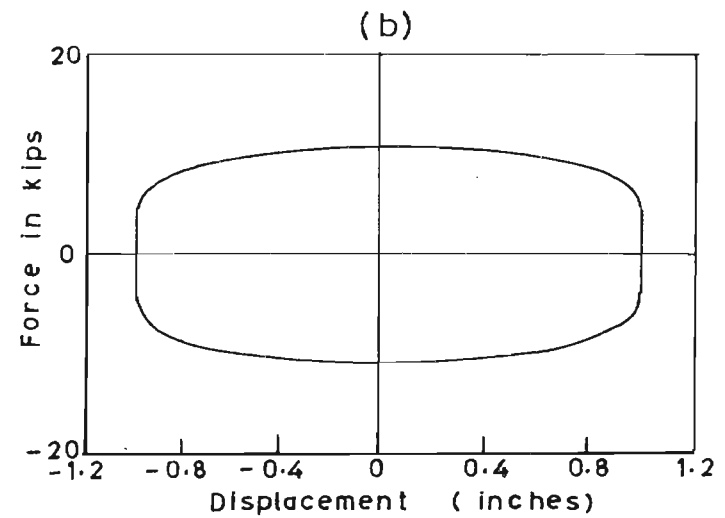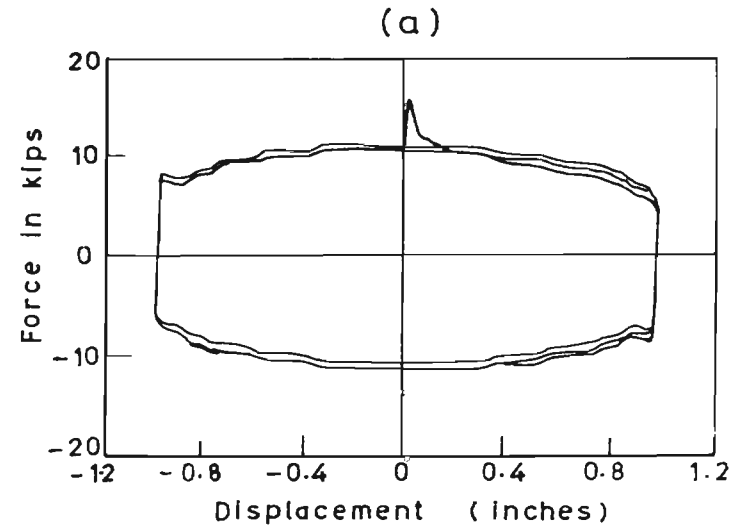[Aiken et al.(1989)] and (b) Simulated

Fig.6.5 Frictional Force-Displacement Characteristics for
Teflon/Stainless Steel Interface: (a) Experimental
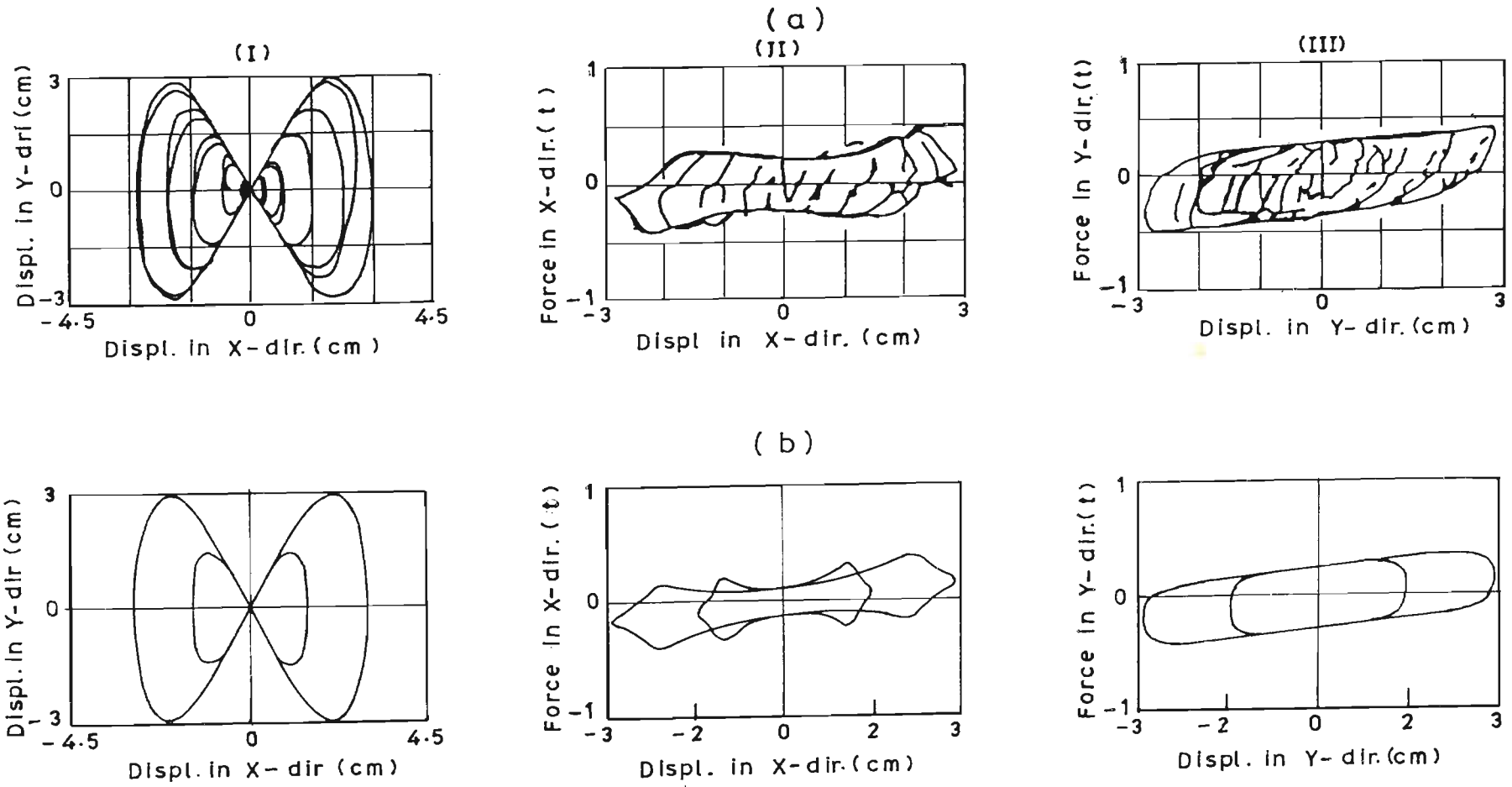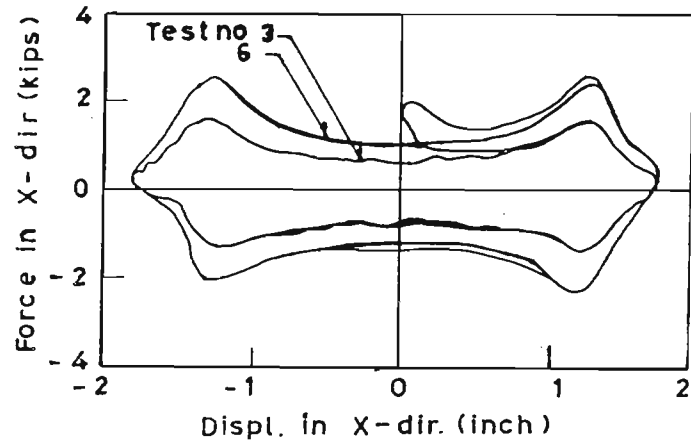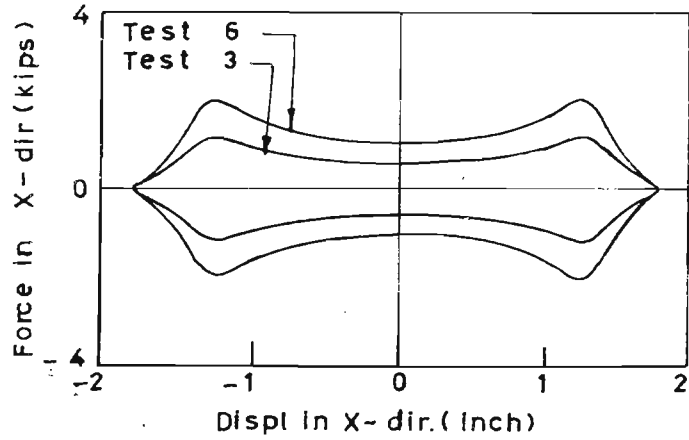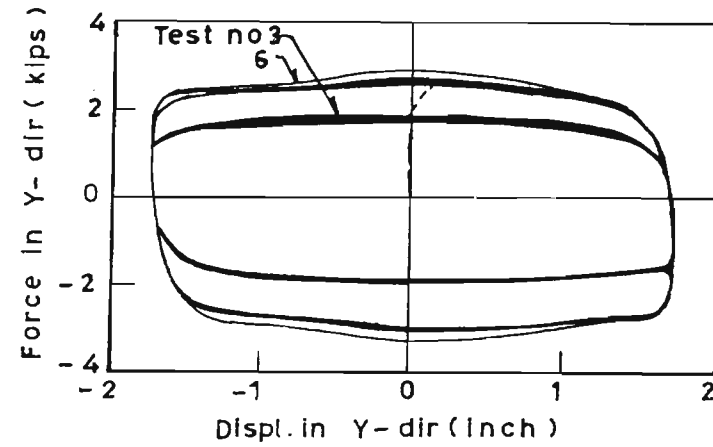[Mokha et al.(1990)] and (b) Simulated

Fig.6.6 Biaxial Hysteretic Behaviour of 1/7th Scale Steel Bar Damper Subjected to 8-Shaped Motion: (a) Experimental Loops in X and Y - Directions [Yasaka et al.(1988)] and (b) Simulated Loops in X and Y -Directions
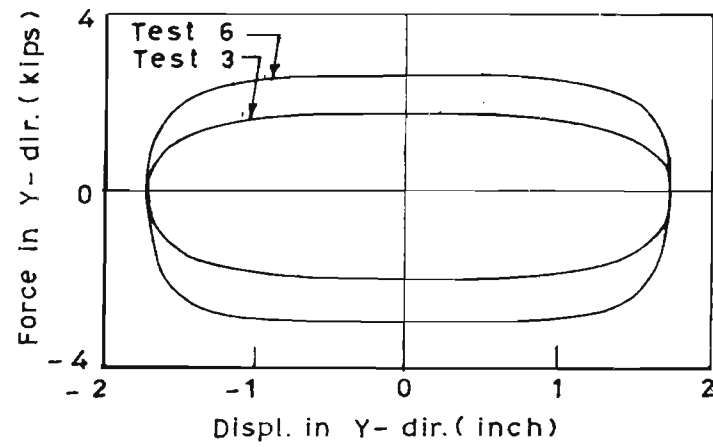
Fig.6.7 Biaxial Hysteretic Behaviour of Teflon/Stainless Steel Frictional Interface
Subjected to 8-Shaped Motion: (a) Experimental Loops in X and Y - Directions
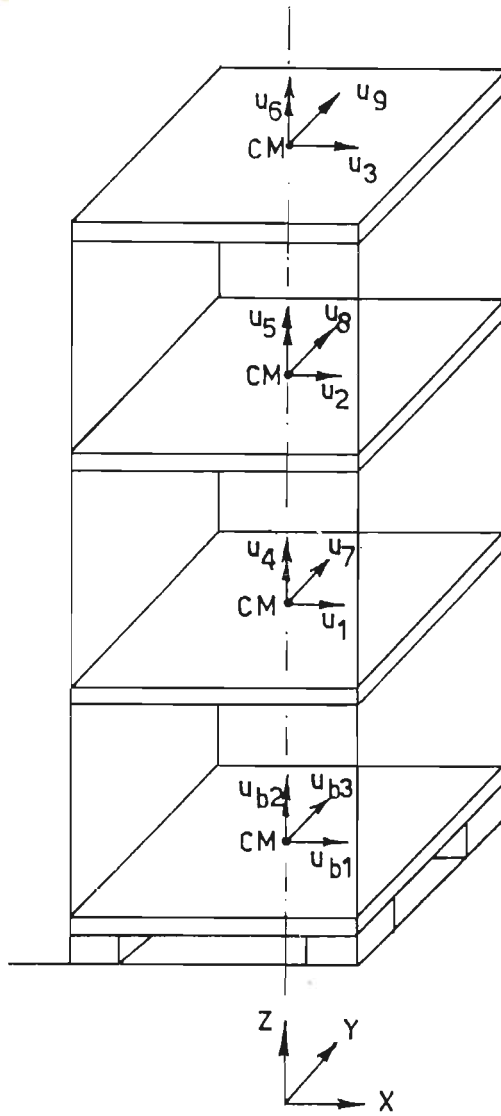[Mokha et al.(1993)] and (b) Simulated Loops in X and Y - Directions

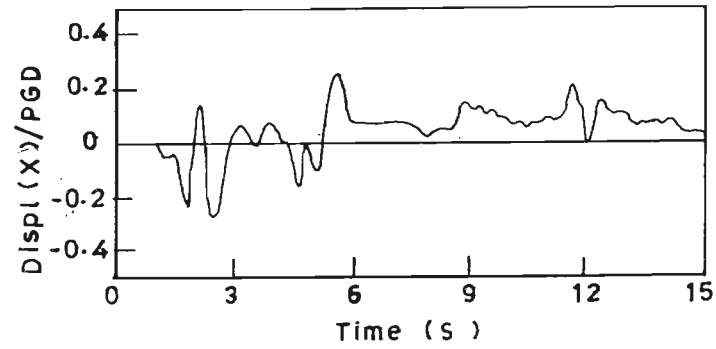Fig.6.8 Structural Model of a Three Storeyed
Shear Frame Building

(a)
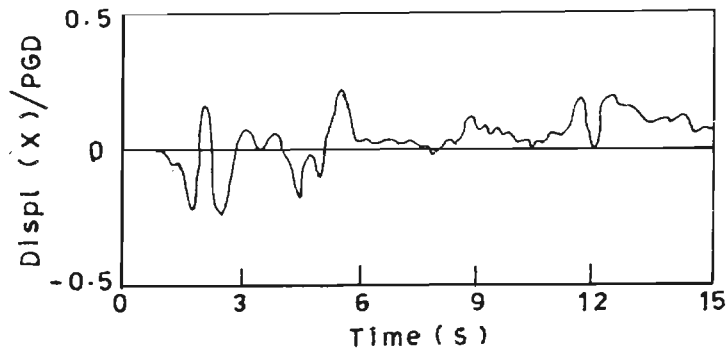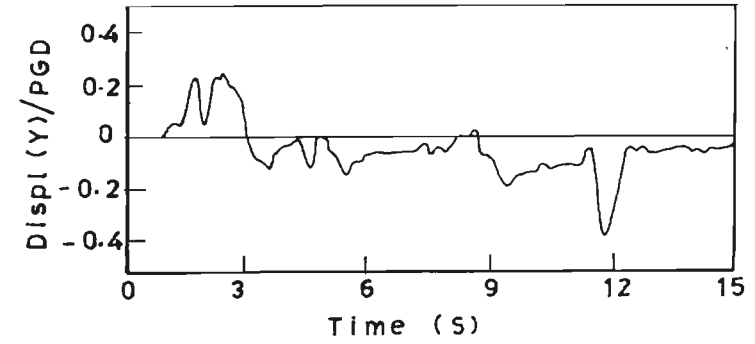
(b)
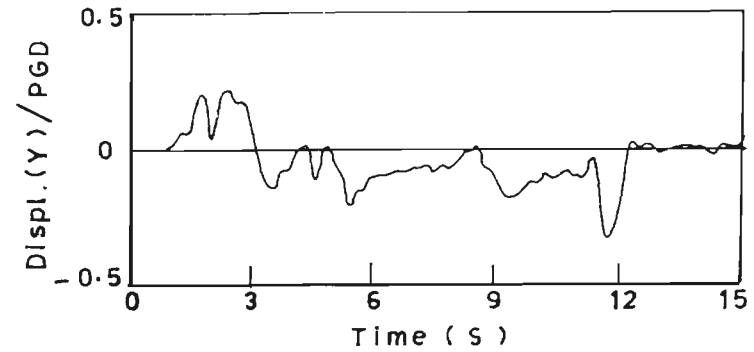
Fig.6.9 Displacement Time History in X and Y-dir of a One Storey
Asymmmetric Frame Isolated by Sliding Isolators: (a)
Nagarajaiah et al.(1990) and (b) Present Study
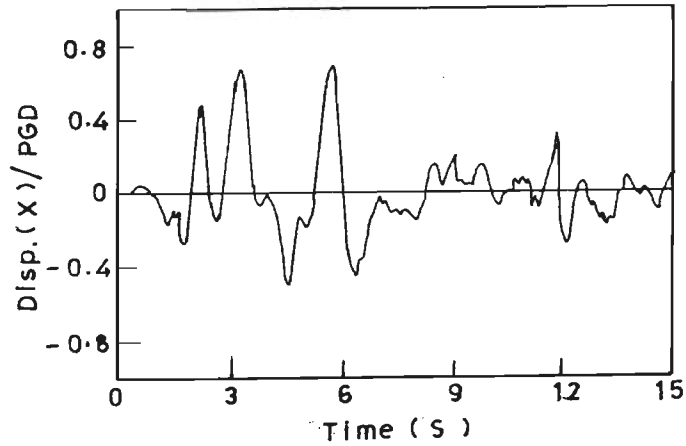
(a)
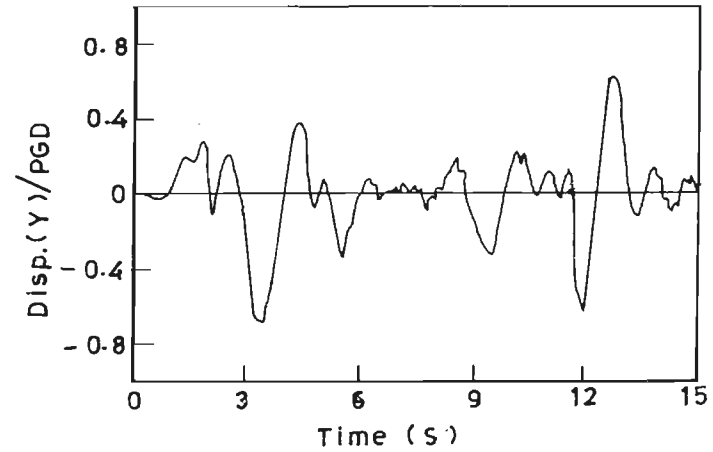
(b)
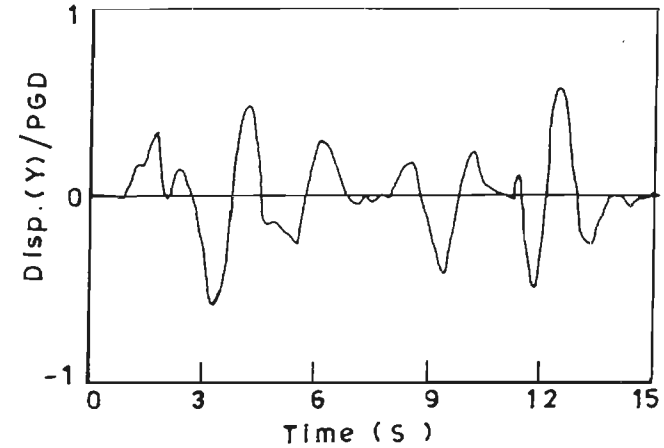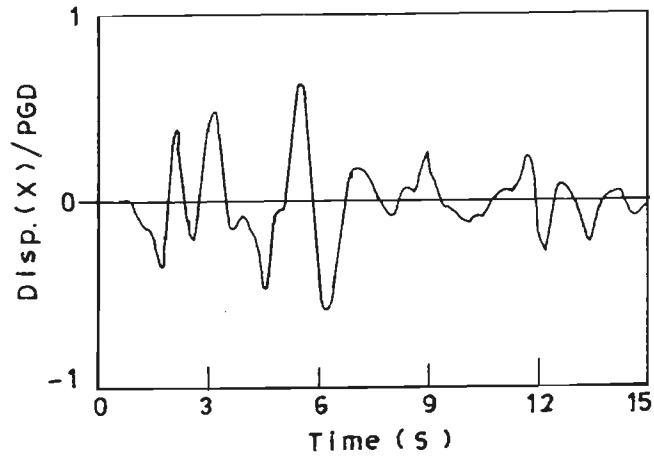
Fig.6.10 Displacement Time History in X and Y-dir of a One Storey
Asymmmetric Frame Isolated by Lead Rubber Bearing: (a)
Nagarajaiah et al.(1991) and (b) Present Study
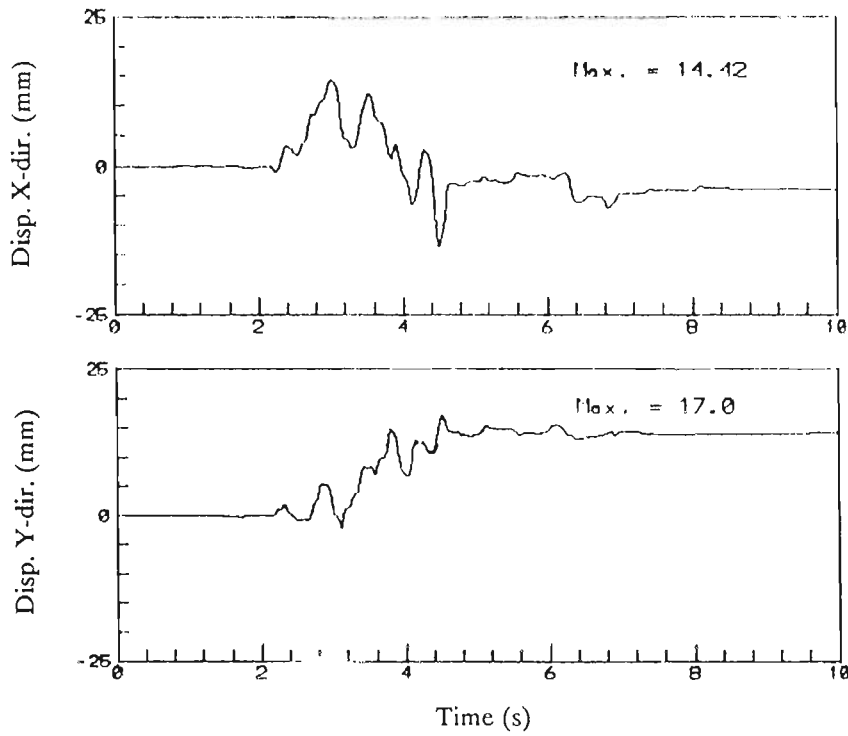
(a) Relative Base Displacement History in X and Y-dir
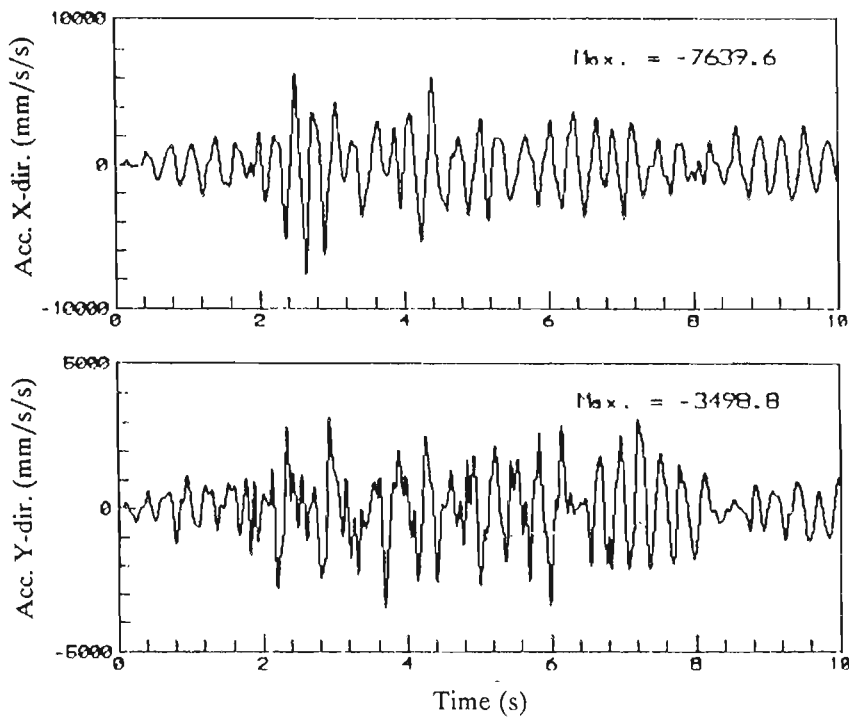
(b) Absolute Roof Acceleration History in X and Y-dir

Fig.6.11 Response of the Structure Isolated by P-F Isolator
Subjected to Bidirectional Koyna Earthquake Motion

137
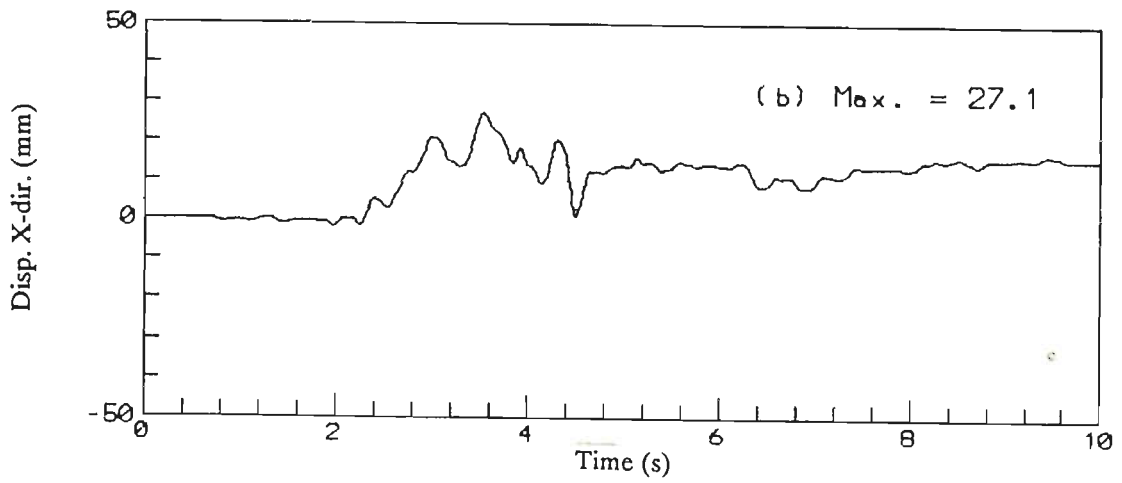
(a) Relative Base Displacement History in X-dir
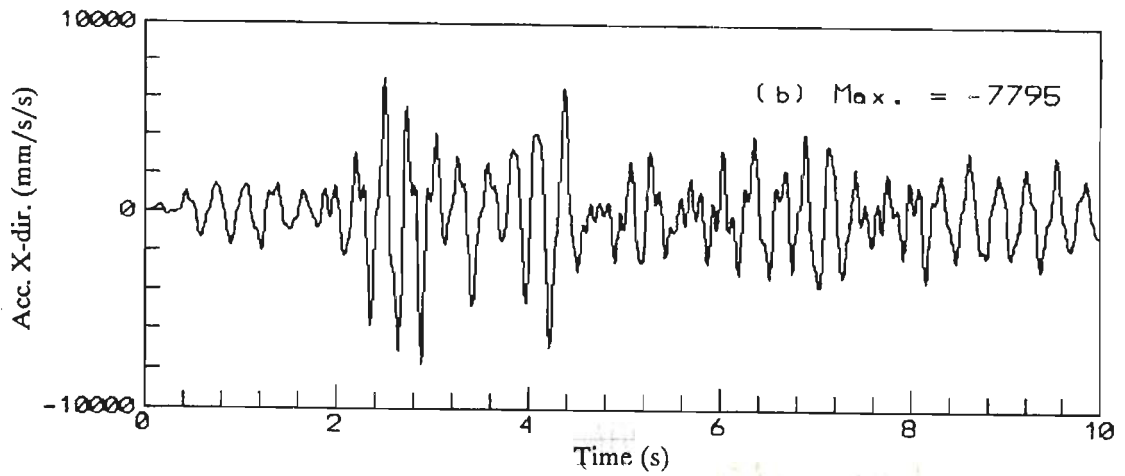
(b) Absolute Roof Acceleration History in X-dir
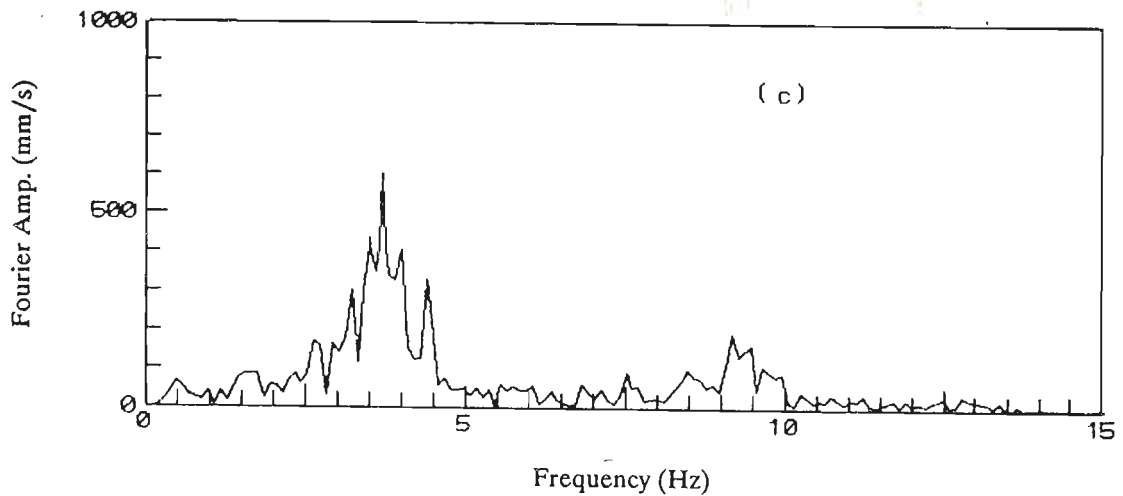
(c) Fourier Amplitude Spectra of Roof Acceleration in X-dir

Fig.6.12 Response of Structure Isolated by P-F isolator
Subjected to unidirectional Koyna (L) Motion
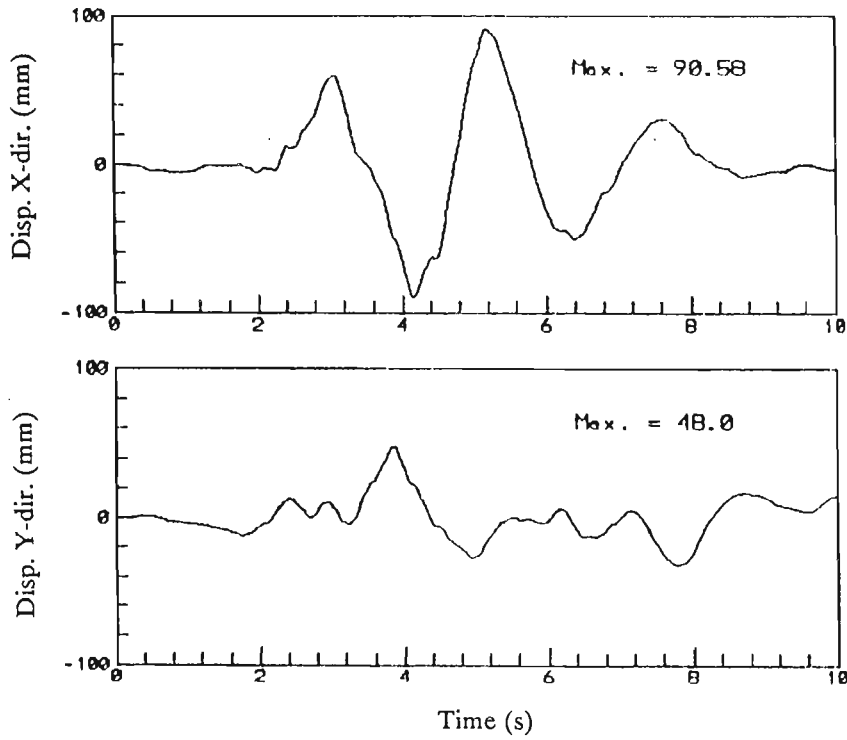
(a) Relative Base Displacement History in X and Y-dir
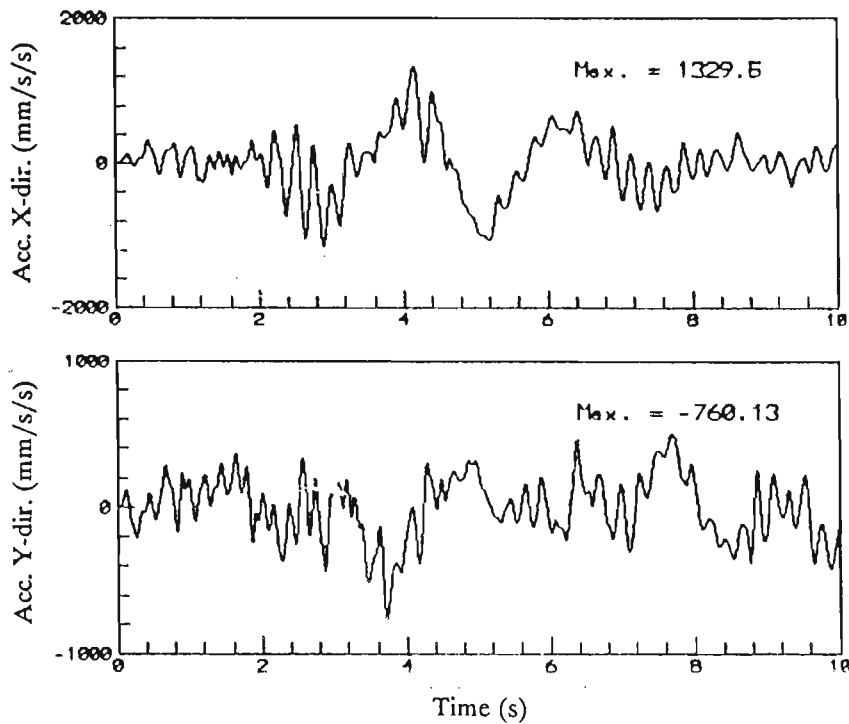
(b) Absolute Roof Acceleration History in X and Y-dir

Fig.6.13 Response of the Structure Isolated by LRB System
Subjected to Bidirectional Koyna Earthquake Motion

139

(a) Relative Base Displacement History in X-dir

(b) Absolute Roof Acceleration History in X-dir
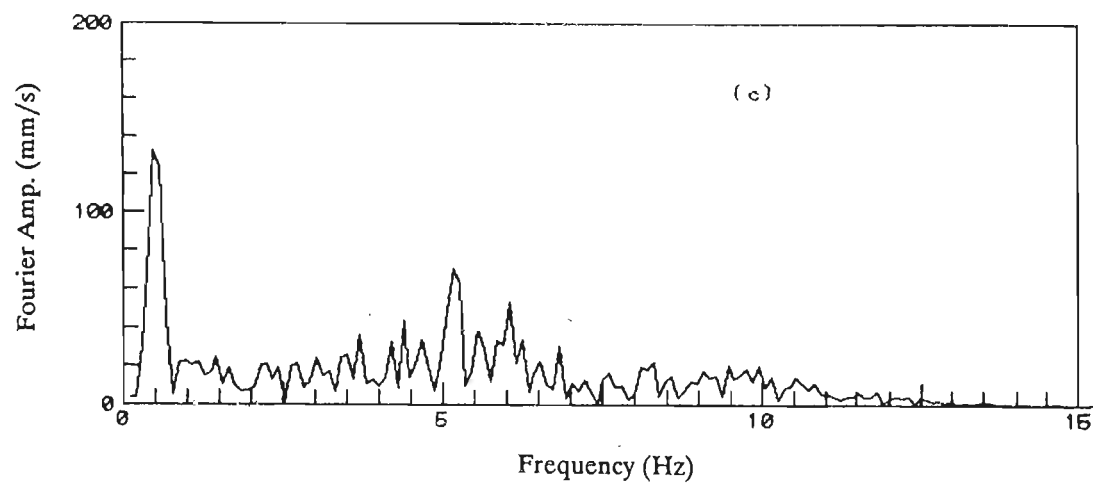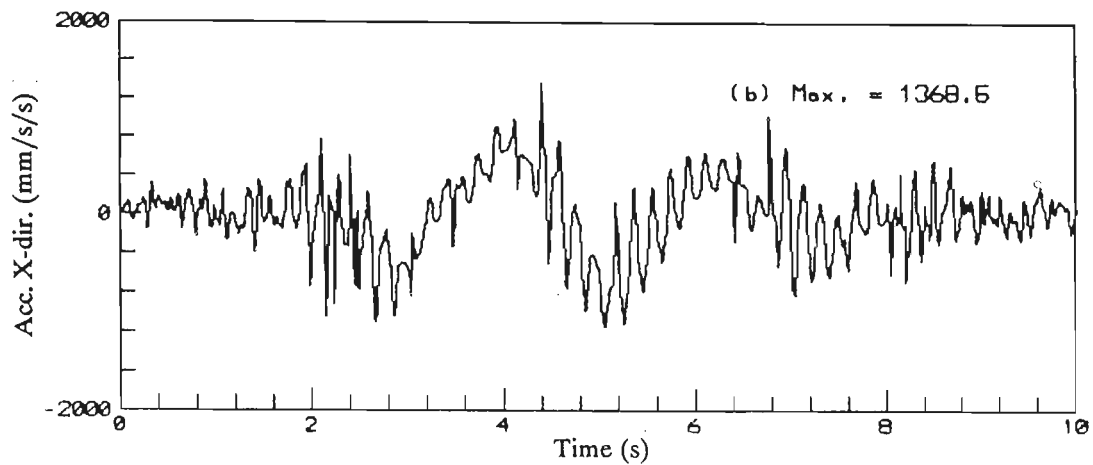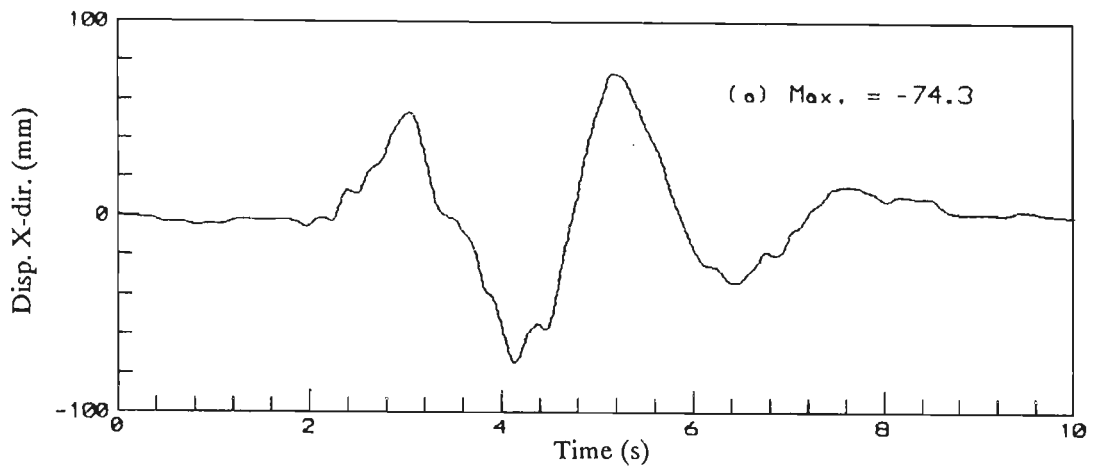
(c) Fourier Amplitude Spectra of Roof Acceleration in X-dir

Fig.6.14 Response of Structure Isolated by LRB System
Subjected to unidirectional Koyna (L) Motion
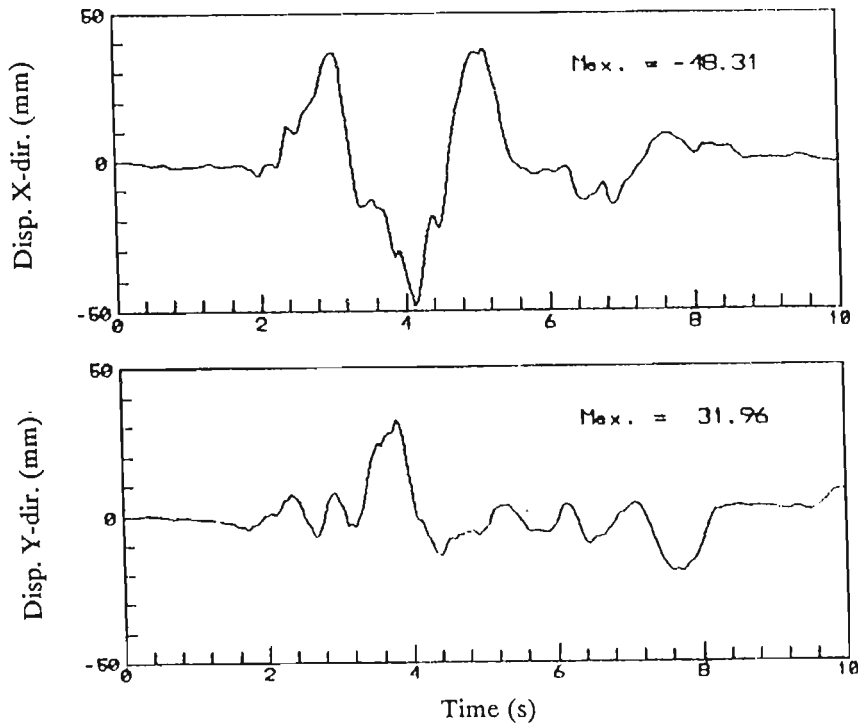
(a) Relative Base Displacement History in X and Y-dir
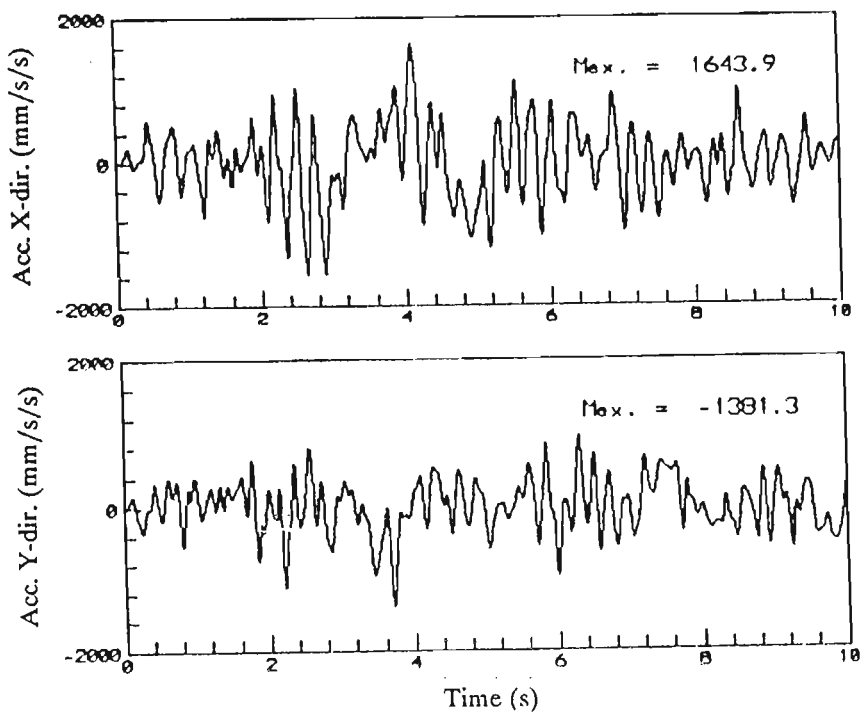
(b) Absolute Roof Acceleration History in X and Y-dir

Fig.6.15 Response of the Structure Isolated by LLRB System
Subjected to Bidirectional Koyna Earthquake Motion
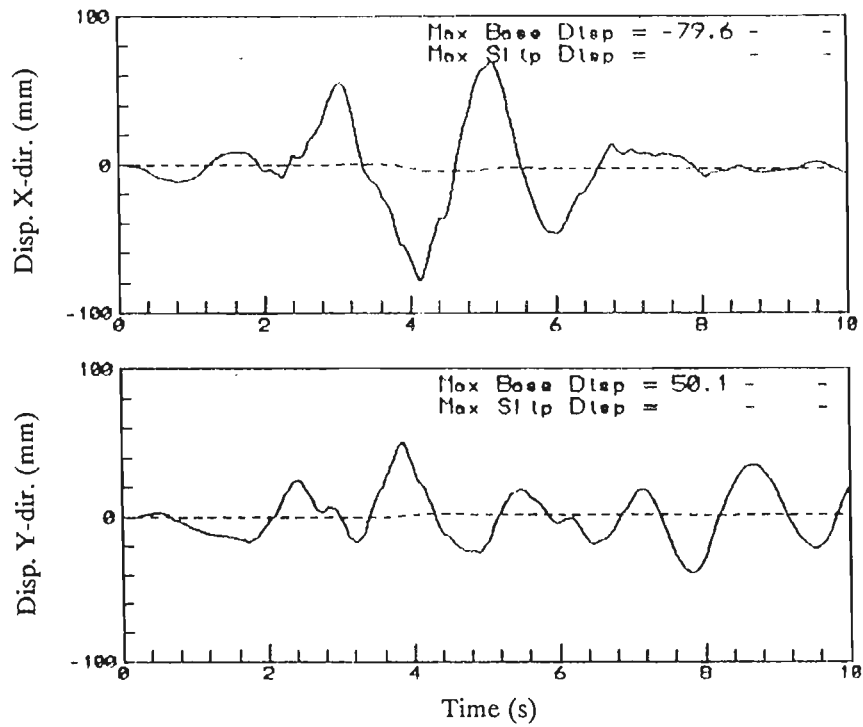
141

(a) Relative Base Displacement History in X and Y-dir
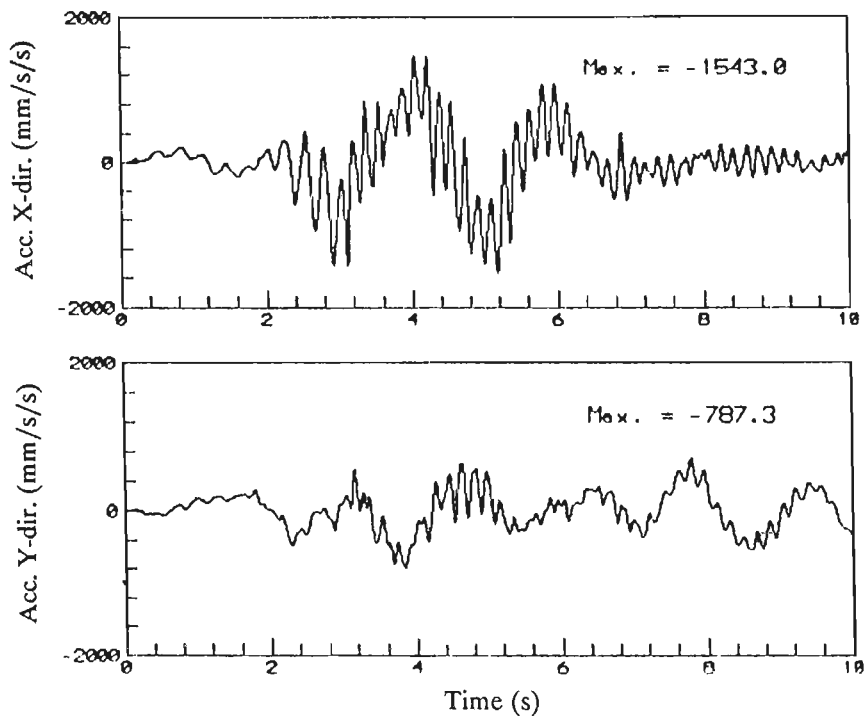
(b) Absolute Roof Acceleration History in X and Y-dir

Fig.6.16 Response of the Structure Isolated by EDF Bearing
Subjected to Bidirectional Koyna Earthquake Motion

142

CHAPTER 7

SUMMARY AND CONCLUSIONS

7.1 General

The present work is undertaken to study the response of base isolated medium-rise framed buildings – both analytically and experimentally. The main objectives of this study are – (i) to develop suitable isolation system for seismic protection and assess its effectiveness in controlling the response of the test structure by Shake Table test (ii) to model hysteretic behaviour of seismic isolation system in light of experimental observations and (iii) to develop a unified solution algorithm, which is simple and practical yet accurate, and also necessary computer programs for computation of seismic response of medium-rise base isolated buildings, subjected to both unidirectional and bidirectional motions. In the course of the study, various other important factors which influences the overall behaviour of the base isolated buildings supported over various isolation systems viz bearing characteristics, effects of flexibility of the superstructure, characteristics of earthquake excitation, effects of different hysteretic models, biaxial interaction in general plane motion and contribution of rocking mode have been examined. The major conclusions are summarized in the subsequent sections.

7.2 Conclusions

7.2.1 Review of Literature

Seismic isolation systems developed so far and their characteristics, analytical and experimental studies on overall behaviour of base isolated buildings have been reviewed in this study. Various base isolation systems developed for earthquake protection of medium-rise buildings are broadly classified into three categoreies. Based on the review of literature, laminated rubber bearing (LRB) with appropriate damping is found to be suitable for seismic isolation of

medium-rise framed buildings considering its low-pass filter characteristics and simple construction and connection details.

7.2.2 Design of Model Bearing and its Characteristics

Main criterion for design of LRB for seismic isolation, are high vertical stiffness and low horizontal stiffness. It is very difficult to achieve these two requirements simultaneously, while designing model LRB for seismic isolation of test structure with small loads.

Buckling load of model LRB have been estimated from different formulae proposed by different investigators. On the basis of compressive load test on model LRB, it is concluded that buckling load predicted by Stanton *et al.*(1989) gives a more realistic value as compared to other formulae.

Shear test carried out on model LRB show that shear modulus and shear stiffness decreases with increasing shear strain level (upto 55% maximum strain) and increasing vertical load. Damping provided by the model LRB increases with increasing vertical load.

7.2.3 Shake Table Test

A three storeyed r.c. framed model has been constructed for the Shake Table test. The dimensions of elements of the model are obtained by geometric scaling of corresponding elements of the prototype, which are designed for Zone-V as per seismic zoning map of India.

Response of a base isolated model have been recorded during free vibration test and shake table test. It is observed that model LRB acts as a low pass filter which eliminates high frequency components of the table acceleration. Peak roof accelerations in three test runs are found to be nearly 50% of peak table accelerations of the respective runs and this establishes the effectiveness of model LRB in controlling the response of the test structure. The behaviour of model LRB is non-linear in nature with high stiffness at low strain level. Rocking mode contribution is present in the response of the isolated structure because of slender shape of model LRB.

7.2.4 Development of Computer Programs and their Validation

Number of computer programs have been written in FORTRAN-77 language on the basis of solution algorithms developed for computation of seismic response of base isolated medium-rise r.c. framed structures, subjected to both unidirectional and bidirectional motions. Validation of computer programs have been performed by comparing the computed results with the measured response of Shake Table test carried out in this study and analytical and experimental results reported in the literature.

7.2.5 Flexibility of Superstructure

Effect of flexibility of the superstructure has been assessed by idealizing the superstructure isolated by different isolation systems as rigid body model and flexible model. Base displacement histories obtained from rigid body model for LRB, LLRB and EDF bearing, give good estimate as compared to that obtained from flexible model. Acceleration time histories for these isolation systems obtained from flexible model are almost similar in pattern with slightly higher amplitude as compared to that obtained from rigid body model. Effect of flexibility is maximum in case of P-F isolation system. Level of base displacement increases considerably in case of flexible model, although pattern of displacement histories in both models are similar. Amplification of acceleration is considerable for this system, although it is less than that of fixed base structure. Base acceleration response in EDF isolation system is found to oscillate about μg acceleration level in the flexible model.

7.2.6 Characteristics of Earthquake Excitation

Seismic base isolation is one of the passive control techniques of earthquake protection of buildings and therefore, characteristics of earthquake motion influence the response of the isolated structure. Base displacement level for LRB, LLRB and EDF isolated systems obtained from flexible model subjected to Koyna earthquake (long.) are less than that subjected to El Centro (N-S) earthquake, although peak ground acceleration is more in former excitation as compared to that in later one. But, this is not so in case of P-F bearing isolated system, because this system can not filter out high frequency component of the

145

earthquake excitations. Amplification of acceleration is more in base isolated system subjected to El Centro (N-S) excitation. Higher modes contribution also increases slightly for LRB, LLRB and EDF isolators. For Koyna earthquake (long.) EDF bearing behaves almost as LRB. Earthquake protection of buildings by base isolation is more effective in controlling the response of the structure under earthquake excitations with most energy contents in the high frequency range.

7.2.7 Hysteretic Modelling of Isolation System

Experimental shear force-displacement hysteresis loops for different isolation system under both unidirectional and bidirectional motion have been simulated by solution algorithm developed in the present study. Simulated hysteresis loops are found to be in good agreement with the experimental hysteresis loops.

Modelling of shear force-displacement characteristics of LRB by non-linear hysteretic model increases the higher mode contributions at the same time decreases the lower mode contributions in the response of isolated structure as compared to that of equivalent linear analysis. Similar behaviour is also observed for lead rubber bearing and EDF isolator. Modelling of hysteresis loop of P-F bearing by visco-plastic model reduces the contribution of higher modes in the response of isolated structure as compared to that of rigid plastic model.

7.2.8 Biaxial Interaction in General Plane Motion

Influence of biaxial interaction between orthogonal components of restoring force of isolation bearings is established by change in shape of hysteresis loops, when the bearings are subjected to bidirectional motion. Comparison of response of isolated structure in a particular direction for unidirectional and bidirectional excitations also reflects the significant effects of biaxial interaction.

Effects of biaxial interaction on the response of isolated structure are more prominent in case of P-F bearing and its effects are considerable for LRB based isolation systems.

The computed response based on proposed solution algorithm of the base isolated structure subjected to bidirectional motion are in good agreement with that obtained from more complex numerical studies reported in the literature.

7.2.9 Rocking Mode of Vibration

Normally contribution of rocking mode of vibration is not significant, if vertical stiffness of the bearing is large. The model LRB designed in this study is exceptionally slender in shape for providing necessary flexibility for seismic isolation of the test model and this is responsible for significant contribution of rocking mode, as indicated by measured response of shake table testing. When, an additional rocking degree of freedom is considered only at the rigid base, response computed from flexible model matches well with the measured response of the test model. Thus, response of the base isolated systems could be reliably predicted by analytical techniques developed in the present study.

7.3 Suggestions for Future Work

Earthquake protection of structures by base isolation is of recent origin. Different types of new seismic isolation systems are coming up in different parts of the world. Application of base isolation technique is gaining acceptance for controlling seismic response of structures. This new aseismic design method will be very useful for earthquake protection of important structures like Fire Station Buildings, Hospital Buildings, Communication Centres, R&D centres with sophisticated equipment, bridges and other life line structures, which should remain undamaged and functional after an earthquake. Therefore, further research in the field of seismic base isolation are necessary for raising security against earthquake disaster. The most relevant suggestions for future research work are as follows:

(1)   Full 3-D analysis taking into account non-linear behaviour of individual isolation bearing, can be carried out for computation of overall response of base isolated structure.

(2)   The response of the base isolated structure is dependent on the characteristics of earthquake motion, which will occur in future.

Therefore, probabilistic method of computation of response of base isolated structure will be more appropriate.

(3) Seismic response of secondary system in a base isolated building is an important area for future research work.

(4) Rehabilitation of old monumental buildings or buildings with historical importance by base isolation can be studied as an alternative to existing retrofitting techniques.

(5) Earthquake protection of other life line structures by base isolation can be studied.

REFERENCES

1. Aiken, I.D., J.M. Kelly and F.F. Tajirian(1989), "Mechanics of low shape factor elastomeric seismic isolation bearings", Report No. UCB/EERC-89/13, Earthquake Engineering Research Center, University of California at Berkeley.

2. Aiken, I.D., J.M.Kelly, P.W. Clark, K. Tamura, M. Kikuchi and T. Itoh(1992), "Experimental studies of the mechanical characteristics of three types of seismic isolation bearings", 10th WCEE, Madrid, Spain, Vol. 4, pp. 2281-2286.

3. Aoyagi, S., T. Mazda, O. Harada and S. Ohtsuka(1988), "Vibration test and earthquake response observation of base isolated building", Proc. 9th WCEE, Tokyo-Kyoto, Japan, Vol-5, pp. 681-687.

4. Arya, A.C., B. Chandra and B. Qamaruddin(1978), "A new building system for improved earthquake performance", 6th Symposium on Earthquake Engg., University of Roorkee, India, Vol. 5, pp. 499-504.

5. Arya, A.S.(1984), "Sliding concept for mitigation of earthquake disaster to masonry building", 8th WCEE, San Francisco, Vol. 5, pp. 951-958.

6. Buckle, I.G., and R.L. Mayes (1990) " Seismic isolation: History, application and performance - A world view", Earthquake Spectra, Vol. 6, No.2, pp. 161-201.

7. Bouc, R.,(1967)[*] "Forced vibration of Mechanical system with hysteresis", Abstract, Proceedings of 4th Conf. on Non-linear Oscillation, Prague, Czechoslovakia.

8. Built, S.M.(1982), "Lead rubber dissipator for base isolation of bridge structures", School of Engineering Report No. 289, Department of Civil Engineering, University of Auckland, New Zealand, August, 1982.

9. Capse, M.S.(1984), "Base isolation from earthquake hazards, an idea whose time has come!", 8th WCEE, San Francisco, Vol. 5, pp. 1031-1038.

10. Capse,M.S. and A.M. Reinhorn(1986), "The earthquake barrier - A solution for adding ductility to otherwise brittle buildings", Proc. of ATC-17 Seminar on base isolation and passive energy dissipation, Applied Tech. Council, San- Francisco, California, pp. 331-342.

11. Clough, R.W. and J. Penzien (1986) "Dynamics of structures", International Student Edition, McGraw Hill Book Company.

12. Constantinou, M.C., and M.A. Adane (1987)[**] "Dynamics of soil-based-isolated structure systems: Evaluation of two models for yielding systems", Report to the National Science Foundation, Deptt. of Civ. Engg., Drextel Univ. Philadelphia, Pa.

13. Constantinou, M.C., and A. Mokha (1989) "A model of friction of Teflon sliding bearings", Report to the National Science Foundation, Deptt. of Civ. Engg., State Univ. of New York, Buffallo, N.Y, April.

14. Constantinou, M., A. Mokha and A. Reinhorn(1990), "Teflon bearings in base isolation II: modelling", J. of Struc. Div., ASCE, Vol. 116, No. 2, pp. 455-474.

15. Delfosse, G.C.(1977), "The Gapec system: a new highly effective aseismic system", 6th WCEE, New Delhi, India, Vol. 3, pp. 135-1140.

16. Delfosse. G.C.(1980), "Full earthquake protection through base isolation system", 7th WCEE, Istanbul, Turkey, Vol. 8, pp. 61-66.

17. Delfosse, G.C. and P.G.Delfosse(1984), "Earthquake protection of a building containing radioactive waste by means of base isolation system", 8th WCEE San Francisco, Vol. 5, pp. 1047-1054.

18. Derham, C.J.(1982), "Basic principles of base isolation", Proc. of the Int. Conf. on Natural rubber for Earthquake Protection of Buildings and Vibration Isolation, Kuala Lumpur, Malaysia, Edited by C.J. Derham, pp. 65-81.

19. Derham, C.J. and H.S. Thomas(1983), "The stability of rubber/steel building bearings", Natural Rubber Technology, Vol. 14, No. 3, pp. 124-132.

20. Derham, C.J., J.M. Kelly and A.G. Thomas(1985), "Non linear natural rubber bearings for seismic isolation", Nuclear Engg. and Design, Vol. 84, pp. 417-428.

21. Fintel, M. and R.F. Khan(1969), "Shock absorbing soft story concept for multistorey earthquake structures", J. of A.C.I Vol. 69, No. 29, pp. 318-390.

22. Fan, F, G. Ahamdi and I.G. Tadjbakhsh(1990), "Multi-story base isolated buildings under a harmonic ground motion – Part I: A comparison of performances of various system ", Nuclear Engg. and Design, Vol. 123, pp. 1-16.

23. Gent, A.N.(1964), "Elastic stability of rubber compression springs", J. of Mechanical Engineering Science, Vol. 6, No. 4, pp. 318-326.

24. Gent, A.N. and P.B. Lindley(1959), *** "The compression of bonded rubber blocks", Proc. of Institution of Mechanical Engineers, Vol. 173, No. 3, pp. 111-122.

25. Gueraud, R., J.P. Noel-leroux, M. Livolant and P Michalopoulos (1985), "Seismic isolation using sliding-elastomer bearing pads", Nuclear Engg. and Design, Vol-84, pp. 363-377.

26. Haringx, J.A.(1948-49), *** "On highly compressive helical springs and and their application to free mountings – Part I, II and III, Philips Research Report.

27. Higashino, M., S. Aizuwa and Y. Huyanizu(1988), "The study of base isolation system for actual use", Proc. 9th WCEE, Tokyo-Kyoto, Japan, Vol-5, pp. 705-710.

28. Hirasawa, M., A. Mikame, Y. Takasaki, T. Miyama, and K. Uchid (1988), "Aseismic design of a base isolated building and verification tests of an isolator", Proc. 9th WCEE, Tokyo-Kyoto, Japan, Vol-5, pp. 723-728.

29. Huffman, G.R.,(1985), "Full base isolation for earthquake protection by helical springs and viscodampers", Nuclear Engg. and Design, Vol. 84, pp. 331-338.

30. I.S.3400 - I, II, X, XIV(1971-80), "Indian Standard Code of Practice for methods of test for vulcanized rubbers.

31. Inaudi, J.A. and J.M. Kelly(1992), "Optimum damping in base isolated structures", 10th WCEE, Madrid, Spain, Vol. 4, pp. 1993-1998.

32. Izumi, M. and H. Yamahara(1988), "Comparisons between earthquake response characteristics of base isolated and ordinary buildings", Proc. 9th WCEE, Tokyo-Kyoto, Japan, Vol-5, pp. 687-692.

33. Jennings, P.C.(1968), "Equivalent viscous damping for yielding structures", J. of Engg. Mech., ASCE, Vol. 94, No. 1, pp. 103-116.

34. Kamke, E.(1959), ** "Differentialgleichungen Losungsmethoden un Losungen", Chelsea Publishing Company, New York.

35. Kan, C.L. and A.K.Chopra (1977) "Elastic earthquake analysis of a class of torsionally coupled buildings", J. of Struc. Div., ASCE, Vol. 103, No. 4, pp. 821-838.

36. Kawamura, S., K. Kitazawa, M. Hisano and I. Nagashima(1988), "Study on a sliding-type base isolation system-system composition and element properties", Proc. 9th WCEE, Tokyo-Kyoto, Japan, Vol-5, pp 735-741.

37. Kelly, J.M.(1986), "Aseismic base isolation: Review and Bibliography", Soil Dyn. and Earthquake Engg., Vol. 5, No. 3, pp. 202-216.

38. Kelly, J.M. and S.B. Hodder(1982), "Experimental study of lead and elastomeric dampers for base isolation systems in laminated neoprene bearings", Bulletin of New Zealand National Society for Earthquake Engg., Vol. 11, No. 4, pp. 219-233.

39. Kelly, J.M.(1991), "Shake table tests of long period isolation system for nuclear facilities at soft soil sites ", Report No. UCB/EERC-91/03, Earthquake Engineering Research Center, University of California at Berkeley.

40. Kelly, J.M. and K.E. Beucke(1983), "Friction damped base isolation system with fail-safe characteristics", Int. J. of Earthquake Engg. and Struc. Dyn., Vol. 11, pp. 33-56.

41. Kimura, O.M. and M. Izumi(1989), "A method of artificial generation of earthquake ground motion", Int. J. of Earthquake Engg. and Struc. Dyn., Vol. 18, pp. 867-874.

42. Koh, C.G. and J.M. Kelly(1989), "Viscoelastic stability model for elastomeric isolation bearings", J. of Struc. Engg., ASCE, Vol. 115, No. 2, pp. 285-302.

43. Lam, H.Y-F(1979), "Analog and digital filters: design and realization", Prentice- Hall, Inc., Englewood Cliffs, New Jersy.

44. Lee, D.M. and I.C. Medland(1978), "Base isolationan historical development, and influence of high mode responses", Bulletin of New Zealand National Society for Earthquake Engg., Vol. 11, No. 4, pp. 219-233.

45. Li, L.(1984), "Base isolation measure for aseismic buildings in China", 8th WCEE, San Francisco, Vol. 6, pp. 791-798.

46. Liauw, T.C., Q.L. Tian and Y.K. Cheung(1988), "Structures on sliding base subject to horizontal and vertical motions", J. of Struc. Div., ASCE, Vol. 114, No. 9, pp. 2110-2129.

47. Lin, B.C. and I. Tadjbakhsh(1986), "Effects of vertical motion on friction-driven isolation systems", Int. J. of Earthquake Engg. and Struc. Dyn., Vol-14, pp. 609-622.

48. Megget, L.M.(1984), "The design and construction of a base isolated concrete frame building in Wellington, New Zealand", 8th WCEE, San Francisco, Vol. 5, pp. 935-942.

49. Miyazaki, M., K. Nakano, Y. Kitagawa, I. Shimoda and Y. Mitsusaka (1988), "Design and its performance verification of a base isolated building using lead rubber bearings in Japan", Proc. 9th WCEE, Tokyo-Kyoto, Japan, Vol-5, pp. 717-722.

50. Mizukoshi, K., A. Yasaka and M. Iizuka(1992), "Failure test of laminated rubber bearings with various shapes", 10th WCEE, Madrid, Spain, Vol. 4, pp. 2277-2280.

51. Mohraz, B.(1976), "A study of earthquake response spectra for different geological conditions", Bulletin of the Seismological Society of America, Vol. 66, No. 3, pp. 915-935.

52. Mokha, A., M. Constantinou and A. Reinhorn(1990), "Teflon bearings in base isolation I: Testing ", J. of Struc. Div., ASCE, Vol-116, No. 2, pp. 438-454.

53. Mokha, A., M. Constantinou, A. Reinhorn and V.A. Zayas(1991), "Experimental study of friction pendulum isolation system", J. of Struc. Div., ASCE, Vol. 117, No. 4, pp. 1201-1217.

54. Mokha, A.S., M.C. Constantinou, A.M. Reinhorn (1993) "Verification of friction model of Teflon bearings under triaxial load", J. of Struc. Div., ASCE, Vol. 119, No. 1, pp. 240-261.

55. Mostaghel, N. and J. Tanbakuchi(1983), "Response of sliding structures to earthquake support motion", Int. J. ofEarthquake Engg. and Struc. Dyn., Vol. 11, pp. 729-748.

56. Mostaghel, N. and M. Khodaverdian(1987), "Dynamics of resilient -friction base isolator (R-FBI)", Int. J. of Earthquake Engg. and Struc. Dyn., Vol. 15, pp. 379-390.

57. Nagarajaiah, S., A. Reinhorn and M. Constantinou (1990) "Analytical modelling of three dimensional behaviour of base isolation devices", Proc. of fourth U.S. National Conf. on Earthquake Engg., Palm

springs, California, Vol. 3, pp. 579-588.

58. NagaraJaiah, S., A.M. Reinhorn and M. Constantinou(1991), "Non-linear dynamic analysis of 3-D-base-isolated structures", J. of Struc. Engg., ASCE, Vol. 117, No. 7, pp. 2035-2054.

59. Nakamura, T., T. Suzuki, H. Okada and T. Takeda(1988), "Study on base isolation for torsional response reduction in asymmetric structures under earthquake motion". 9th WCEE, Tokyo-Kyoto , Japan, Vol. 5, pp. 675-680.

60. Nakamura, T., T. Tsunoda and A. Teramura(1992) "Study on soft-landing mechanism in base-isolation device", 10th WCEE, Madrid, Spain, Vol. 4, pp. 2005-2011.

61. Pan, T.C. and J.M. Kelly(1983), "Seismic response of tortionally coupled base isolated structures", Int. J. of Earthquake Engg. and Struc. Dyn., Vol. 11, pp. 749-770.

62. Pan, T.C. and J.M. Kelly(1984), "Seismic response of base isolated structures with vertical-rocking coupling", Int.J of Earthquake Engg. and Struc. Dyn., Vol. 12, pp. 681-702.

63. Park, Y.J., Y.K. Wen and A.H.S. Ang(1986), "Random vibration of hysteretic systems under bi-directional ground motions", Int. J. of of Earthquake Engg. and Struc. Dyn., Vol. 14, pp. 543-557.

64. Paul, D.K.,(1982) "Efficient dynamic solution for single and coupled multiple field problems", Ph.D thesis, Univ. of Swansea, C/Ph/64/82.

65. Robinson, W.H. and A.G. Tucker(1977), "A lead-rubber shear damper", Bulletin of New Zealand National Society for Earthquake Engg., Vol. 10, No. 3, pp. 151-153.

66. Robinson, W.H.(1982), "Lead rubber hysteretic bearings suitable for protecting structures during earthquakes", Int. J. of Earthquake Engg. and Struc. Dyn., Vol. 5, pp. 593-604.

67. Serino, G., G. Bonacina, R. Spade(1992), "Implications of shaking table tests in the analysis and design of base isolated structures", 10th WCEE, Madrid, Spain, Vol. 4, pp. 2405-2410.

68. Shimoda, I., S. Nakano, Y. Kitagawa and M. Miyazaki(1988), "Experimental study on base isolated building using lead rubber bearing through vibration tests", Proc. 9th WCEE, Tokyo-Kyoto, Japan, Vol-5, pp. 711-716.

69. Shimosaka, H., K. Ohmata, H. Shimoda, T. Koh and T.Arakawa (1988), "An earthquake isolator effectively controlling the displacement by employing the ball screw type damper with magnetic damping ", Proc. 9th WCEE, Tokyo-Kyoto, Japan, Vol-5, pp. 827-832.

70. Shustov, V.(1992), "Base isolation: Fresh insight", 10th WCEE, Madrid, Spain, Vol. 4, pp. 1983-1986.

71. Skinner, R.I., J.M. Kelly and A.J. Heine(1975), "Hysteretic dampers for earthquake-resistant structures", Int. J. of Earthquake Engg. and Struc. Dyn., Vol. 3, No. 3, pp. 287-296.

72. Skinner, R.I., J.L. Beck and G.N. Bycroft(1975), "A practical system for isolating structures from earthquake attack", Int. J. of Earthquake Engg. and Struc. Dyn., Vol. 3, No. 3, pp. 297-309.

73. Skinner, R.I., G.N. Bycroft and G.H. McVerry(1976), "Practical system for isolating nuclear power plants from earthquake attack", Nuclear Engineering and Design, Vol. 36, pp. 287-297.

74. Skinner, R.I.(1984), "Base isolated structures in New Zealand", 8th WCEE, San Francisco, Vol. 5, pp. 927-934.

75. Skinner, R.I., G.H. Mc Verry and W.H. Robinson(1992), "Developments in understanding, analysing and designing structures with aseismic isolation", 10th WCEE, Madrid, Spain, Vol. 4, pp. 1977-1982.

76. Stanton, J.F., G. Scroggins, A.W. Taylor, C.W. Roeder(1989), "Stability of laminated rubber bearing", J. of Engg. Mech., ASCE, Vol. 116, No. 2, pp. 351-371.

77. Stiemer, S., F.L. Zhou(1984), "Curved plate energy absorbers for earthquake resistant structures", 8th WCEE, San Francisco, Vol. 5, pp. 967-974.

78. Su, L., G. Ahamdi and I.R. Tadjbakhsh(1989), "Comparative study of base isolation systems", J. of Engg. Mech. Div., ASCE, Vol-115, No. 9, pp. 1976-1992.

79. Suzuki, H., N. Kaizu, M. Takeuchi, and K. Takahashi (1992) "Theoretical study and development of new base-isolation systems of power equipment", 10th WCEE, Madrid, Spain, Vol. 4, pp. 1999-2003.

80. Takeda, T., S. Hirano, J. Yoshihara, Y. Nawaoka, H. Uchida and M. Nakamura(1988), "Study on base isolation system for earthquake protection and vibration isolation by laminated high-damping rubber", Proc. 9th WCEE, Tokyo-Kyoto, Japan, Vol-5, pp. 729-734.

81. Teramura, A., T. Takeda, T. Tsunoda, M. Seki, M. Kageyama and A. Nohata(1988), "Study on earthquake response characteristics of a base isolated full scale building", Proc. 9th WCEE, Tokyo -Kyoto, Japan, Vol-5, pp. 693-698.

82. Thomas, A.G.,(1982) "Design of laminated bearings I", Proc. of Conf. Natural Rubber for Earthquake Engg. Protection of Buildings, Kualalumpur, Malaysia, pp. 229-246.

83. Tyler, R.G.(1977), "Dynamic test on PTFE sliding layers under earthquake conditions", Bulletin of the New Zealand National Society for Earthquake Engg., Vol. 10, No. 3, pp. 129-138.

84. Tylor, R.G. and W.H. Robinson(1985), "Test on lead-rubber bearings", Proc. 2nd U.S.-New Zealand Workshop on Seismic Resistance of Highway Bridges, ATC-12-1, pp.217-221.

85. Wen, Y.K.(1976) "Method of random vibration of hysteretic systems", J. of Engg. Mech. Div., ASCE, Vol. 102, No. 2, pp. 249-263.

86. Wen, Y.K.,(1980) "Equivalent linearization for hysteretic systems under random excitations", J. of Appl. Mech., ASME, Vol. 47, pp. 543-557.

87. Yasaka, A., H. Koshida and M. Iizuka(1988a), "Base isolation system for earthquake protection and vibration isolation of structures", Proc. 9th WCEE, Tokyo-Kyoto, Japan, Vol. 5, pp. 699-704.

88. Yasaka, A., K. Mizukoshi, M. Izuka, Y. Takenaka, S. Maeda and N. Fuzimoto(1988b), "Biaxial hysteresis model for base isolation devices", Summeries of technical papers of annual meeting, Architectural Inst. Of Japan, Tokyo, Japan, Vol. 1, pp. 395-400.

89. Younis, C. and I.G. Tadjbakhsh(1984), "Response of a sliding structures to base excitation", J. of Engg. Mech., ASCE, Vol. 110, No. 3., pp. 417-432.

90. Zayas, V.A., S.S Low and S.A. Mahin(1989), "A simple pendulum technique for achieving seismic isolation", Earthquake Spectra, Vol. 6, No. 2, pp. 317-334.

91. Zienkiewicz, O.C., D.K. Paul and A.H.C. Chan (1988) "Unconditionally stable staggered solution procedure for soil-pore fluid interaction problems", Int. J. of Num. Meth. Engg., Vol. 26, pp. 1039-1055.

---

*, **, *** Not seen in original.

* Referred from cross reference of Wen (1976).

** Referred from cross reference of Constantinou and Mokha (1990).

*** Referred from cross reference of Aiken et al.(1989).